Introducing stable isotopes into small molecule to elucidate functional analysis of biologically active compounds

（生理活性物質の機能解明を目指した低分子安定同位体標識法の検討）

Doctoral dissertation

北海道大学大学院農学院
農学専攻／生命フロンティアコース　博士後期課程

ZHANG Wen (章　文)

TABLE OF CONTENTS

Acknowledgement

First and foremost, I would like to express my sincere gratitude to Prof. Makoto Hashimoto for providing me with the opportunity to join the Ecological Chemistry Laboratory and for his invaluable support in completing my studies and obtaining my doctoral degree. In addition, he has also offered significant assistance in both my personal life and career. Over the past three years, he has dedicated himself to mentoring me from 6:00 a.m to 9:00 p.m each day, efficiently addressing my inquiries, which has been crucial for smooth proceeding of my research. Whenever I faced challenges and setbacks in my research, his innovative viewpoint consistently guided me toward effective solutions. From him, I have not only learned the importance of a rigorous academic attitude but have also been deeply influenced by his divergent thinking and passion for research, which I intend to apply in my future endeavors.

I would also like to thank Prof. Yasuko Sakihama for her assistance throughout my research process. Her meticulous guidance enabled me to quickly adapt to the research methodologies of the Ecological Chemistry Lab. I am also grateful to associate professor Yuta Murai, who joined our lab later on, for his support in experiments and manuscript preparation, particularly for his help in measuring MS for me. His approachable demeanor, coupled with his enthusiasm and rigor in academic research, has greatly benefited me. Additionally, I would like to extend my gratitude to all my colleagues in the laboratory from the time I entered the Ecological Chemistry Laboratory until my impending graduation, for their assistance and encouragement during my experiments.

I am also thankful for the support provided by the DX FELLOWSHIP scholarship from Hokkaido University over the past three years, which has been instrumental in my living expenses and research endeavors (JPMJSP2119).

Finally, I wish to convey my profound appreciation to my beloved family. Their care and encouragement over the years have enabled me to overcome the challenges and obstacles in my life and studies. I am especially grateful to my boyfriend, who has repeatedly guided and supported me through various difficulties, allowing me to face all challenges head-on. I will carry your love and support with me as I embark on a new phase of my life.

Abbreviations

TfOH	trifluoromethanesulfonic acid
TfOD	deuterated trifluoromethanesulfonic acid
MFW	fresh weight of mycelia
ESI-MS	electro spray ionization mass spectrometry
FD-MS	field desorption mass spectrometry
PDA	potato dextrose agar
PDB	potato dextrose broth
PIG	potato infusion with glucose
TLC	thin layer chromatography
NMR	nuclear magnetic resonance
HPLC	high performance liquid chromatography
mM	millimolar
rpm	rotations per minute
μM	micromolar

1. Introduction and brief summary

1.1. Introduction: stable isotopes

Biomolecules are composed of atoms from various elements, each exhibiting distinct chemical properties that are determined by their position in the periodic table, which is based on the number of protons in their nuclei (atomic number). Stable isotopes are atoms of the same element that differ in the number of neutrons within their nuclei, resulting in variations in atomic mass. The term "isotope" refers to the different isotopes of the same element occupying the same ("iso") position ("topos") in the periodic table[1]. Most elements possess multiple naturally occurring isotopes; as the name suggests, stable isotopes are those that do not undergo radioactive decay. While it is common for one isotope to be more abundant, every element in nature invariably exists as a mixture of its isotopic forms. For instance, carbon typically has 6 protons and 6 neutrons, yielding an atomic mass of 12; however, 1.11% of carbon on Earth possesses an additional neutron, resulting in a mass of 13. Although ^{13}C is significantly less abundant than ^{12}C, it is not rare: a 50-kilogram human body contains approximately 137 grams of ^{13}C, equivalent to over 6×10^{24} atoms[2, 3].

Table 1.1 Summary of the more commonly used stable isotopes for tracer work including their natural abundance[4]

Element	Stable isotopes	%Natural abundance
Hydrogen	^{1}H	99.985
	^{2}H (D)	0.015
Carbon	^{12}C	98.89
	^{13}C	1.11
Nitrogen	^{14}N	99.63
	^{15}N	0.37
Oxygen	^{16}O	99.76
	^{17}O	0.037
	^{18}O	0.204

Sulfur	^{32}S	95.00
	^{33}S	0.76
	^{34}S	4.22
Silicon	^{28}Si	92.21
	^{29}Si	4.9
	^{30}Si	3.09
Iron	^{54}Fe	5.82
	^{56}Fe	91.66
	^{57}Fe	2.19
	^{58}Fe	0.33
Zinc	^{64}Zn	48.89
	^{66}Zn	27.81
	^{67}Zn	4.11
	^{68}Zn	18.57
	^{70}Zn	0.62
Selenium	^{74}Se	0.87
	^{76}Se	9.02
	^{77}Se	7.58
	^{78}Se	23.52
	^{80}Se	49.82

Since the 1930s, when stable isotope tracers were first isolated and implemented, they have provided the scientific community with invaluable insights into the metabolic mechanisms underlying diseases[5], aging[6], and genetic disorders[7]. While stable isotopes are primarily utilized in the study of biological systems, their application is not confined to this domain; they have found extensive use in fields such as art, forensics, and geology[8-10]. By substituting one or more of the naturally occurring isotopes in target compounds—such as 12 carbon, 14 nitrogen, 16 oxygen, or 1 hydrogen (Table 1)—with their heavier and less abundant stable isotope counterparts, namely 13 carbon (^{13}C), 15 nitrogen (^{15}N), 18 oxygen (^{18}O), or 2 hydrogen (^{2}H or D), stable isotope tracers can be created. These labeled compounds can then be introduced into the systems under investigation, allowing for the monitoring of the fate of the compound and/or its

metabolites over time, thereby providing dynamic measurements of metabolism within the system.

1.2. Brief summary of the study

Isotopic labeling is a powerful technique extensively used in many aspects such as pharmaceutical industry. This technique involves incorporating either stable isotopes, such as deuterium (D) and carbon-13 (^{13}C), or radioactive isotopes, such as tritium (T) and carbon-14 (^{14}C), into molecules. By tracking these labeled molecules, researchers gain unique and invaluable insights into the pharmacokinetics and pharmacodynamics of new drug candidates. There are two main methods to achieve stable isotopic labeling into bioactive molecules, chemical labeling and metabolic labeling.

In this research, both two methods were performed, and isotopic labeling compounds were successfully obtained with high yield and effects. Deuterium-labeled indole-3-propionoic acid (IPA) was achieved through chemical synthesis under mild reaction conditions and ^{13}C-labeled squalene was obtained through metabolic biosynthesis in filamentous fungus *Trichoderma virens* PS1-7, which can be used to elucidate the metabolic pathways of indole derivatives and steroidal substances in living organisms individually.

1.2.1. Chemical synthesis of deuterium-labeled indole-3-propionoic acid (IPA) through H/D exchange with deuterated trifluoromethanesulfonic acid (TfOD)

Indole-3-propionic acid (IPA), a member of the plant auxin family, plays an important role in biological activity. Deuterium incorporation via H/D exchange is one of the simplest ways to prepare deuterated compounds, however, there are few reports for the preparation of their deuterated derivatives for IPA. In this research, H/D exchange with deuterated trifluoromethanesulfonic acid (TfOD), can achieve our aim easily. The reactions can be conducted in a temperature-dependent manner according to the chemical stability of the ligands without the use of special reagents. The detailed analysis of H/D exchange of IPA revealed that the reaction proceeded swiftly at low temperature. The effective H/D exchange of indole-3-alkanoic acids will be helpful not only in plant regulation studies but also in drug development.

1.2.2. Metabolic biosynthesis of ^{13}C-enriched squalene in filamentous fungi *Trichoderma virens* PS1-7 in the presence of butenafine hydrochloride, squalene epoxidase inhibitor.

Squalene is a primary metabolite of almost all triterpenoids with polyene structure and has been attracting attention from the pharmaceutical and cosmetics industries. Filamentous fungi have biosynthesis of various terpenoids via mevalonate pathway, but few accumulations of squalene were observed under normal cell growth culture conditions. I investigated the accumulation of squalene in filamentous fungi by inhibiting squalene epoxidase, which is the first enzyme in squalene metabolism. Squalene epoxidase is essential enzymes for fungi homeostasis to biosynthesis of important steroids (ex. ergosterol). Moderate inhibition of the enzyme is required to maintain both cell growth and squalene accumulation. It is optimized that filamentous fungi, *Trichoderma virens* PS1-7, produced squalene up to 429.93 ± 51.60 mg/L after culturing for 7 days in the medium consisted of potato infusion with glucose at pH 4.0, in the presence of 200 μM butenafine hydrochloride. I conducted other eight *Trichoderma virens* strains, which are available from NBRC, because *Trichoderma virens* PS1-7 is housekeeping fungi. All *Trichoderma virens* strains were found to be suitable for squalene accumulation. I found that PS1-7 is one of the most suitable strains for squalene accumulation among *Trichoderma virens*. The results means that filamentous fungi *Trichoderma virens* PS1-7 can be a potential source of producing squalene with the presence of squalene epoxidase inhibitor, butenafine hydrochloride, which heavily upgraded squalene accumulation than that without butenafine. Through further optimizing cultivation conditions, the squalene can be accumulated up to 608.94 ± 46.87 mg/L in PS1-7 by culturing up to 28 days. Based on that result, [U-$^{13}C_6$]-glucose was utilized to biosynthesize [U-^{13}C]-labeled squalene in the presence of exogeneous butenafine. The biosynthesized squalene, which is C30 triterpene, contained up to 30 atoms of stable isotope ^{13}C from mass spectrometry. The high incorporation of ^{13}C enables to measure ^{13}C-^{13}C COSY, which is not easy to measure in natural product, to elucidate structural analysis of labeled squalene. The accumulation of stable isotope squalene in filamentous fungi can be utilized to analyze terpene metabolites derived from squalene.

1.2.3. Metabolic biosynthesis of ^{13}C-enriched squalene in filamentous fungi *Trichoderma virens*

Viridin and viridiol are useful compounds with potent bioactivities, including antibacterial and antifungal activities. Additionally, they strongly inhibit phosphoinositide 3-kinases, which are associated with tumor cell survival. However, despite their benefits, methods for the large-scale production of viridin, viridiol, and their derivatives are limited. Therefore, in this study, we developed a simple production and purification method for these compounds. NBRC 9169 showed viridin and viridiol accumulation of 47.80 ± 4.71 and 61.92 ± 4.39 mg/L after seven days of incubation at pH 3 and pH 2, respectively. Additionally, we established an efficient method to irreversibly convert viridin into β-viridin at high yields reaching 76% using the TEA/$CHCl_3$ system, thus facilitating further research on β-viridin. Notably, we determined the absolute configuration of β-viridin, which has been unknown for more than 70 years since its discovery. Our findings revealed the potential of NBRC 9169 for the biosynthesis of ^{13}C-labeled viridin and viridiol using [U-$^{13}C_6$]-glucose. Future studies should elucidate the detailed biosynthetic pathways of ^{13}C-labeled viridin and viridiol. Moreover, it will be expected to reveal a group of unidentified gene clusters responsible for the biosynthesis of viridin and viridiol using our unique culturing techniques to produce highly enriched ^{13}C- furanosteroids.

2. Chemical labeling: H/D exchange with trifluoromethanesulfonic acid-D

2.1. Introduction

With the progress of techniques for mass analysis, stable isotope-labeled bioactive ligands have become attractive tools in the field[11]. Deuterium is one of the simplest stable isotopes and can be utilized for post-introductions to bioactive compounds. Hydrogen-deuterium exchange (H/D exchange)[12-14] at a specific position and universal hydrogen-deuterium exchange in acidic conditions[15] and/or metal catalysis[16] in aromatics have been reported in the literature. Indole-3-propionic acid (IPA) is well known as not only a plant auxin but also a potent neuroprotective antioxidant and drug for Alzheimer's disease. Partial deuteration on the indole moiety of IPA was reported using photolysis in D_2O, with deuteration degrees up to 40%[17]. There are few reports on a high H/D exchange for the indole moiety on IPA. Recently, we developed a method for effective H/D exchange for natural aromatic α-amino acids and their corresponding peptides with deuterated trifluoromethanesulfonic acid (TfOD) at a temperature lower than room temperature without a side-effect on stereochemistry[18-22]. We report in this paper the details of the H/D exchange of IPA and indole-3-alaknoic acid derivatives with TfOD under mild conditions.

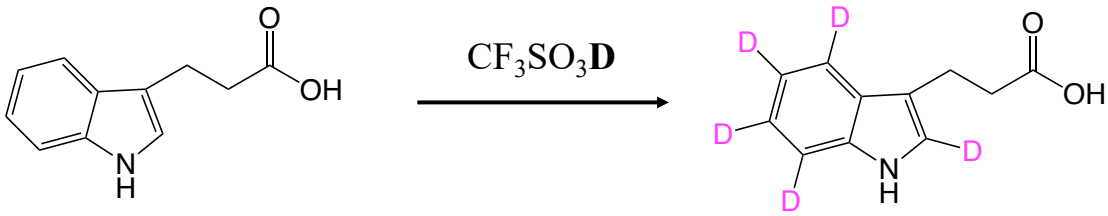

2.2. Results and discussion

2.2.1. H/D exchange of Indole-3-propionic acid (IPA, 1)

Indole-3-propionic acid (IPA, 1) was dissolved in deuterated trifluoromethanesulfonic acid (TfOD, 40 eq) at rt or 30 °C. The progress of H/D exchange was monitored using 1H-NMR. The results are summarized in Table 1. The priority of H/D exchange for the indole ring was observed as H-2 > H-5 > H-4, 6 and 7. A partial H/D exchange was

observed at β-methylene. Complete H/D exchange could not be achieved when the reaction was conducted at rt within 5 days, but no deuterated starting material 1 was observed from 1H-NMR analysis. The reaction conducted at 30 °C for 4 days afforded over 80% H/D exchange at all protons expect the α-position (Table 1). The reaction at higher temperature promoted side reactions for 1. The intramolecular cyclization to form 5-membered ring also promoted at higher temperature in the strong acid condition. Ester forms of IPA was subjected to H/D exchange with TfOD.

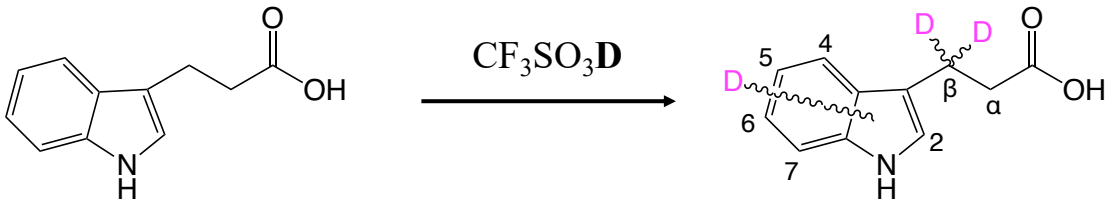

1 1-D

Table 2.1 H/D exchange of indole-3-propionic acid (1) with TfOD

Temperature	Time (h)	2	4	5	6	7	α	β
rt	12	92	58	88	50	50	0	26
	36	93	69	90	51	47	0	38
	120	93	86	90	76	71	0	64
30 °C	6	94	46	75	35	32	0	14
	12	94	57	87	44	47	0	27
	36	94	85	89	68	61	0	49
	48	96	91	91	79	71	0	58
	60	96	92	91	80	76	0	60
	72	96	94	92	80	85	0	79
	96	96	94	92	82	90	0	86

2.2.2. H/D exchange of IPA methyl ester (IPA-OMe, 2)

IPA methyl ester (IPA-OMe, 2) was subjected to H/D exchange with TfOD in a shortened reaction time (Table 2). H/D exchange on the indole moiety of IPA-OMe (2) was faster than that of IPA (1) and prevent intramolecular cyclization. The results

promoted the reactions are conducted at higher temperature (up to 60 °C). The deuterium incorporation at the β-position of the propionic acid moiety proceeded in a time-dependent manner. On the other hand, the deuterium incorporations on the indole moiety proceeded in a temperature-dependent manner until 60 °C. Methyl ester was hydrolyzed in alkaline conditions, and deuterium enrichment on the indole ring of IPA was obtained.

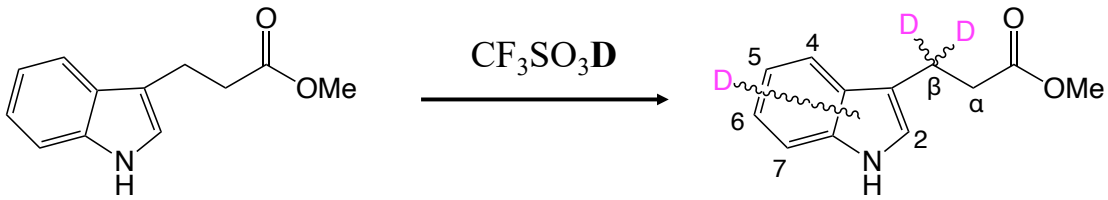

2 2-D

Table 2.2 H/D exchange of indole-3-propionic acid methyl ester (2) with TfOD

Temperature	Time (h)	2	4	5	6	7	α	β
rt	1	93	19	37	20	16	0	0
	2	94	27	63	26	32	0	0
	6	95	44	65	53	36	0	6
	12	97	67	89	64	32	0	26
40 °C	1	95	57	87	62	47	0	0
	2	95	65	90	62	51	0	5
	3	97	77	91	62	60	0	7
	4	97	81	92	62	60	0	10
	12	97	84	93	83	78	0	48
	72	97	90	93	88	89	0	84
60 °C	1	92	86	89	85	84	0	0
	2	92	89	91	85	85	0	10
	3	92	90	91	87	86	0	18
	4	92	92	92	90	88	0	25

2.2.3. H/D exchange of Indole-3-acetic acid (IAA, 3)

The established methods for IPA (1) and IPA-OMe (2) were applied to other indole alkanoic acid derivatives. Indole-3-acetic acid (IAA, 3), which is the shortest alkanoic acid moiety, was treated with TfOD (Table 3). Deuterium incorporations were observed at 4 °C. The α-methylene of IAA did not participate in the H/D exchange. H/D exchange on the indole ring was achieved within an hour at 40 °C. Intramolecular cyclization to form 4-membered ring was prevented. It has been reported H/D exchange of IAA with acidic condition (DCl or D_2SO_4). But the methods are conducted at higher temperature (over 100 °C) and long reaction time (over 12 h) due to less acidic condition. H/D exchange to be carried out at low temperatures and in short reaction times. TfOD archive the unique advantage of H/D exchange to be carried out at low temperatures and in short reaction times[23, 24].

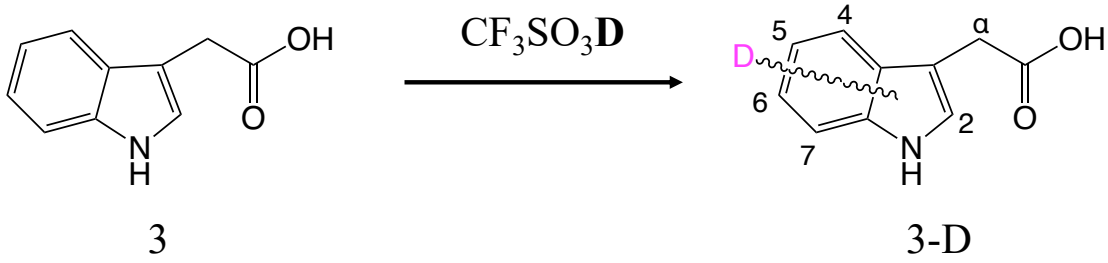

3 3-D

Table 2.3 H/D exchange of indole-3-acetic acid (3) with TfOD

Temperature	Time (min)	2	4	5	6	7	α
4 °C	60	0	2	0	0	3	0
	480	83	83	80	58	78	0
40 °C	15	82	80	88	76	69	0
	30	88	87	93	86	81	0
	45	91	90	93	90	87	0
	60	90	90	93	90	86	0

2.2.4. H/D exchange of Indole-3-butyric acid (IBA, 4)

Indole-3-butyric acid (IBA, 4) was treated with TfOD (Table 4). The deuterium incorporations were specifically observed at the 2-position of the indole and γ-position

of the alkanoic moiety at rt. The reaction conducted at 40 °C improved this incorporation into the indole rings. But higher temperature promoted intramolecular cyclization to form 6-membered ring.

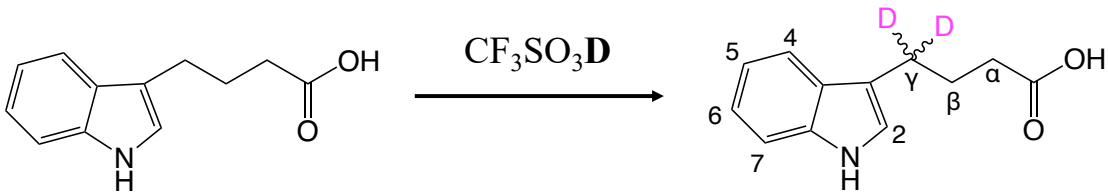

4 4-D

Table 2.4 H/D exchange of indole-3-butyric acid (4) with TfOD

Temperature	Time (h)	2	4	5	6	7	α	β	γ
rt	0.5	61	0	0	0	0	0	0	14
	1	74	0	0	0	0	0	0	36
	2	75	0	0	0	0	0	0	57
	3	79	0	0	0	0	0	0	61
	4	85	0	0	0	0	0	0	79
	6	86	0	0	0	0	0	0	89
	8	88	0	0	0	0	0	0	92
40 °C	1	95	26	46	17	10	0	5	82
	1.5	96	35	51	23	12	0	5	83
	2	98	44	66	37	16	0	6	88
	3	98	50	72	42	20	0	5	88
	4	98	55	79	51	22	0	5	90

2.3. Conclusion

Deuterium incorporation via H/D exchange is one of the simplest ways to prepare deuterated compounds, which are utilized to elucidate not only of biological activities but also reaction mechanisms. It has been reported that many H/D exchange reactions under acidic conditions proceed at higher temperature and with a longer reaction time. Indole-3-alkanoic acids are well known as plant growth regulators (auxins), but there

are few reports for the preparation of their deuterated derivatives for IAA[23, 24] and IBA[25]. The many reported reactions were conducted at high temperature. H/D exchange with deuterated trifluoromethanesulfonic acid (TfOD), which was recently reported by us, can overcome these problems. The reactions can be conducted in a temperature-dependent manner according to the chemical stability of the ligands without the use of special reagents (e.g., complex metal). The detailed analysis of H/D exchange of indole-3-alkanoic acids revealed that the reaction proceeded swiftly at low temperature. The effective H/D exchange of indole-3-alkanoic acids will be helpful not only in plant regulation studies but also in drug development.

2.4. Experimental section

General. All reagents used were analytical grade. Deuterated trifluoromethanesulfonic acid was purchased from Aldrich. NMR spectra were measured by using an EX 270 spectrometer (JEOL, Tokyo, Japan). HRMS-ESI spectra were obtained with a Waters UPLC ESI-TOF mass spectrometer (Waters, Milford, CT, USA). H/D exchange of Indole-3-alakanoic acid derivatives were conducted up to 150 mg scale for each compound.

3-(1*H*-Indol-3-yl-2,4,5,6,7-d5)propanoic-2,2-d_2 acid (1-D). 3-(1H-indol-3-yl)propanoic acid (**1**, 26.5 mg, 0.14 mmol) was dissolved in TfOD (0.5 mL, 5.65 mmol) at 0 °C. The reaction mixture was stirred at 30 °C for 96 h and slowly poured into 3.5 mL D_2O on ice. The aqueous solution was extracted with ethyl acetate. The organic layer was washed with brine, dried over $MgSO_4$, filtered, and concentrated. The residue was purified by column chromatography (ethyl acetate: n-hexane, 1:1) to afford colorless solid (19.8 mg, 72 %). ^{1}H-NMR (270 MHz, CD_3OD) δ: 7.47 (0.06H, s, H-4), 7.27 (0.10H, s, H-7), 7.03 (0.18H, s, H-6), 6.96 (0.08H, s, H-5), 6.95 (0.04H, s, H-2), 3.00 (0.28H, t, J 7.6 Hz, H-b), 2.62 (2H, t, J 7.6 Hz). ^{13}C-NMR (67.8 MHz, CD_3OD) δ: 177.5, 138.0, 128.4, 122.8 (t, J 24.0 Hz), 121.8 (t, J 25.1 Hz), 118.7 (t, J 22.8 Hz), 114.8 (t, J 23.1 Hz), 111.8 (t, J 25.1 Hz), 36.0, 21.8 (m). HRMS-ESI (m/z) $[M + H]^+$ calcd for $C_{11}H_5D_7NO_2^+$ 197.1302, found 197.1284.

Methyl 3-(1*H*-indol-3-yl-2,4,5,6,7-d_5)propanoate (2-D). 3-(1H-indol-3-yl)propanoic acid (**1**, 2.0 g, 10.6 mmol) was dissolved in 53 mL methanol. Concentrated H_2SO_4 (1.7 mL) was added at 0 °C. The reaction mixture was stirred at room temperature overnight,

poured into 88 mL of H_2O, extracted with CH_2Cl_2 (100 mL × 2), dried with $MgSO_4$, filtered, and concentrated to afford methyl 3-(1H-indol-3-yl)propanoate (**2**) as a pale brown solid (1.80 g, 84%). Compound **2** (143.0 mg, 0.70 mmol) was dissolved in TfOD (2.5 mL, 28.3 mmol) at 0 °C. The reaction mixture was stirred at 60 °C for an hour and slowly poured into 20 mL of D_2O on ice, and then extracted with $CHCl_3$ (10 mL × 3). The organic layer was washed with brine (5 mL × 3), dried over $MgSO_4$, filtered, and concentrated to afford pale yellow solid (103.0 mg, 70%). ^{1}H-NMR (270 MHz, CD_3OD) δ: 7.47 (0.11H, s, H-4), 7.27 (0.15H, s, H-7), 7.03 (0.10H, s, H-6), 6.96 (0.08H, s, H-5), 6.95 (0.08H, s, H-2), 3.72 (s, 3H), 3.00 (2H, t, J 7.6 Hz), 2.62 (2H, t, J 7.6 Hz). ^{13}C-NMR (67.8 MHz, CD_3OD) δ: 177.5, 138.0, 128.4, 122.8 (t, J 23.8 Hz), 121.8 (t, J 25.0 Hz), 118.7 (t, J 22.0 Hz), 114.8 (t, J 22.2 Hz), 111.8 (t, J 25.1 Hz), 51.5, 34.7, 20.6. HRMS-ESI (m/z) $[M + H]^+$ calcd for $C_{12}H_9D_5NO_2^+$ 209.1333, found 209.1350.

Hydrolysis of 2-D. Compound **2-D** (63.0 mg, 0.30 mmol) was dissolved in methanol (3.5 mL), and 1 M NaOH (1.2 mL) was added slowly. The reaction mixture was stirred at room temperature overnight and washed with CH_2Cl_2. The aqueous layer was acidified with 2 M HCl and extracted with ethyl acetate (20 mL × 2). The organic layer was dried over $MgSO_4$, filtered and concentrated. The residue was purified by column chromatography (ethyl acetate: n-hexane, 1:1) to give 3-(1H-indol-3-yl-2,4,5,6,7-d5)propanoic acid as a colorless solid (56.2 mg, 96 %).

2-(1*H*-Indol-3-yl-2,4,5,6,7-d$_5$)acetic acid (3-D). 2-(1H-indol-3-yl)acetic acid (**3**, 24.6 mg, 0.14 mmol) was dissolved in TfOD (0.5 mL, 5.65 mmol) at 0 °C. The reaction mixture was stirred at 40 °C for 45 min and slowly poured into 3.5 mL of D_2O on ice, and then extracted with ethyl acetate. The organic layer was washed with brine, dried with $MgSO_4$, filtered, and concentrated. The residue was purified by column chromatography (ethyl acetate: n-hexane, 1:1) to afford a colorless solid (24.8 mg, 98%). ^{1}H-NMR (270 MHz, CD_3OD) δ: 7.52 (0.10H, s, H-4), 7.33 (0.13H, s, H-7), 7.14 (0.09H, s, H-6), 7.08 (0.10H, s, H-5), 7.00 (0.07H, s, H-2), 3.72 (2H, s). ^{13}C-NMR (67.8 MHz, CD_3OD) δ: 176.5, 137.9, 128.6, 124.4 (t, J 26.8 Hz), 121.9 (t, J 24.6 Hz), 119.0 (t, J 24.6 Hz), 118.4 (t, J 24.6 Hz), 108.7 (t, J 25.0 Hz), 31.9. HRMS-ESI (m/z) $[M + H]^+$ calcd for $C_{10}H_5D_5NO_2^+$ 181.1020, found 181.1045.

4-(1*H*-Indol-3-yl-2-d)butanoic-4,4-d$_2$ acid (4-D). 4-(1H-indol-3-yl)butanoic acid (**4**, 434.4 mg. 0.17 mmol) was dissolved in TfOD (0.6 mL, 6.78 mmol) at 0 °C. The mixture was stirred at rt for 8 h and slowly poured into 3.5 mL D_2O on ice. The aqueous solution

was extracted with ethyl acetate. The organic layer was washed with brine, dried with $MgSO_4$, and filtered. The residue was purified by column chromatography (ethyl acetate: n-hexane, 1:1) to afford a colorless solid (31.7 mg, 91%). ^{1}H-NMR (270 MHz, $CDCl_3$) δ: 7.60 (1H, t, J 3.8 Hz, H-4), 7.35 (1H, d, J 7.9 Hz, H-7), 7.19 (0.12H, t, J 7.3 Hz, H-6), 7.11 (1H, t, J 7.3 Hz, H-5), 6.99 (0.07H, s, H-2), 2.83 (0.16H, dd, J 12.5, 6.6 Hz, H-g), 2.43 (2H, t, J 7.4 Hz), 2.05 (2H, q, J 6.9 Hz) ^{13}C-NMR (67.8 MHz, $CDCl_3$) δ: 179.2, 136.3, 127.4, 122.0, 119.3, 118.9, 115.1 (t, J 24.6 Hz), 111.1, 33.4, 24.9, 24.2 (m). HRMS-ESI (m/z) $[M + H]^+$ calcd for $C_{12}H_{11}D_3NO_2^+$ 207.1207, found 207.1188.

3. Biosynthesis of ^{13}C squalene

3.1. Introduction

3.1.1. squalene

Squalene is a lipid compound classified as a triterpene, first identified in 1906 by Manmaru Tsujimoto at the Tokyo Industrial Research Institute, extracted from the liver oil of the black dogfish[26]. Subsequently, in 1926, Heilbron and colleagues elucidated its structure, naming it squalene due to its discovery in deep-sea sharks (Squalus spp.)[27]. The structure of squalene is illustrated in Figure 3.1.

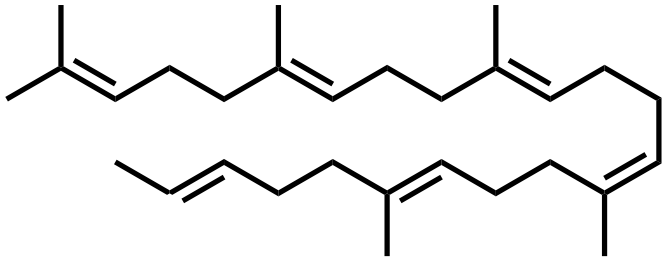

Figure 3.1 Structure of squalene

Squalene serves as a crucial intermediate in the biosynthesis of all triterpenoids, playing an essential role in the production of sterols and hopanoids. Consequently, a wide range of organisms, from bacteria to humans, are known to biosynthesize squalene[28]. Additionally, squalene remains in a liquid state at room temperature and is secreted by human skin[29].

Squalene is recognized as a potent antioxidant, capable of protecting cells from free radicals and reactive oxygen species by preventing lipid peroxidation[30]. Furthermore, it has been demonstrated to inhibit tumor formation in the colon, lungs, and skin, exhibiting chemopreventive and immunomodulatory activities, which have garnered significant interest from the pharmaceutical and medical industries[31, 32]. Moreover, due to its emollient properties that help maintain skin moisture and softness, squalene is also utilized in cosmetic formulations[33]. The demand for squalene, with its diverse functional applications, has been steadily increasing; the global market, valued at $129 million in 2020, is projected to reach $184 million by 2025, with an average annual growth rate of 7.3%[34].

Currently, the primary commercial source of squalene is the liver of deep-sea sharks, which typically contains 40-60% squalene. For instance, Hadimoto et al. reported that in the Okinawa dogfish (Centrophorus moluccensis), approximately 83% of the liver is composed of liver oil, with about 95% of that being squalene[35]. Due to rising demand and concerns over overfishing leading to potential extinction of these deep-sea sharks, there is an urgent need to explore alternative sources of squalene. Some plants have been reported to accumulate squalene; for example, olive oil contains significant amounts of squalene, ranging from 200 mg to 700 mg per 100 g of biomass, while amaranth seeds contain 6-8% squalene in their oil[34, 36]. However, the long lifecycle of plant resources and limitations on arable land due to climatic factors render plant-derived squalene insufficient to meet global industrial and food demands[37].

In light of these challenges, microorganisms have emerged as promising new sources of squalene. Although microorganisms do not accumulate squalene in quantities comparable to sharks or plants, they exhibit rapid growth rates and numerous reports of genetic modifications, making them suitable candidates for squalene production. For instance, the model eukaryote Saccharomyces cerevisiae (yeast) accumulates squalene at a rate of 1.6 mg/g CDW (cell dry weight)[38]. Other organisms, such as Aspergillus nidulans (0.3 mg/g CDW)[39] and the industrial yeast Saccharomyces uvarum (14.3 mg/g CDW)[40], also possess the ability to accumulate squalene. Additionally, microalgae such as Aurantiochytrium sp. strain 18W-13a (1.29 g/L)[41] and Schizochytrium limacinum strain SR21 (16.34 mg/g CDW)[42] have been reported to accumulate substantial amounts of squalene. Research is being conducted to further enhance squalene accumulation in these various wild-type microorganisms through strategies such as optimizing culture conditions[43], genetically modifying existing squalene biosynthetic pathways[44], and employing appropriate inhibitors (e.g., terbinafine) to block competing pathways.

Conversely, research utilizing filamentous fungi has not yet been conducted. This may be attributed to the challenges associated with genetic modification compared to the model organism S. cerevisiae, as well as the relatively low squalene accumulation in wild-type strains compared to Traustochytrids. Nevertheless, filamentous fungi inherently possess the mevalonate pathway responsible for squalene biosynthesis and are capable of producing a diverse array of secondary metabolites, including terpenes, suggesting their potential as a viable source of squalene.

3.1.2. biosynthetic pathway of terpenes

Terpenoids are compounds that are biosynthesized by plants, insects, fungi, and bacteria. Terpenes are classified based on the number of isoprene units, with the basic structure being isoprene (C5). They are categorized into hemiterpenes (C5), monoterpenes (C10), sesquiterpenes (C15), diterpenes (C20), triterpenes (C30), and sesterterpenes (C40), depending on the number of isoprene units present in the molecule. These terpenoids originate from isopentenyl diphosphate (IPP) and its isomer, dimethylallyl diphosphate (DMAPP), which are synthesized via the mevalonate pathway[45]. Additionally, some plants and bacteria have been reported to possess alternative biosynthetic pathways leading to IPP and DMAPP[46, 47]. Currently, it is known that the mevalonate pathway primarily exists in eukaryotes and archaea, while the non-mevalonate pathway is predominantly found in bacteria.

As previously mentioned, in filamentous fungi, which are eukaryotes, terpenoids are biosynthesized through the mevalonate pathway. In this pathway, terpenoids are synthesized starting from acetyl-CoA, leading to the production of mevalonic acid, which is subsequently phosphorylated to yield isopentenyl diphosphate (IPP) and its isomer dimethylallyl diphosphate (DMAPP)[45]. IPP and DMAPP are then linked head-to-tail by dimethylallyltransferase to form geranyl diphosphate (GPP), which serves as the precursor for monoterpenes. GPP is further combined with DMAPP by farnesyl diphosphate synthase to synthesize farnesyl diphosphate (FPP), the precursor for sesquiterpene biosynthesis. Moreover, two molecules of FPP are joined by squalene synthase to produce squalene, which is subsequently cyclized to yield sterol-type triterpenes, including ergosterol[48]. Additionally, FPP can be converted into geranylgeranyl diphosphate (GGPP) through the action of geranylgeranyl diphosphate synthase, which serves as the precursor for diterpenes[49]. The biosynthetic pathways of these terpenoids are illustrated in Figure 3.2[50].

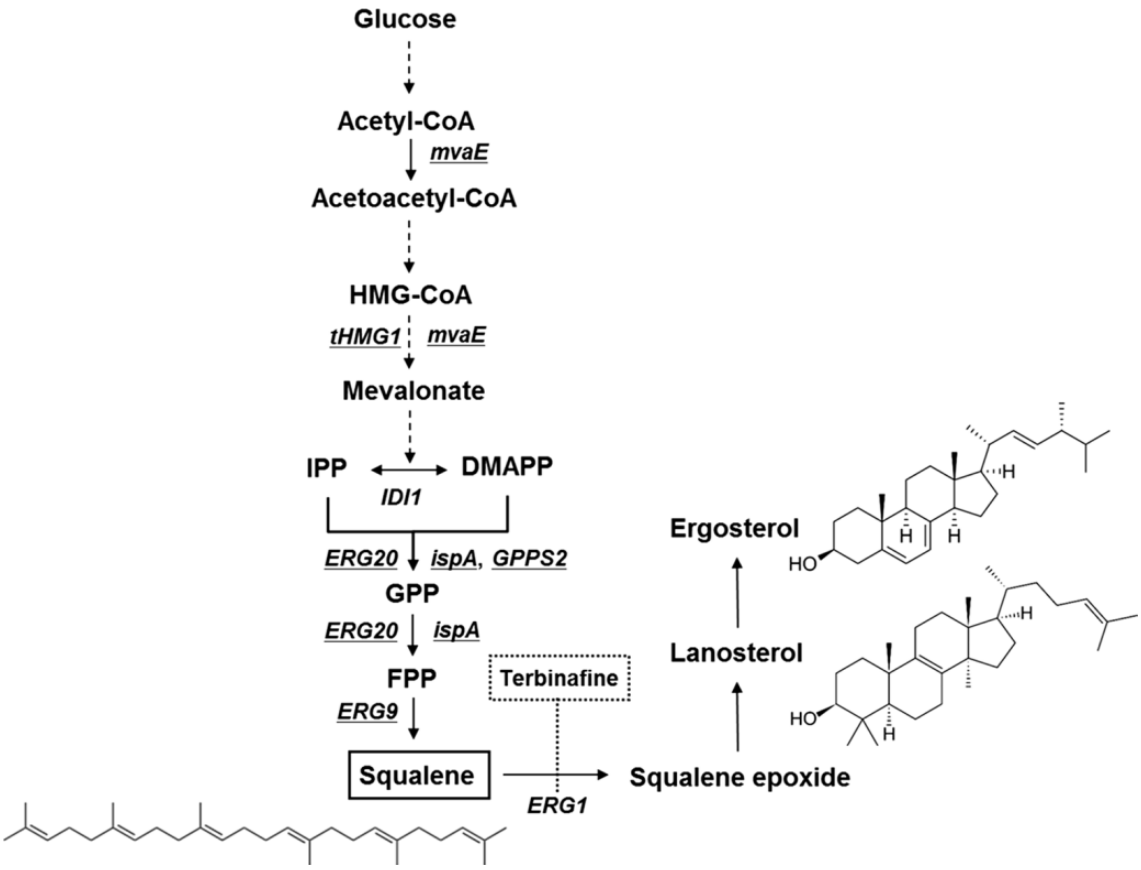

Figure 3.2 Biosynthetic pathways of terpenoids, with solid lines indicating single-step reactions and dashed lines representing multi-step reactions[50].

3.1.3. Butenafine hydrochloride

Squalene is oxidized to squalene epoxide by the enzyme squalene epoxidase and subsequently metabolized into sterols and other compounds. Given that sterols are essential molecules for living organisms[51], squalene is typically metabolized rapidly and does not accumulate within microbial cells. Squalene epoxidase inhibitors are specific inhibitors of the aforementioned enzyme, leading to the inhibition of sterol biosynthesis, which can result in lethality as an antifungal agent. Additionally, it has been reported that these inhibitors impede the metabolism of squalene, causing its accumulation within microbial cells[52].

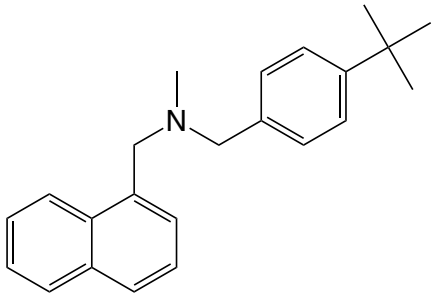

Figure 3.3 Structure of butenafine

3.2. Results and discussion

3.2.1. Prescreening results of the suitable filamentous fungus and concentration of butenafine to produce squalene

Squalene is used as a crucial precursor to synthesize sterols, such as ergosterol which is an essential component of cell membranes and its accumulation without any interfere is nearly undetectable under normal growth in fungi cells[50]. It is well known that the biosynthesized squalene is initially oxidated by squalene epoxidase (SQE) in the sterol metabolic pathway, giving the hypothesis that squalene accumulation will be increased through partial inhibiting the activity of SQE[53]. Butenafine hydrochloride, a benzylamine antifungal derivative, has been widely reported to block the biosynthesis of ergosterol by restraining the SQE activity, resulting in the improvement of squalene accumulation[54]. But complete inhibition of SQE will promote cell death. It is important to set up the butenafine concentration for cell growth and squalene accumulation.

We chose 13 species of filamentous fungus belonging to 4 genera to conduct prescreening experiments to find out the suitable one as our main species in the further research about squalene production. The fresh weight of the mycelia (MFW) indicates that the growth of the majority of fungi used in this study was significantly inhibited upon the addition of butenafine, and this inhibition intensified with increasing concentrations of butenafine hydrochloride. However, the sensitivity of different fungal genera to butenafine concentrations varied. For instance, 1 μM of butenafine reduced the growth of mycelium of *Penicillium spinulosum* NBRC5793 by 82% (Table 3.3), while a concentration of 1200 μM only resulted in a 33% reduction in the mycelia of *Rhizopus oryzae* NBRC5418 (Table 3.1). More importantly, the production of squalene exhibited considerable differences among various fungal genera. The optimal

concentration of butenafine ranged from 10 to 600 μM, with significant variations in squalene production. For example, *R. oryzae* NBRC9364 achieved a maximum squalene production of 0.79 mg/L at 100 μM butenafine, whereas the production without the inhibitor was only 0.47 mg/L. In contrast, for *T. virens* ps1-7, the squalene accumulation under the presence of 200 μM butenafine reached 336 mg/L, compared to a yield of 0.36 mg/L without the inhibitor. Furthermore, in all strains, there was almost no accumulation of squalene in the culture filtrate; the majority was retained within the fungal cells. This is believed to be due to squalene being a primary metabolite essential for growth, which is directly utilized for the synthesis of sterols for cell membrane formation in the absence of any inhibitors.

Table 3.1 The squalene accumulation and fresh weight of mycelia for different species of *Rhizopus* with different butenafine concentration for cultivated in 200 mL PDB medium (pH no adjustment, 5.0) at 25 ℃, 100 rpm for 7 days.

Species	Concentration of butenafine (μM)	MFW (g/L)	Squalene (mg/L)	
			Mycelia	Culture filter
sp. SH35	0	6.67	1.24	ND
	200	6.14	18.93	0.89
	400	5.92	23.71	0.55
	600	5.86	29.64	0.26
sp. SH36	0	7.84	0.32	ND
	200	8.02	21.07	0.89
	400	6.77	36.40	0.55
	600	5.89	6.67	0.26
oryzae I-1	0	11.41±0.15	2.85±0.74	0.05±0.03
	200	10.13±1.00	67.23±7.60	3.12±0.96
	400	8.86±0.41	70.13±5.06	13.67±2.19
	600	4.92±1.44	70.53±26.18	2.02±0.34
	800	3.43±0.22	40.83±7.26	0.81±0.20
oryzae NBRC9364	0	2.29±0.19	0.47±0.11	ND
	100	3.66±0.82	0.79±0.21	0.11

	200	2.41±0.27	0.49±0.08	ND
	300	2.64±0.30	0.37±0.08	ND
	400	2.05±0.08	0.66±0.03	ND
oryzae NBRC5418	0	7.86	0.92	ND
	400	7.32	6.61	ND
	800	6.31	1.15	ND
	1200	5.29	0.15	ND

Table 3.2 The squalene accumulation and fresh weight of mycelia for different species of *Mortierella isaberina* with different butenafine concentration for cultivated in 200 mL PDB medium (pH no adjustment, 5.0) at 25 ℃, 100 rpm for 7 days.

Species	Concentration of butenafine (μM)	MFW (g/L)	Squalene (mg/L)	
			Mycelia	Culture filter
NBRC7824	0	10.79	0.14	ND
	100	9.785	ND	0.06
	200	8.12	178.42	0.15
	300	9.28	132.24	0.04
	400	1.61	26.07	0.34
	600	0.82	3.40	0.04

Table 3.3 The squalene accumulation and fresh weight of mycelia for different species of *Penicillium spinulosum* with different butenafine concentration for cultivated in 200 mL PDB medium (pH no adjustment, 5.0) at 25 ℃, 100 rpm for 7 days.

Species	Concentration of butenafine (μM)	MFW (g/L)	Squalene (mg/L)	
			Mycelia	Culture filter
NBRC5793	0	15.50	0.09	ND
	1	2.85	1.39	ND
	10	2.43	12.26	ND
	20	1.56	8.16	ND
	30	1.55	8.10	ND

	50	0.43	2.04	ND
	100	0.28	1.43	ND
	150	0.41	2.49	ND
	200	0.37	1.78	ND
	400	0.15	0.89	ND
	600	0.16	1.18	ND
	800	0.19	1.27	ND

Table 3.4 The squalene accumulation and fresh weight of mycelia for different species of *Trichoderma* with different butenafine concentration for cultivated in 200 mL PDB medium (pH no adjustment, 5.0) at 25 ℃, 100 rpm for 7 days.

Species	Concentration of butenafine (μM)	MFW (g/L)	Squalene (mg/L)	
			Mycelia	Culture filter
virens PS1-7	0	10.72±1.00	0.36±0.04	ND
	100	7.09±0.88	279.48±12.29	0.22±0.07
	200	5.29±0.19	336.35±53.02	0.33±0.13
	300	2.91±1.41	113.64±84.57	0.05±0.04
	400	1.08±0.20	3.00±0.61	ND
reesei NBRC31326	200	0.95	22.17	-
virens NBRC8349	200	3.12	215.24	-
virens NBRC9166	200	3.85	168.41	-
virens NBRC30547	200	4.75	326.85	-
virens NBRC31959	200	3.60	260.81	-

The results above indicate that *Trichoderma* strains possess a higher capacity for squalene production compared to other strains. It has been reported that *Trichoderma* species produce a wealth of secondary metabolites, including numerous terpenoids and it is believed that *Trichoderma* initially engages in the mevalonate pathway for terpenoid biosynthesis and exhibit a robust metabolic flux for the production of various terpenoid compounds, suggesting a high potential for squalene production.

Mortierella is a type of oilseed microorganism with a lipid content exceeding 20% of its dry weight, which also includes various microalgae that produce substantial amounts of squalene. This high lipid storage capacity within their cells is considered one of the reasons why the *Mortierella isabelline* NBRC7824 produces significant quantities of squalene. Furthermore, this finding suggests that other oilseed microorganisms, including those in the *Mortierella* genus, may possess a high potential for squalene production.

Rhizopus exhibits a wide range of squalene production capabilities depending on the species. Our laboratory isolated strain I-1, which, upon TLC analysis, was identified as a high squalene-producing strain; however, the maximum yield of squalene remained around 70 mg/L. In contrast, no significant decrease in fresh weight of mycelia or increase in squalene was observed in strain NBRC9364 under approximately 800 μM butenafine hydrochloride conditions, indicating that NBRC9364 may be less sensitive to butenafine. Our laboratory analyzed the SQE gene of strains NBRC9364 and I-1, finding no differences in the sequence from 370 bp to the stop codon, suggesting that this region of the gene has not been characterized. Variations in sensitivity may lead to differences in production capabilities.

The optimal concentration of butenafine hydrochloride for the production of squalene by the *Penicillium spinulosum* NBRC5793 is relatively low, at 10 μM, and its sensitivity to butenafine hydrochloride surpasses that of other strains. From a cost-reduction perspective, a lower optimal concentration of butenafine hydrochloride is preferable; however, the squalene production remains around 12 mg/L, indicating a limited potential for this strain as an alternative source of squalene.

Among the 13 species examined, the *T. virens* PS1-7 exhibited a squalene production of approximately 340 mg/L, demonstrating its high squalene production capacity. Therefore, in the subsequent chapter, we will investigate the optimal cultivation conditions for squalene production using the PS1-7 strain.

3.2.2. Effect of initial pH of culture liquid for squalene accumulation

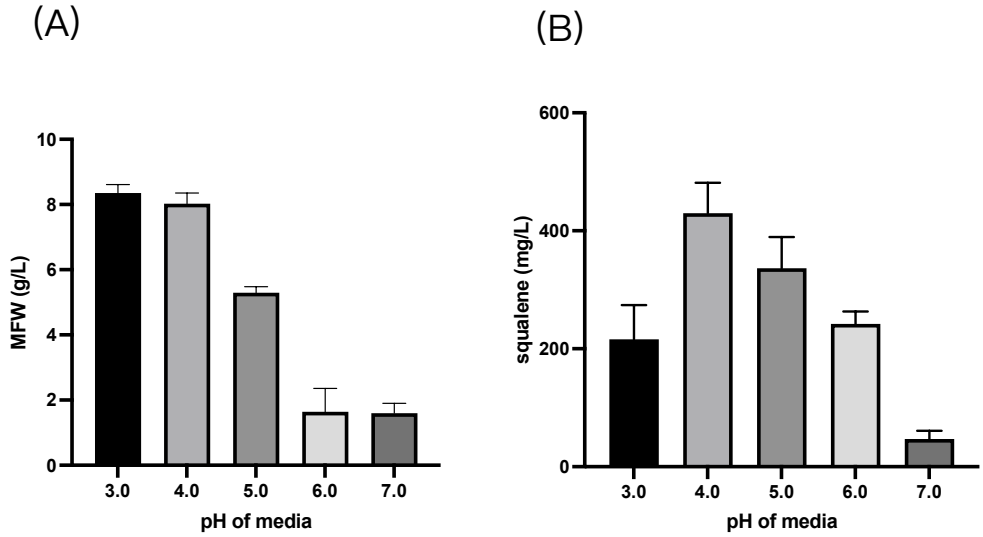

Figure 3.4 The squalene accumulation and cell growth status for *T. virens* PS1-7 of different medium pH (MFW (A) and squalene accumulation in mycelia (B) of different medium pH from 3.0 ~ 7.0) cultivated in PDB medium with 200 μM butenafine hydrochloride at 25 ℃, 100 rpm for 7 days. Data are means ± S.D. (n=3).

Table 3.5 Squalene accumulation of *T. virens* PS1-7 from culture filtrate and mycelia in different pH

pH	MFW (g/L)	Squalene (mg/L)	
		Culture filtrate	Mycelia
3.0	8.35±0.26	0.03 ± 0.03	215.87 ± 58.09
4.0	8.03±0.33	0.09 ± 0.11	429.93 ± 51.60
5.0	5.29±0.19	0.33 ± 0.13	336.35 ± 53.02
6.0	1.64 ± 0.72	0.06 ± 0.04	242.17 ± 21.04
7.0	1.60 ± 0.30	0.13 ± 0.03	47.04 ± 13.82

The pH of the medium has a strong influence on cell membrane function, cell metabolism, alimentation and biosynthesis activity[55]. The pH of liquid media is much more adjustable compared to solid media, *T. virens* were cultured in liquid media of different pH ranged from 3.0 to 7.0. Figure 3.4 showed that the MFW of *T. virens* PS1-7 under pH 3.0 is highest among all the conditions and the MFW decreased at higher pH. The squalene accumulation in cell body were maximized at pH 4.0. Meanwhile the squalene accumulation from culture liquid, which accounts for 10% in the mycelia, also

showed the same pH dependent manner (Table 3.5). Results showed that the accumulation of squalene was highest at pH 4.0 with the value achieving 429.93 ± 51.60 mg/L. A decreasing trend of squalene was also observed at pH 3.0. It can be confirmed that the optimum initial pH of the medium for squalene production of the PS1-7 strain is 4.0.

3.2.3. Effect of culture temperature for squalene accumulation

It's been well reported that the temperature of living surroundings has nonnegligible effects on microbial metabolism[56, 57]. Squalene production of *S. cerevisiae* Y2805 was affected by the culture temperature[50]. *T. virens* PS1-7 was pre-investigated on potato broth agar medium (PDA) from 15 to 40 °C.

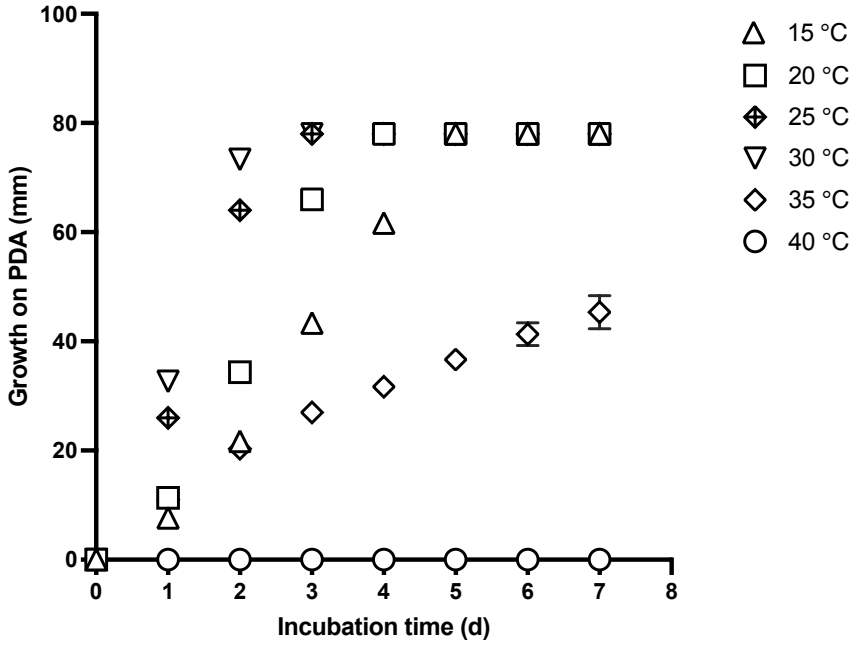

Figure 3.5 Time growth status of PS1-7 on PDA plate until 7 days at different temperature from 15 ~ 40 °C. Data are means ± S.D. (n=3).

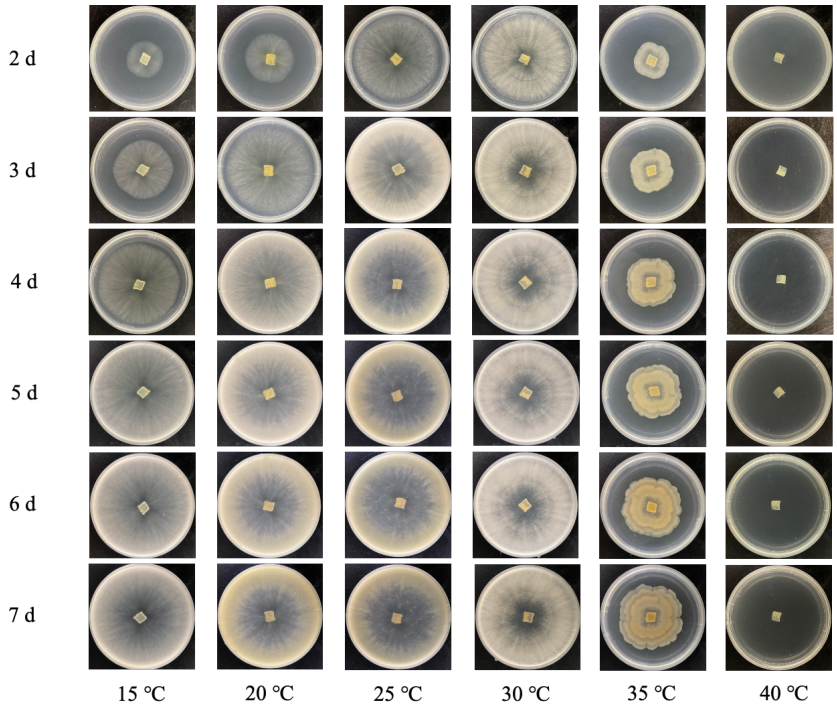

Figure 3.6 Growth status of PS1-7 on PDA plate under different temperature from 2 ~ 7 days.

As shown in the Figure 3.5 and 3.6, the optimum culture temperature for PS1-7 strain on PDA plate was 25 and 30 °C. The growth was clearly inhibited over 35 °C, and was completely suppressed while no visible growth inhibition was observed less than 15 °C, but the growth rate decreased on PDA plate. Based on these results, the range of the temperature in liquid culture was subjected at 20, 25 and 30 °C.

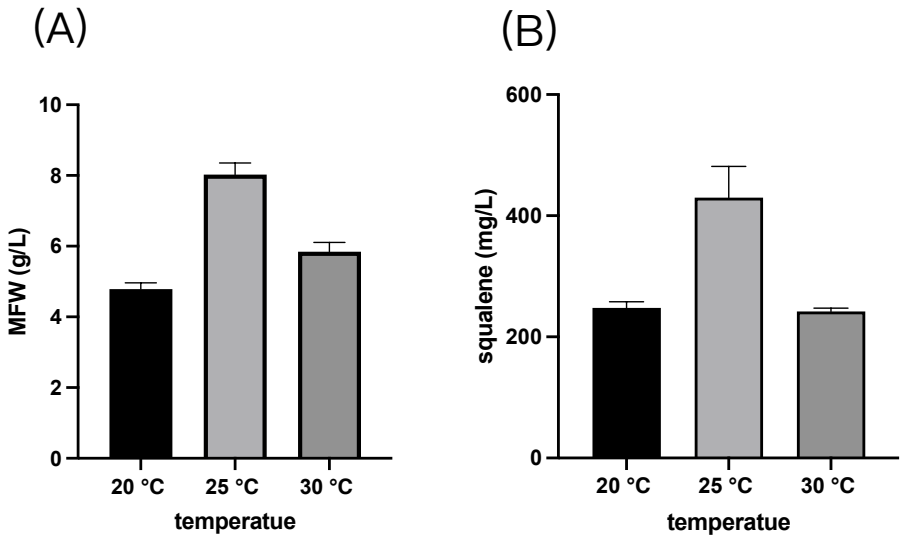

Figure 3.7 The squalene accumulation and cell growth status of different temperature from 20 ~ 30 °C (MFW (A) and squalene accumulation in mycelia (B) of different medium temperature) cultivated in 200 mL PDB medium (pH adjusted to 4.0) with 200 μM butenafine hydrochloride at 100 rpm for 7 days. Data are means ± S.D. (n=3).

Figure 3.7(A) showed that the optimum culturing temperature for the MFW of PS1-7 is 25 °C, and the squalene accumulation suggested same tendency as the MFW between these temperatures (Figure 3.7(B)). All the results from solid PDA plate and liquid culture indicated that the optimal culture temperature for squalene production for PS1-7 was 25 °C.

3.2.4. Effect of different carbon source for squalene accumulation

Glucose is the main carbon source in glycolysis, and fructose is metabolized by multiple enzymes and incorporated into glycolysis. Disaccharides such as sucrose and starch are metabolized in the same manner as monosaccharides such as glucose after being decomposed. Glycerol is metabolized to dihydroxyacetone phosphate (DHAP) and incorporated into glycolysis after being phosphorylated. Whether these carbon sources can be used depends greatly on the physiological characteristics of the strain. Squalene productions were verified based on utilization of carbon sources for fungus which accumulated squalene without SQE inhibitor in the cell body[55, 56]. However, the potato dextrose broth (PDB) normally used is commercially available and it has already contained glucose. The potato infusion powder (PI) does not contain exogeneous glucose and can be used as a supplementary material to the media with different kinds of saccharides as carbon sources at 20 g/L.

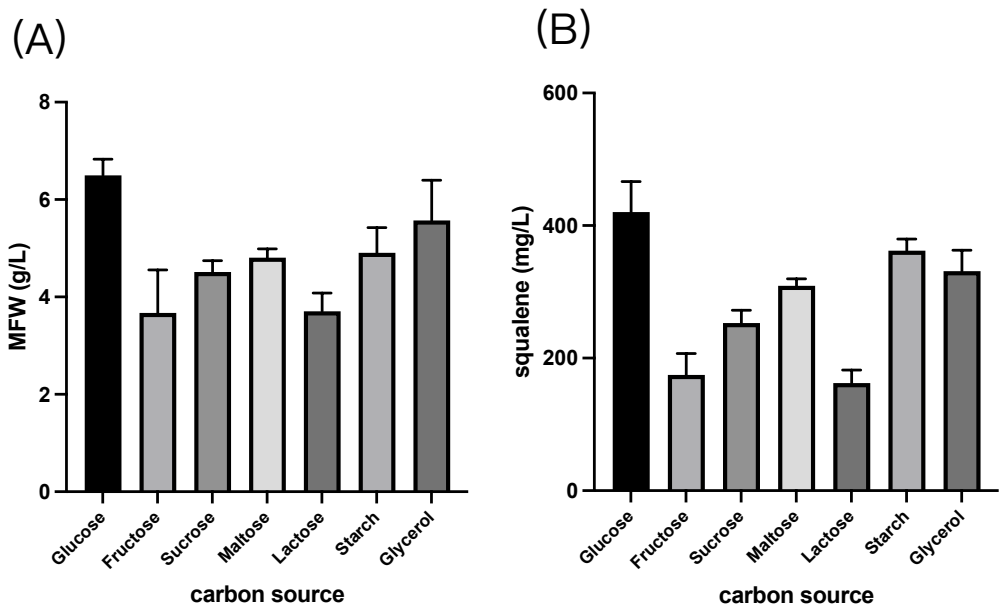

Figure 3.8 The squalene accumulation and cell growth status for PS1-7 from different carbon sources (20 g/L) with PI (4 g/L) cultivated in 200 mL medium with 200 μM butenafine hydrochloride at 25 ℃, 100 rpm for 7 days (MFW (A) and squalene accumulation in mycelia (B) from different carbon sources). Data are means ± S.D. (n=3).

As shown in the Figure 3.8, PS1-7 produced some degree of squalene with glucose at 420.53 ± 45.70 mg/L which was consistent with the that of PDB media. The results indicated that PS1-7 utilized carbon source for growth and biosynthesis of metabolites as order: Glucose > Starch ≒ Glycerol ≒ Maltose > Sucrose > Fructose > Lactose. The orders are slightly different from squalene accumulation in yeast-like fungus at normal conditions [58]. Therefore, the optimum carbon source for PS1-7 producing squalene is glucose.

3.2.5. Effect of exogeneous precursors on squalene accumulation

Squalene is a kind of essential metabolite in fungi and the biosynthetic pathway is quite complicated and affected by many substances. There are lots of precursors and crucial enzymes participating in the biosynthesis of squalene, and several kinds of intermedia (thiamine, pyruvic acid, acetate, mevalolactone, ergosterol and lanosterol) were selected to put into the culture medium to check the effects on producing squalene of

PS1-7. Figure 3.9 suggested the biosynthesis pathway of squalene and effective positions of the precursors used in this study.

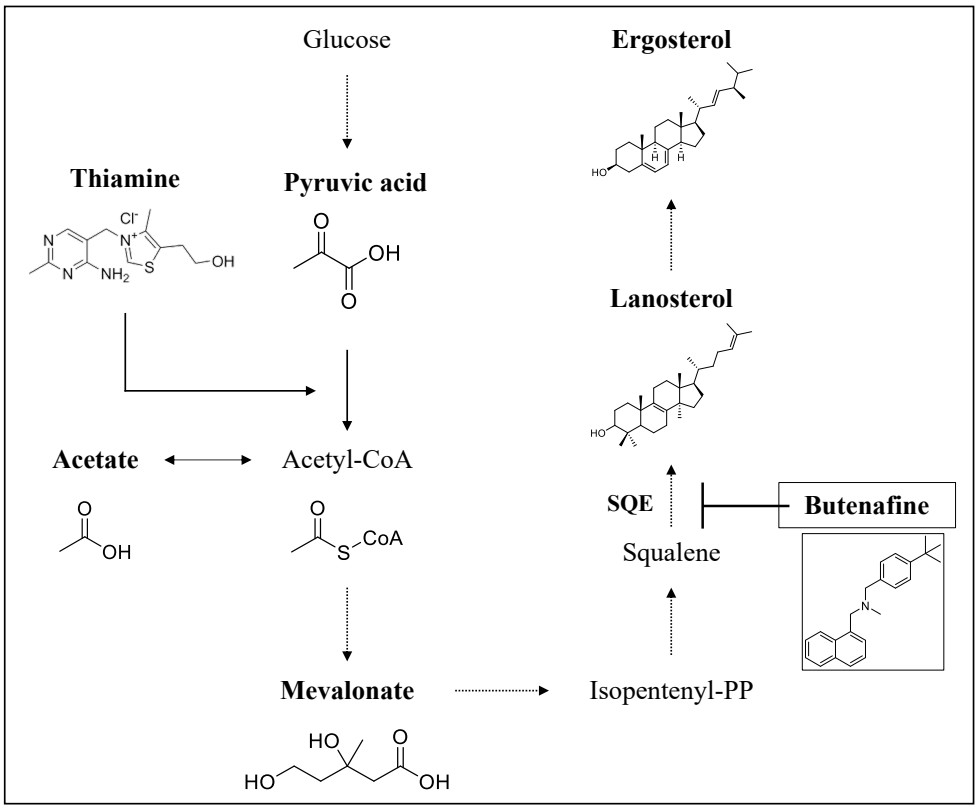

Figure 3.9 The precursors used in this study and biosynthesis pathway of ergosterol. The solid line indicates a one-step reaction, and the dashed line indicates a multiple-step reaction; PP: an abbreviation for diphosphate. Thiamine-HCl, pyruvic acid, mevalonolactone, ergosterol and lanosterol were added into 200 mL PIG medium at pH 4.0 with 200 μM butenafine individually at 25 ℃, 100 rpm.

Table 3.6 Squalene accumulation of PS1-7 in the medium with different kinds of precursors present

Precursors	Concentration of precursors	MFW (g/L)	Squalene in mycelia(mg/L)
-	-	6.50 ± 0.34	420.53 ± 45.70
Thiamine-HCl	100 μM	6.78	247.07
	500 μM	5.90	250.11
	1000 μM	5.45	249.58
NADPH	1 mM	3.40	149.86

Pyruvic acid	10 g/L	0.67 ± 0.14	185.16 ± 18.46
Mevalolactone	10 g/L	8.00	322.28
Ergosterol	10 g/L	7.84	276.05
	100 g/L	7.15	227.05
Lanosterol	30 g/L	7.00	358.65
	60 g/L	6.30	384.39
	90 g/L	9.70	319.68
	120 g/L	7.75	270.56

Among all the exogeneous precursors, none of them increased the production of squalene obviously and some additives even had adverse effects such as growth inhibition (Table 3.6). The results showed that even though certain intermediates are present in large quantities in tightly controlled metabolic systems in the body of organisms, the metabolism of these products requires a considerable number of coenzymes and metabolism-related factors, and if these substances are not sufficient, the additional products cannot be used effectively, such as thiamine hydrochloride which acts as an essential part of coenzyme. Organic acids are known to have antimicrobial activity. Matsuda et al. found an MIC of 0.5% v/v for acetic acid at pH 4.0 and > 5.0 % v/v for pyruvate acid in a test for antimicrobial activity of organic acids using common fungi[59]. Since pyruvic acid is a normal and important metabolic intermediate of many microorganisms, it should have poor antibacterial activity against cells, however in this experiment, a significant growth inhibitory effect was confirmed in the 10 g/L (0.79% v/v) pyruvic acid-added group. Different from acetic acid which inhibited the growth of PS1-7, 10 mM mevalolactone neither showed such effects on restraining the growth status of the fungi nor enhance the production of squalene. The results suggested that even if mevalonate is present in a large amount, it may not be effectively utilized due to insufficient coenzymes such as NADPH required for metabolism as aforementioned description. Same with other exogeneous substances, no positive results on improving production of squalene were observed with lanosterol and ergosterol into the media. All the symptoms suggested that the metabolism in fungi cells is rather complicated and self-adjusted which will not easily be upgraded to produce squalene by adding the intermediates into the culturing liquid.

3.2.6. Effects of supplement of glucose into the media on producing squalene

Since squalene accumulation is associated with cell growth and might be enhanced with the increase of cell weight, long term culturing with the supplement of glucose were investigated until 28 days. 20 g/L glucose was supplied into the flask at 7th, 14th and 21st day of culturing respectively.

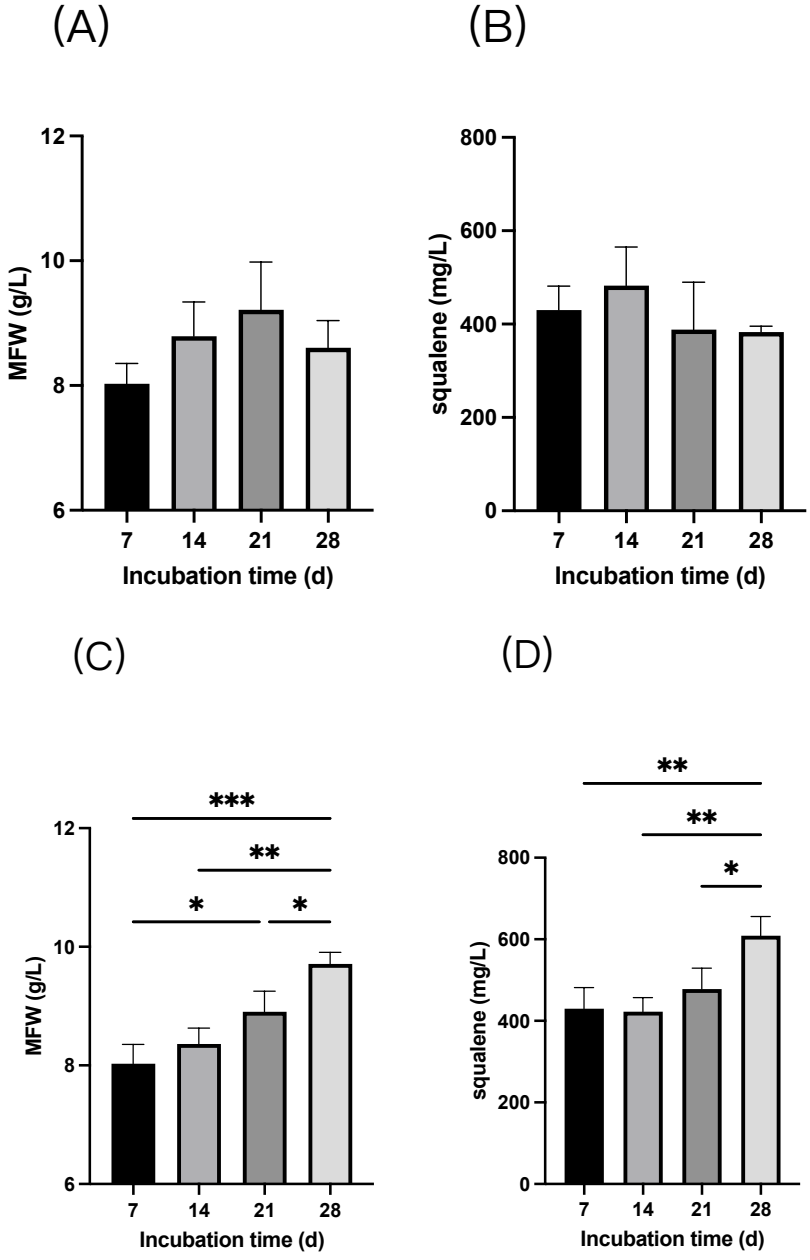

Figure 3.10 The squalene accumulation and cell growth status for PS1-7 of control group with/without additional glucose with 200 μM butenafine hydrochloride at 25 ℃, 100 rpm for 7 days (MFW (A) and squalene accumulation in mycelia (B) without additional glucose (inicial glucose: 20 g/L); MFW (C) and squalene accumulation in

mycelia (D) with additional glucose (20 g/L every 7 days)). Data are means ± S.D. (n=3); *, **, ***mean values are significantly different between these two groups at P < 0.05, 0.01, 0.001 individually.

MFW ranged from 8 to 9 g/L without adding glucose (Figure 3.10(A)), and there was no significant difference on squalene accumulation with the prolongation of cultivation time and the squalene content reached maximum at 482.37 ± 82.67 mg/L after 14 days of culture (Figure 3.10(B)). In addition, in the group without adding glucose, initial glucose was completely consumed in 14 days culture on TLC analysis (Figure 3.11). In the glucose-added group treated at each 7 days, MFW increased in a day dependent manner (Figure 3.10(C)). On the other hand, in the glucose-added group, squalene accumulation increased in a time dependent manner, reaching 608.94 ± 46.87 mg/L at 28 days of culture (Figure 3.10(D)).

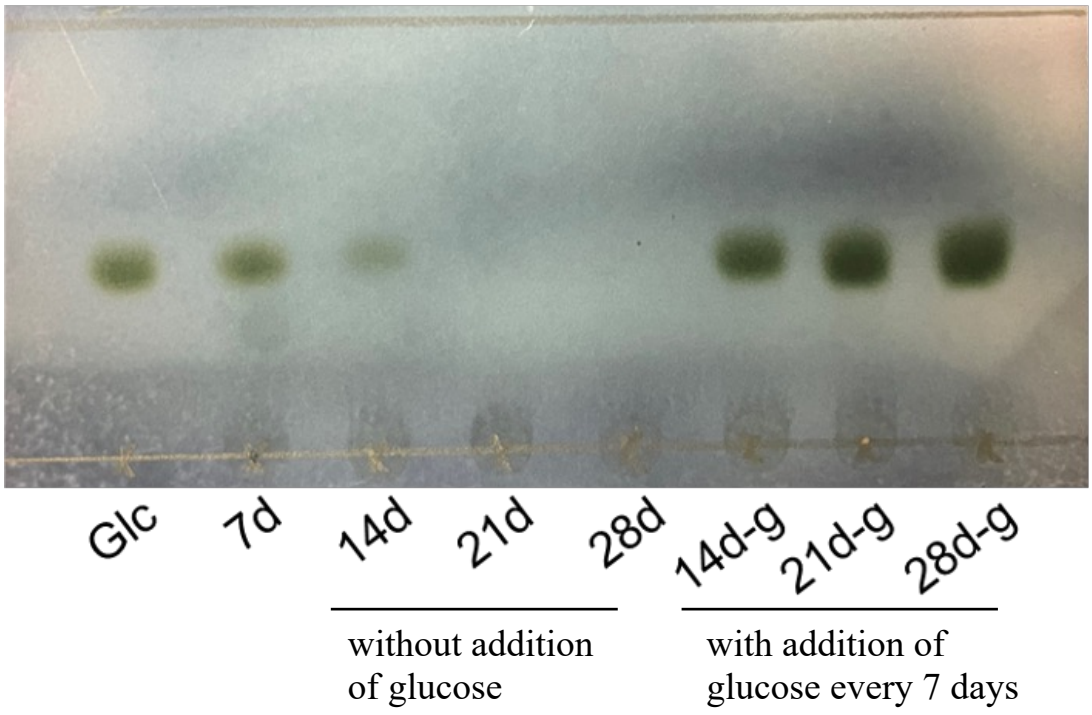

Figure 3.11 Analysis results the amount of glucose in the medium (with/without glucose addition) at 200 μM butenafine hydrochloride; Glc: Glucose standard; Developing solvent: 1-butanol : 2-propanol : AcOH : H_2O = 7 : 5 : 2 : 4, Detection: Anisaldehyde-H_2SO_4.

It is known from several previously published reports that biosynthesized squalene might be metabolized into other compounds in the later stage of culture causing the decrease of squalene[55, 60]. In this study, the squalene accumulation with butenafine also showed a downward trend after 14 days when the carbon source was insufficient, because the initial glucose in the medium was completely consumed after 14 days of cultivation, and squalene accumulation became static state until 28 days. On the other hand, the addition of glucose every 7 days improved squalene accumulation because the growth phase was promoted by glucose addition, and continuous increasement of squalene accumulation was observed until 28 days.

3.2.7. Biosynthesis of ^{13}C labeled squalene using [U-$^{13}C_6$]-glucose in culture media replacing normal glucose

In filamentous fungi, biosynthesized squalene is normally utilized to downstream metabolism immediately and is not stored in the cell body. And the possible precursors for biosynthesis of squalene did not affect squalene accumulation (Figure 3.9). These results promoted us that enrichment of stable isotope labeled squalene can be accumulated with inoculation of [U-$^{13}C_6$]-glucose in cultivation of PS1-7 with butenafine hydrochloride.

PS1-7 was cultured with 1g [U-$^{13}C_6$]-glucose and 0.2 g PI powder in 50 mL water at pH4.0 with exogeneous 200 μM butenafine. The cell growth and squalene accumulation are almost same with 200 mL scale. After extraction from cell body, 26.2 mg biosynthesized squalene was isolated. The isolated squalene was subjected to NMR analysis.

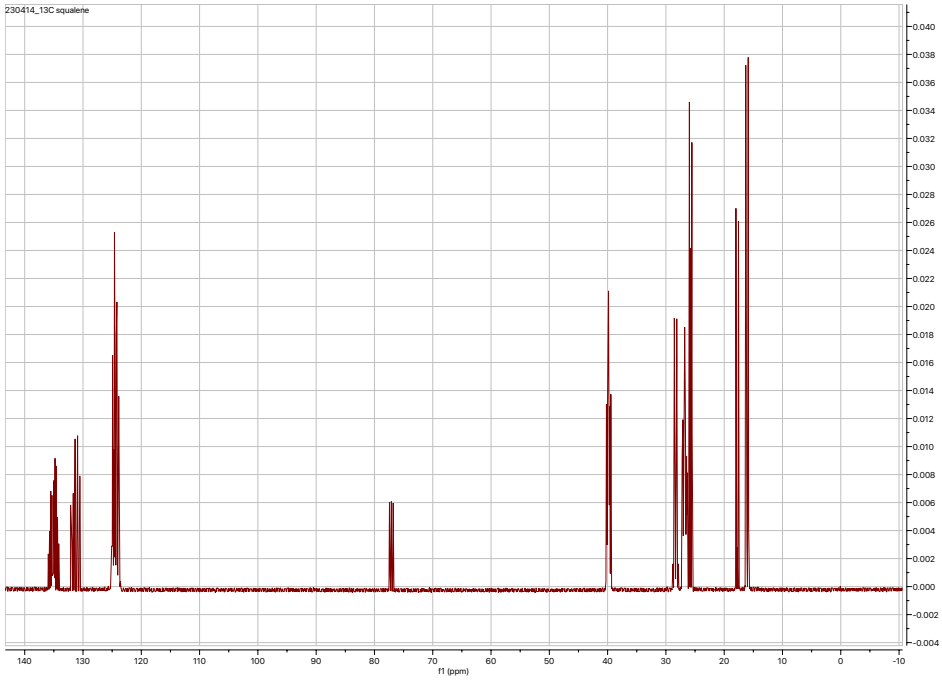

Figure 3.12 ^{13}C-NMR spectrum of biosynthesized ^{13}C enriched squalene in $CDCl_3$.

Table 3.7 ^{13}C-^{13}C coupling constants of ^{13}C-squalene

δ (ppm)	J (Hz)	Carbon-position
16.10	d, 42.14	6, 10, 15, 19-Me
17.77	d, 42.14	2, 23-Me
25.77	d, 42.87	1, 24-Me
28.35	d, 41.90	12, 13-CH_2
26.78	ddd, 12.28, 32.39, 43.83	4, 8, 17, 21-CH_2
39.83	m	5, 9, 16, 20-CH_2
124.43	m	3, 7, 11, 14, 18, 22-CH
135.08	m	6, 10, 15, 19-C
131.31	m	2, 23-C

(A) ^{13}C-^{13}C COSY (32 scans)

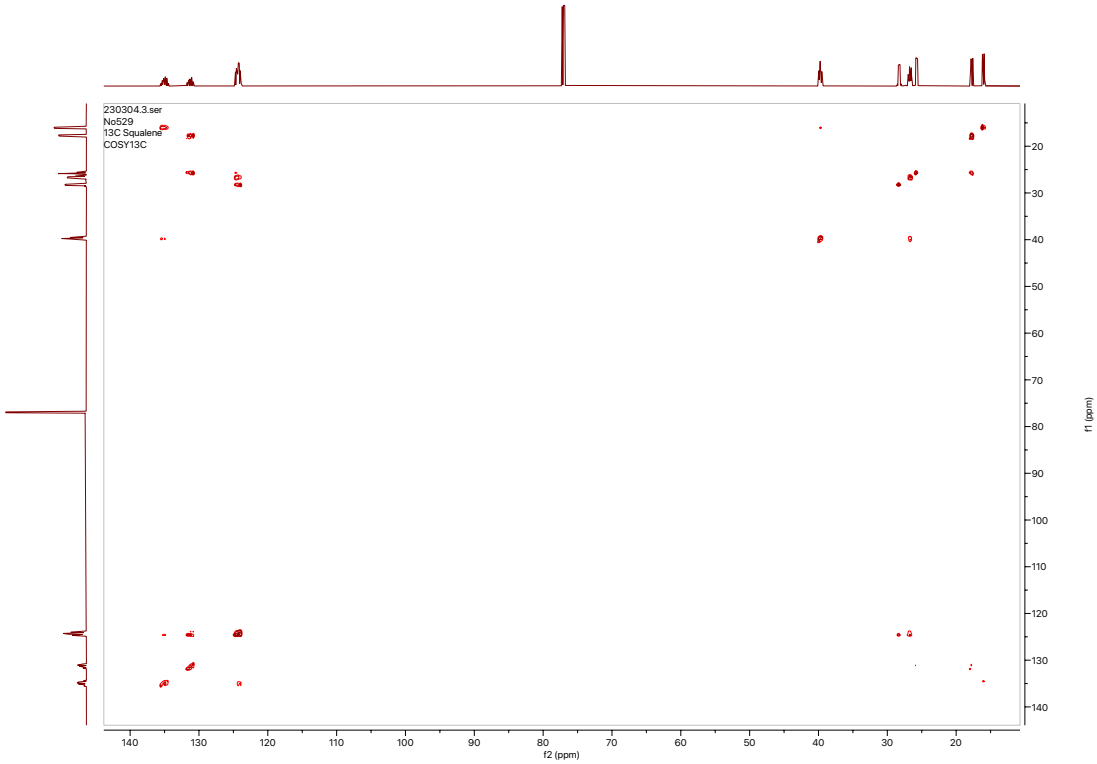

(B) INADEQUATE (128 scans)

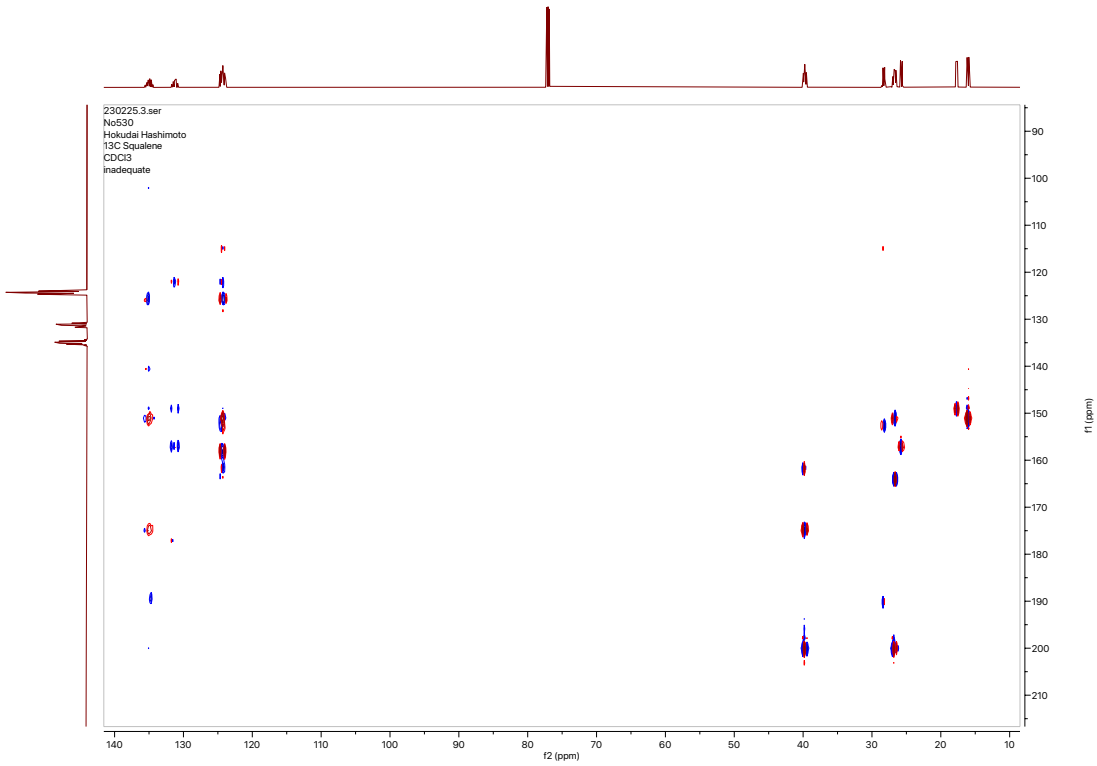

Figure 3.13 ^{13}C-^{13}C COSY (A) and INADEQUATE (B) spectrum of ^{13}C labeled squalene. INADEQUATE (B): part of 2-bond correlations from methyl moiety were sometimes observed due to high ^{13}C incorporations.

^{13}C-NMR was measured by shorter scan (256 times, Figure 3.12) and ^{13}C-^{13}C coupling of isolated squalene were clearly observed at all carbon (Table 3.7). The high incorporation of ^{13}C atom afforded ^{13}C-^{13}C COSY (Figure 3.13(A)) and INADEQUATE (Figure 3.13(B)) in short scanning measurement.

(A)

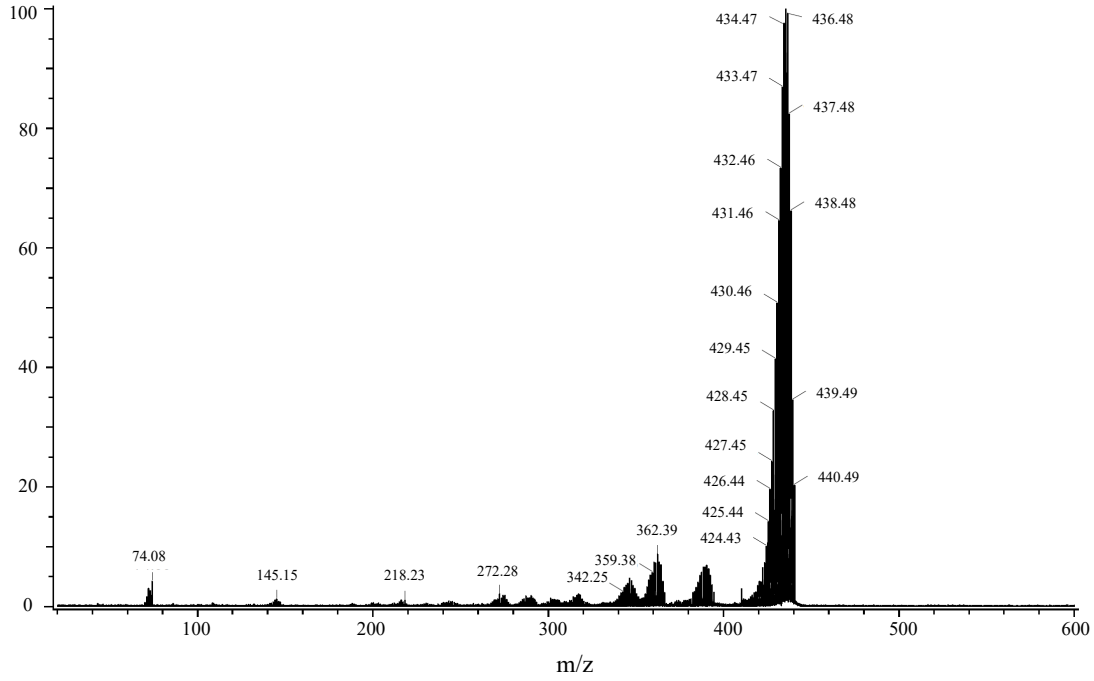

(B)

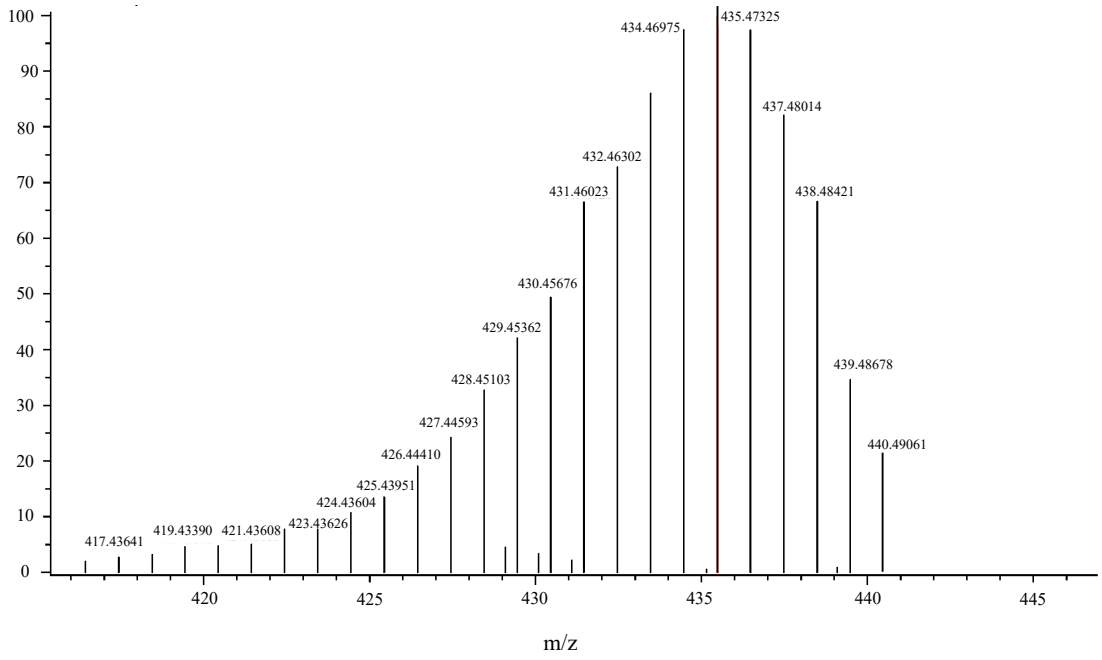

Figure 3.14 FD-MS spectrum (A: full view; B: m/z 415 ~ 445) of ^{13}C labeled squalene

It is shown in the FD-MS analysis of ^{13}C-enriched squalene with maximum 30 ^{13}C incorporated (m/z 440.49061) in the structure, the squalene with 25 ^{13}C was detected as the main species (m/z 435.47325)**.** The sample was also subjected to EI-MS (Figure 3.14).

(A) EI-MS spectrum of ^{13}C labeled squalene

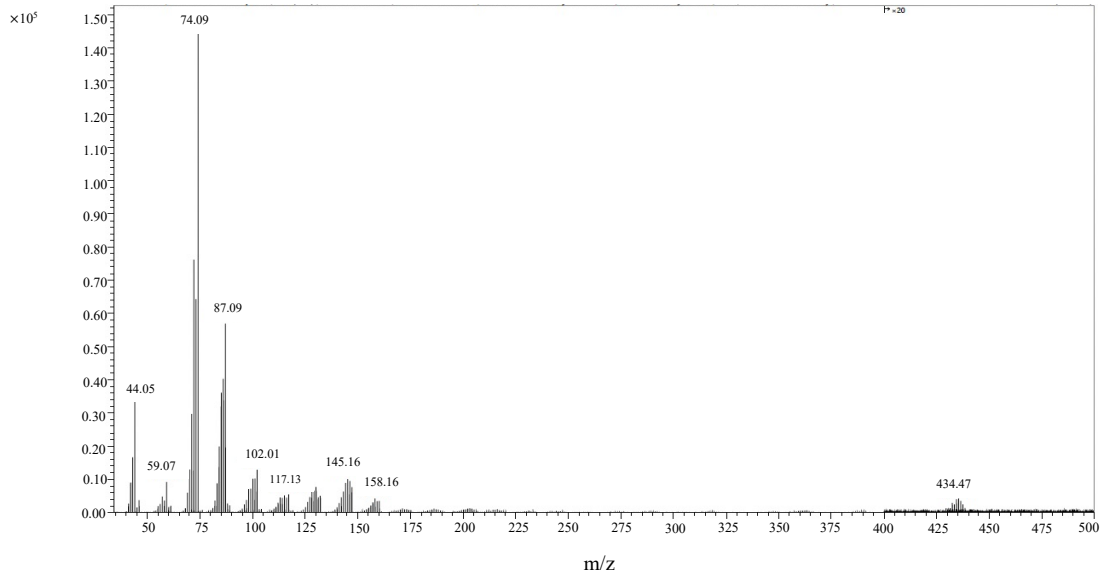

(B) EI-MS (m/z 425 ~ 455) spectrum of ^{13}C labeled squalene

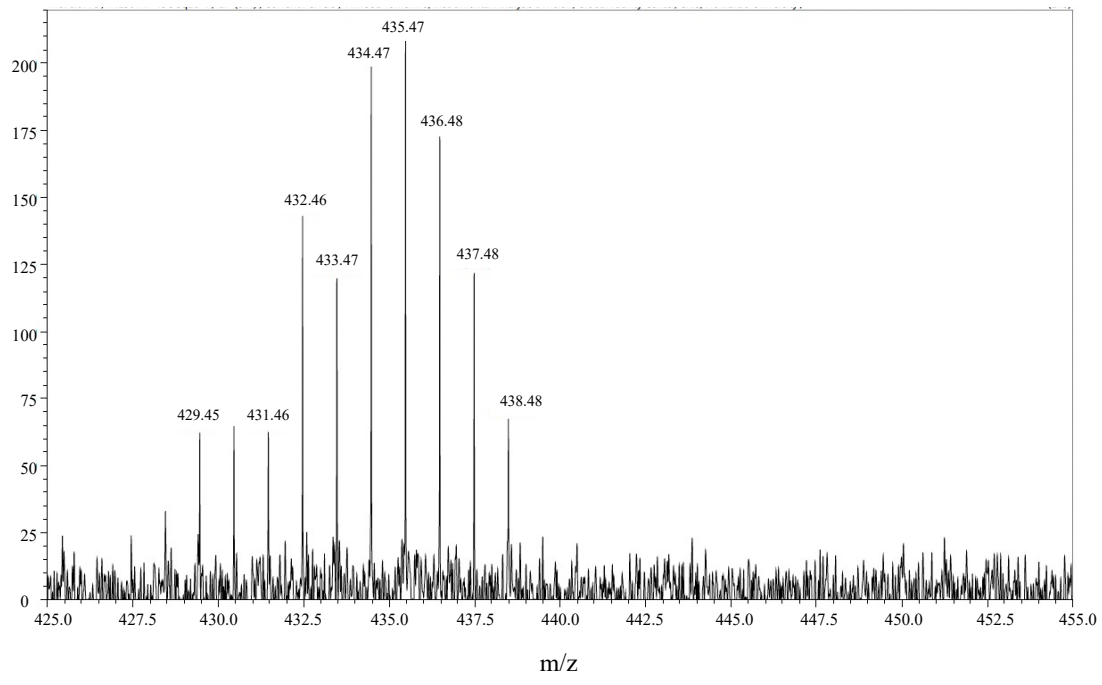

(C) EI-MS spectrum of unlabeled squalene

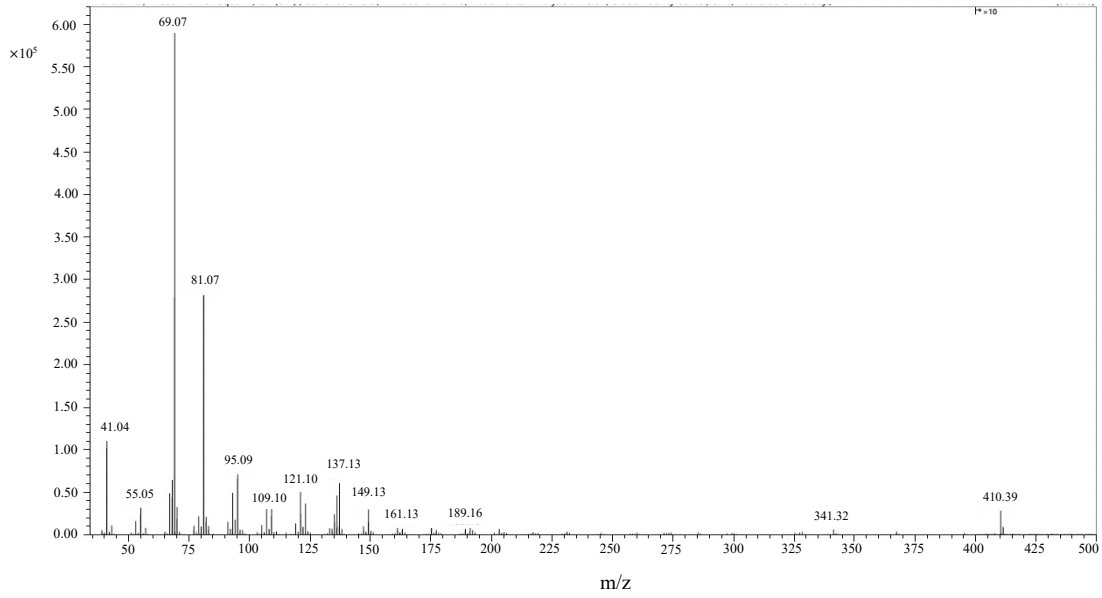

(D) FD-MS spectrum of unlabeled squalene

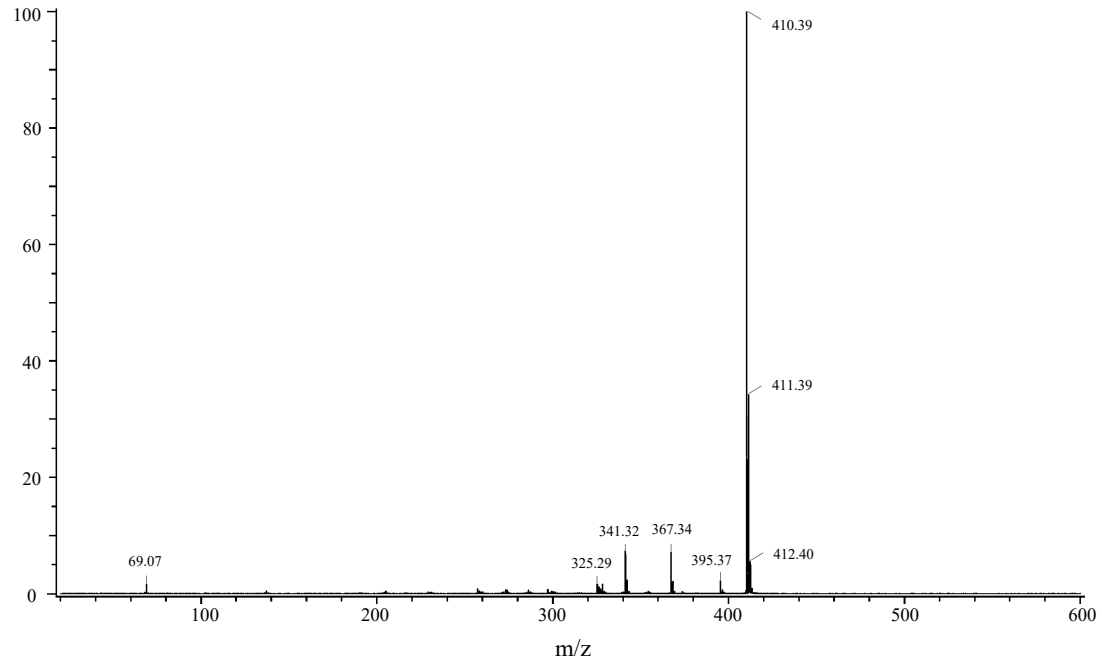

Figure 3.15 MS spectrum of biosynthesized squalene (A: full view, B: m/z 425 ~ 445 of EI-MS spectrum of ^{13}C-labeled squalene; C: EI-MS spectrum, D: FD-MS spectrum of unlabeled squalene).

From EI-MS, fragmentation of $^{13}C_5H_9$ (m/z 72 ~ 74) indicated that incorporation of ^{13}C-atom to C5 unit estimated 3, 4 and 5 respectively. Mass proportions for $^{13}C_{10}H_{17}$

fragmentations (m/z 142 ~ 147) also estimated ^{13}C-atoms incorporation from 6 to 10 and major kind is 8. Molecular ion of ^{13}C-squalene was also detected (m/z 423 ~ 438). It is consisted with the results of C_5 and C_{10} fragmentations, which were ^{13}C incorporated of 3 ~ 5 and 6 ~ 10 respectively and FD-MS results (Figure 3.15). It has been reported that lycopene was biosynthesized in the tomato cell culture with ^{13}C-glucose and ^{13}C incorporations in the first cell culture was calculated as 80%[61]. Our results of ^{13}C incorporations into squalene reached 78% and was identical with previous reports.

There are few reports about isotope labeled squalene. The ^{14}C radioisotope labeled squalene has been previously biosynthesized from [2-^{14}C]-mevalonate with cell-free system of fungus[62-65]. The labeled positions of squalene were predicted based on the biosynthetic route, but it was not described clearly. SQE inhibitors, which act important role for accumulation of squalene in our system, also promoted increasement of radioisotope incorporation to squalene in cell-free system[62]. Furthermore, in-vitro biosynthesis system sometimes afforded complicated non-saponifiable lipids mixture, which needs to isolate labeled squalene effectively[66]. There are few reports on the preparations of ^{13}C-labeled squalene through chemical synthesis. Hoshino et al has been reported the chemical synthesis of ^{13}C-stable-isotope labeled squalene at C_{10} and C_{15} position from [3-^{13}C]-ethyl acetoacetate at 5% overall yield in 6 steps[66].

To our best knowledge, this is the first report for biosynthesis of uniformly ^{13}C-enriched squalene, which will be utilized to elucidate the biosynthesis of squalene and confirmed chemical structure by NMR and mass spectrometry. Because the biosynthesized squalene is accumulated in *T. virens* fungus body, not in culture liquid, the extraction and isolation of labeled squalene is easier than cell-free systems.

3.3. Conclusion

Here we confirmed that filamentous fungi can be a potential source of producing squalene, and *Trichoderma virens* PS1-7 has quite strong ability than other kinds of filamentous fungi. Through optimizing cultivation conditions and carbon sources, the squalene accumulation of PS1-7 can reach 608.94 ± 46.87 mg/L at 28 days. Furthermore, the filamentous fungi can be utilized in biosynthesis of ^{13}C-labeled squalene with ^{13}C-glucose. The accumulations of squalene in filamentous fungi will be

utilized to be one of squalene source and to analyze terpene metabolites derived from squalene with stable isotope labeled squalene.

3.4. Experimental section

3.4.1. Chemicals

Potato dextrose broth was purchased from BD Difco, USA; potato infusion powder was obtained from Millipore, USA; butenafine hydrochloride was purchased from BLD pharm; [U-$^{13}C_6$]-Glucose was purchased from Cayman, US.

3.4.2. Microorganisms

Table 3.8 Information of strains used in this study

Species	Name	Origin
Rhizopus oryzae	I-1	isolated by our lab
Rhizopus oryzae	NBRC9364	purchased from NBRC
Rhizopus oryzae	NBRC5418	purchased from NBRC
Rhizopus microsporus	NBRC31987	purchased from NBRC
Rhizopus sp.	SH35	obtained from HABA
Rhizopus sp.	SH36	obtained from HABA
Trichoderma virens	PS1-7	isolated by our lab
Trichoderma virens	NBRC9166	purchased from NBRC
Trichoderma virens	NBRC30547	purchased from NBRC
Trichoderma virens	NBRC31959	purchased from NBRC
Trichoderma reesei	NBRC31326	purchased from NBRC
Mortierella isabellina	NBRC7824	purchased from NBRC
Penicillium spinulosum	NBRC5793	purchased from NBRC

NBRC: Biological Resource Center of the National Institute of Technology and Evaluation (Japan).

These fungi were pre-cultured on potato dextrose agar (PDA) plate at 25 ℃.

3.4.3. Cryopreservation of strains used in this study

The fungal strains utilized in this study were cryopreserved at -80°C in accordance with the guidelines outlined in NBRC News No. 3 (June 1, 2010), Section 2: Microbial Preservation Methods (2).

Upon reaching the edge of the plate and achieving sufficient growth, the mycelial mass was excised using a cork borer and immersed in the glycerol solution detailed in Table 3.9. The samples were allowed to stand at 4°C for one hour to facilitate the permeation of the solution into the mycelium. At this stage, 4 to 5 pieces of mycelial fragments were added to each vial (CryoKING® Cryogenic Vials, BIOLOGIX, USA). Subsequently, the samples were rapidly frozen in liquid nitrogen and stored at -80°C. Additionally, the glycerol solution was autoclaved prior to use and aliquoted into cryovials at a volume of 1 mL each.

Table 3.9 Glycerol solution for cryopreservation of fungi

Reagent	Volume/Weight
Glycerol	10 mL
Trehalose	5.0 g
MilliQ Water	90 mL

The revival of the cryopreserved strains was performed by immersing the vials in a 30°C water bath for approximately three minutes for rapid thawing, after which the mycelial discs were directly inoculated onto subculture plates without disintegration.

3.4.4. Subculture of filamentous fungi, inoculation into liquid medium

The filamentous fungi were cultured at 25°C in the dark using PDA plate. The hyphal tips, which elongated and reached the edges of the plate, were excised into 7 mm squares with a spatula and subsequently inoculated onto new subculture plates.

For inoculation into liquid media, plates were selected where the hyphae had sufficiently extended to the edges and had formed conidia. A single 7 mm square piece of mycelium was cut with a spatula and inoculated into autoclaved liquid medium. Furthermore, to minimize the impact of changes in the strain's characteristics due to increased subculturing on PDA medium, only those plates with subculture counts of 10 or fewer were utilized for inoculation into liquid media.

3.4.5. Growth and cultivation conditions

All fungi cells were pre-incubated in 200 mL of liquid medium (PDB (20 g/L); PIG (4 g/L PI + 20 g/L glucose); pH of liquid medium was adjusted with 1 M H_2SO_4 or 5 M

KOH) for 42 hours in a shaking incubator at 25 ℃ and 100 rpm followed by 800 μL butenafine stock liquid (50 mM solution in ethanol) being added into flasks individually, and then continuously cultivated for 7 days as the same conditions with pre-incubation. 15 ~ 40 °C was chosen to pre-screen suitable temperature for growth of PS1-7 on PDA plate (24 g/L Potato dextrose broth, 15 g/L agar). A 7 mm square piece from the edge of previous subculturing plate was cut out and cultured on new PDA plates in above temperatures for 7 days, photo of plate was taken and diameter of the mycelial was measured every day.

Screenings carbon sources subjected in 4 g/L potato infusion powder with 20 g/L different carbohydrates (glucose, fructose, sucrose, lactose, maltose, starch and glycerol). Other basic conditions were same with the conditions above.

1 g [U-$^{13}C_6$]-glucose and 0.2 g potato infusion powder were dissolved in 50 mL water and pH was adjusted to 4.0 as the medium to incubate PS1-7. Other basic conditions were same with the aforementioned conditions.

3.4.6. Squalene extraction and quantification

The harvested fungi cells of each bottle were filtrated and immersed in 70 mL acetone individually for 3 days to extract squalene. The crude acetone extract was dried over Na_2SO_4 to remove the water and then concentrated to dryness under reduced pressure and re-dissolved in 1 mL of acetone for squalene quantification.

Squalene was quantified using HPLC system: L-6250 Intelligent Pump (Hitachi, Tokyo, Japan) and L-4000 UV Detector (Hitachi, Tokyo, Japan). The column used was Wakosil-II 5C18 HG φ4.6 mm×250 mm (Wako, Osaka, Japan). The mobile phase is 100% MeOH, and the detection wavelength is 205 nm [67].

3.4.7. NMR analysis

The product was analyzed using NMR, to identify the squalene. The purified ^{13}C labeled squalene was dissolved in $CDCl_3$ and analyzed using ^{1}H and ^{13}C-NMR (400 MHz, JNM-ECS400, JEOL Ltd., Tokyo, Japan; 700 MHz, Avans III, Brucker, Tokyo, Japan).

3.4.8. Mass analysis

The identification of obtained squalene was performed using the EI-TOF MS analyser (JMS-2000GC, JEOL Ltd., Tokyo, Japan) and FD-MS analyser (JMS-T100GCV, JEOL Ltd., Tokyo, Japan).

4. Biosynthesis of ^{13}C viridin and viridiol

4.1. Introduction

Viridin and viridiol (Figure 4.1), belonging to the family of furanosteroid family, are biosynthesized by the filamentous fungus, *Trichoderma virens*, which is a biocontrol agent for various bacteria and fungi[68]. Furanosteroids strongly inhibit phosphatidylinositol 3-kinases, which are associated with tumor cell proliferation [69]. Therefore, structure–activity relationship studies of furanosteroids can aid in the development of effective pesticides and therapeutics[70, 71]. Chemical synthesis of viridin and viridiol involves 17–18 steps, with an extremely low overall yield of approximately 2%[72-74]. Viridin is unstable in neutral and alkaline media[75]. Strongly acid alumina is used as the adsorbent for the chromatography to avoid the isomerization of viridin during purification[76-78]. These reports highlight the difficulty of producing and isolating viridin on a large scale. Structure and ^{1}H nuclear magnetic resonance (NMR) spectroscopic data of β-viridin, an isomer of viridin, have been reported[79]; however, its exact structure remains unknown, and the Chemical Abstracts Service number of β-viridin has been registered without stereochemistry.

Many studies have investigated the biosynthetic pathways of viridin and viridiol. Isotope analysis is a simple but powerful strategy to assess metabolic profiles and pathways. Previous studies using ^{13}C- and ^{14}C-labeled mevalonates and acetate confirmed that viridin is formed from lanosterol (Figure 4.1)[80-83] and that the carbonyl group neighboring the methoxy group in viridin is reduced to the hydroxy group in viridiol[84]. The detailed gene cluster of demethoxyviridin, the precursor of viridin, has been proposed[85]; however, the pathways involved in the biosynthesis of viridin and downstream furanosteroid compounds remain unclear. Therefore, practical production methods for viridin, β-viridin, and viridiol are urgently needed to facilitate their application as therapeutic agents for various diseases, including cancer.

In this study, we screened nine *T. virens* and identified out the most suitable culture conditions to produce and isolate pure viridin (pH 3) and viridiol (pH 2) on a large scale. Using [U-$^{13}C_6$]-glucose as the sole carbon source, we successfully obtained [U-^{13}C]-viridiol and [U-^{13}C]-viridiol, which can be used to elucidate the biosynthetic pathways of furanosteroids. To the best of our knowledge, this study is the first to demonstrate

the X-ray structure of β-viridin crystal and reveal the irreversible conversion of viridin into β-viridin.

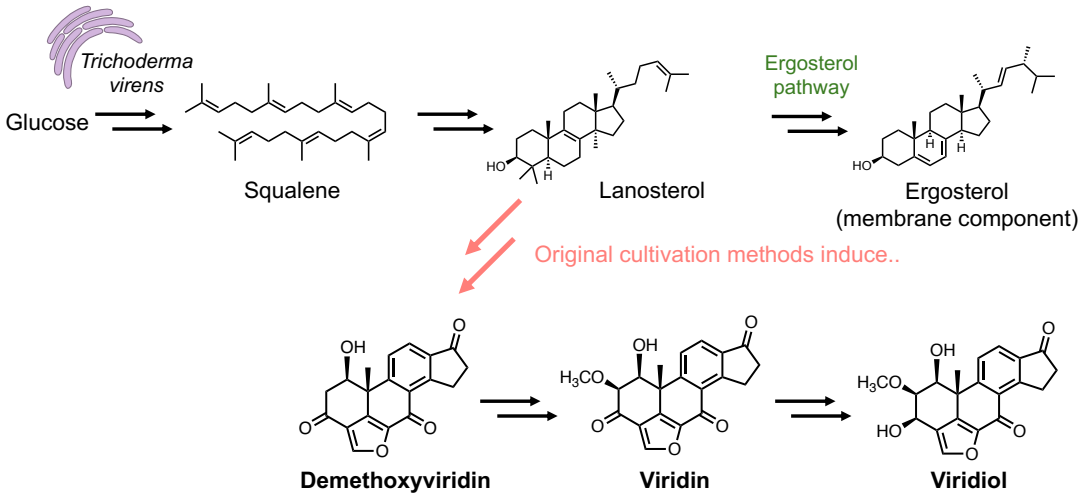

Figure 4.1 Structures and biosynthetic pathway of viridin and viridiol

4.2. Results and discussion

4.2.1. Determination of optimal pH for viridin and viridiol accumulation

First, to determine the optimal pH conditions for the viridin or viridiol production, *T. virens* PS1-7 was cultured in the PIG medium at different pH values (2.0–5.0). This was based on our previous report on the significant impacts of pH on cell growth and squalene accumulation in the filamentous fungus, *T. virens* [86]. Although cell growth of PS1-7 was strongly inhibited in a strong acidic environment, viridin exhibited the highest accumulation (24.99 ± 10.14 mg/L) at pH 3 but none at pH 2. In contrast, viridiol exhibited significant accumulation (52.60 ± 5.23 mg/L) at pH 2, which was a harsh condition for fungal survival (Table 4.1).

Table 4.1 Accumulation of viridin and viridiol in the culture filter, and the fresh weight of mycelia (MFW) of *T. virens* PS1-7 at different pH in 200 mL PIG medium at 25 °C and 100 rpm for seven days. Data are represented as the mean ± standard deviation (S.D.; n = 3).

pH	MFW (g/L)	viridin (mg/L)	viridiol (mg/L)

2	6.17 ± 0.29	*N.D.	52.60 ± 5.23
3	9.93 ± 0.36	24.99 ± 10.14	31.29 ± 5.59
4	10.80 ± 0.57	16.00 ± 3.13	17.99 ± 7.12
5	13.40 ± 0.10	12.60 ± 2.74	11.13 ± 1.74

*N.D., not detected.

Next, stability of viridin was checked in the culture filter. The culture filter was separated from the mycelia after five days of incubation at pH 3, and the pH was adjusted to 2, 3, 4, and 5, followed by two days of incubation. Notably, viridin remained stable at pH 2, but its stability drastically decreased at pH 5 (Figure 4.2). Although the specific enzyme involved in its biosynthesis pathway remains unknown, viridin is suggested to be the precursor of viridiol[84]. These results suggest that the activity of the reductive enzyme involved in the conversion of viridin into viridiol is enhanced under low pH conditions.

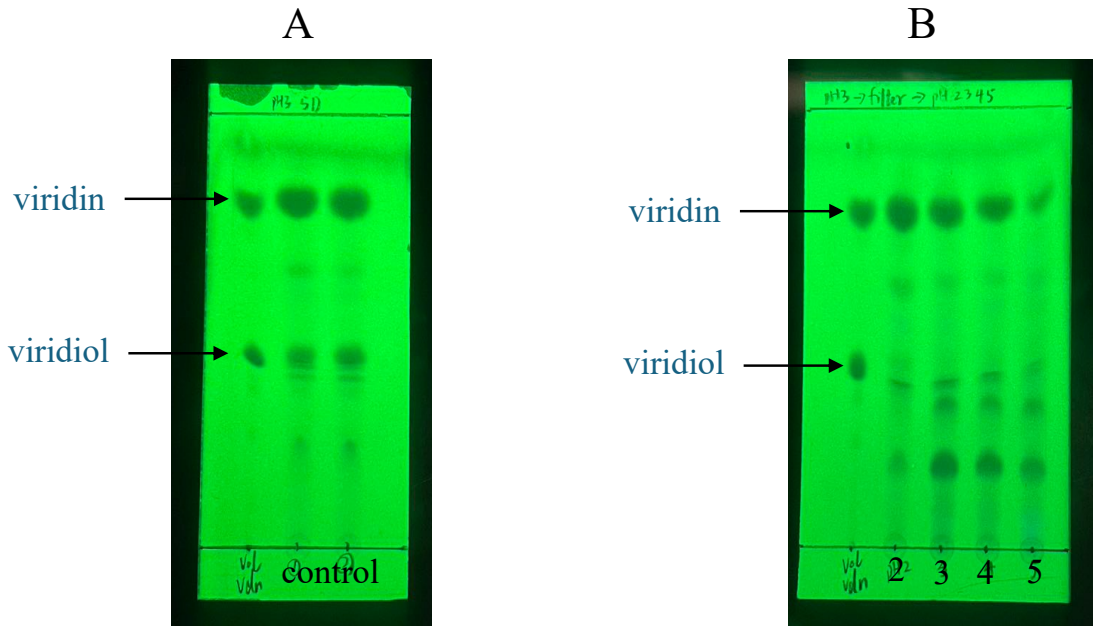

Figure 4.2 Stability of viridin in culture filter. (A) *T. virens* PS1-7 was cultivated in 200 mL PIG pH 3 medium at 25 ℃, 100 rpm for 7 days; (B) *T. virens* PS1-7 was cultivated in 200 mL PIG pH 3 medium at 25 ℃, 100 rpm for 5 days, then culture filter was separated from mycelia followed by pH adjusted to 2, 3, 4 and 5 relatively, then continued 2 days' incubation.

4.2.2. Screening of filamentous strain for viridin accumulation

Next, we used filamentous fungus *T. virens* strains for efficient production of viridin and viridiol at pH 2 and 3. As shown in Table 4.2, at pH 3, each filamentous fungal strain produced viridin, with NBRC 9168 and 9169 exhibiting the highest production of 42.29 ± 6.32 and 47.80 ± 4.71 mg/L, respectively. In contrast, NBRC 8350 and NBRC 9166 barely produced viridin. At pH 2, no viridin production was observed, indicating that the lack of viridin accumulation in the culture liquid at pH 2 was not due to a random effect. PS1-7, NBRC 8349, and NBRC 9169 exhibited the highest viridiol production of 52.60 ± 5.23, 52.77 ± 7.48, and 61.92 ± 4.39 mg/L, respectively (Table 4.3).

Table 4.2 Viridin and viridiol accumulation in the culture filter, and the fresh weight of mycelia (MFW) for nine *T. virens* at pH 3 in 200 mL PIG medium at 25 ℃ and 100 rpm for seven days. Data are represented as the mean ± S.D. (n=3)

strain (*T. virens*)	MFW (g/L)	viridin (mg/L)	viridiol (mg/L)
PS1-7	9.93 ± 0.36	24.99 ± 10.14	31.29 ± 5.59
NBRC 30547	8.57 ± 0.58	15.67 ± 1.35	2.32 ± 0.41
NBRC 8350	10.33 ± 0.26	2.57 ± 1.30	15.03 ± 1.35
NBRC 9168	6.40 ± 0.18	42.29 ± 6.32	2.09 ± 2.03
NBRC 31959	6.15 ± 0.68	14.08 ± 7.29	17.85 ± 9.96
NBRC 9166	10.17 ± 0.68	3.68 ± 2.02	5.20 ± 2.21
NBRC 6355	9.93 ± 0.47	10.54 ± 3.87	0.49 ± 0.08
NBRC 8349	9.43 ± 1.62	30.97 ± 5.74	12.51 ± 6.30
NBRC 9169	6.92 ±0.15	47.80 ± 4.71	4.02 ± 1.55

Table 4.3 Viridin and viridiol accumulation in the culture filter, and the fresh weight of mycelia (MFW) for nine *T. virens* at pH 2 in 200 mL PIG medium at 25 ℃ and 100 rpm for seven days. Data are represented as the mean ± S.D. (n=3)

strain (*T. virens*)	MFW (g/L)	viridin (mg/L)	viridiol (mg/L)
PS1-7	6.17 ± 0.29	*N.D.	52.60 ± 5.23
NBRC 30547	2.87 ± 0.12	N.D.	18.01 ± 0.50
NBRC 8350	5.28 ± 0.46	N.D.	17.78 ± 1.96

NBRC 9168	2.58 ± 0.20	N.D.	28.91 ± 3.06
NBRC 31959	3.80 ± 0.15	N.D.	13.71 ± 0.89
NBRC 9166	2.83 ± 0.20	N.D.	2.06 ± 0.39
NBRC 6355	4.68 ±0.78	N.D.	8.67 ± 2.27
NBRC 8349	5.35 ± 0.71	N.D.	52.77 ± 7.48
NBRC 9169	6.60 ± 0.63	N.D.	61.92 ± 4.39

*N.D., not detected.

4.2.3. Purification of viridin and viridiol from *T. virens*

Avent et al. reported that viridin is easily isomerized into β-viridin during purification [76]. Therefore, a new purification method is needed for fungal culture media. Based on the above screening experiments, a crude medium was prepared by cultivating NBRC 9169 in PIG medium at pH 2 and 3 for 10 d. After the medium was filtered and extracted with diethyl ether, viridin (118.1 mg/L) was successfully purified by recrystallization in one step, without isomerization into β-viridin, by adding acetone to the organic phase under -20 °C. In contrast, viridiol (75.6 mg/L) was obtained via silica gel purification of the ethyl acetate extract of the culture filtrate.

4.2.4. X-ray crystallography of β-viridin

β-viridin is a secondary metabolites produced by soil fungi[76, 79]; however, its absolute configuration remains unknown. Here, evaluation of viridin stability on silica gel revealed that viridin was partially converted to another compound, whose polarity was close to that of viridin maintained on silica gel for one hour (Figure 4.3). The detected spots increased when viridin was kept on the silica gel for longer periods (> 12 h). However, the levels of other unknown compounds also increased (Figure 4.4).

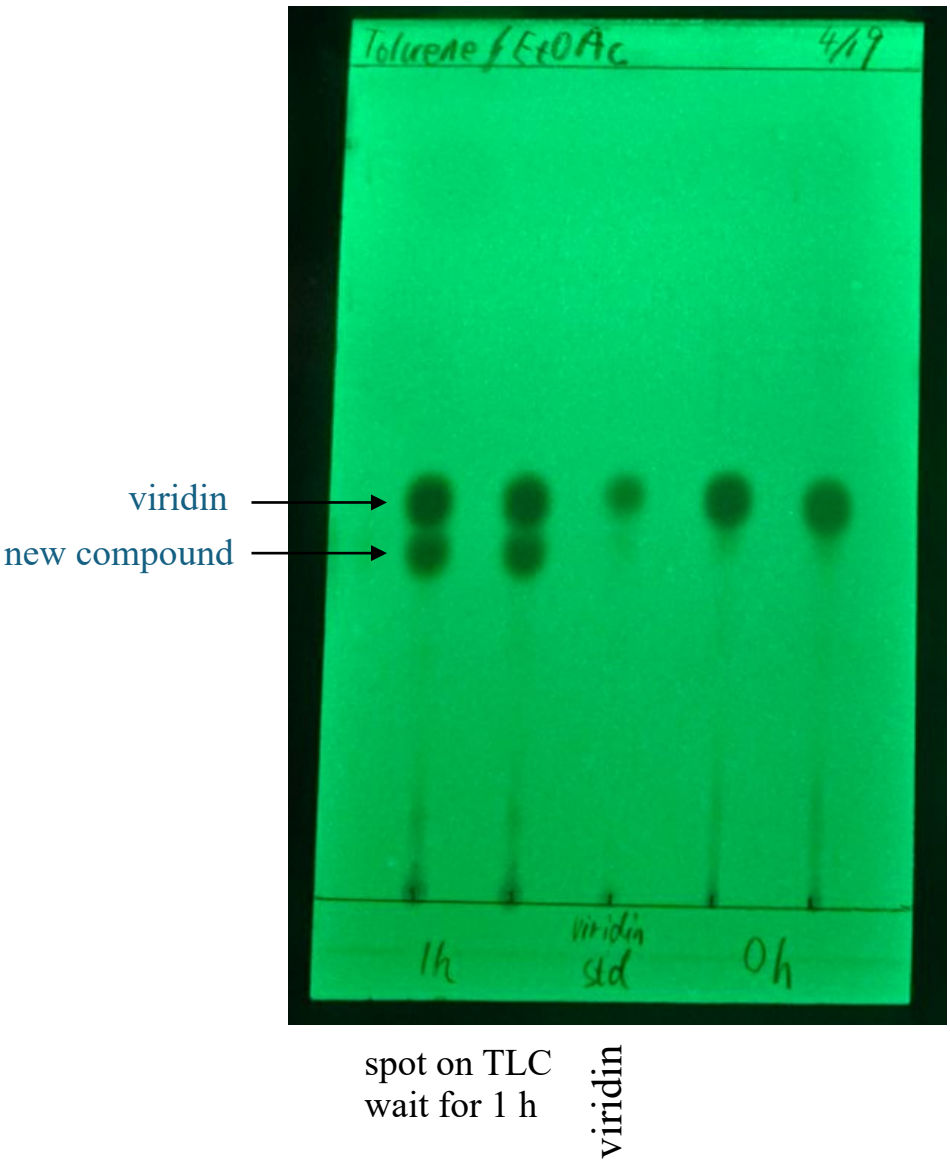

Figure 4.3 Result of spotting viridin on TLC plate for 1 hour under UV 254 nm

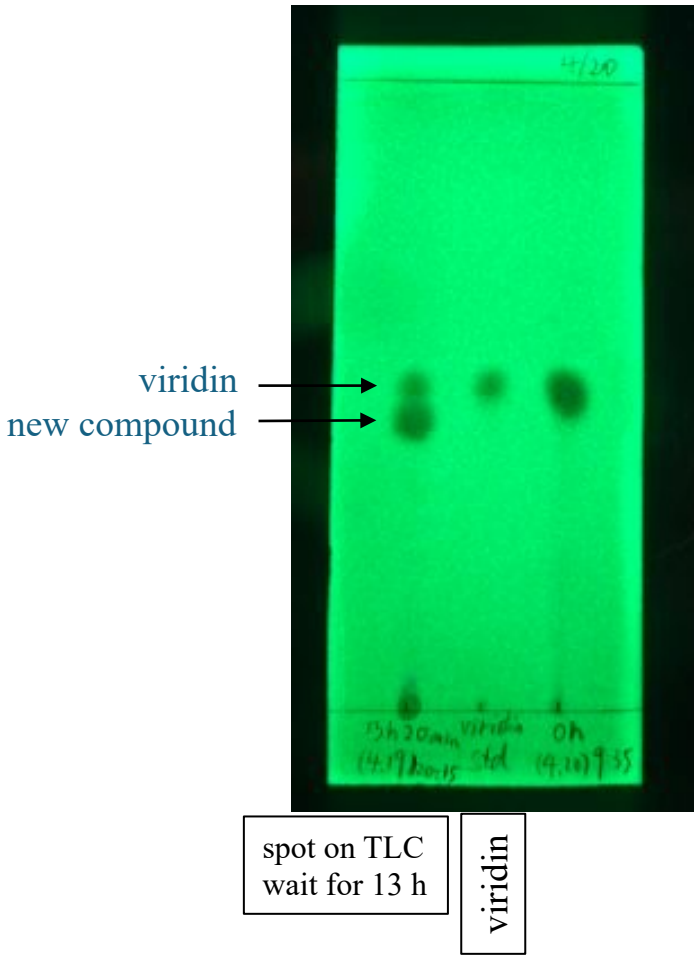

Figure 4.4 Result of spotting viridin on TLC plate for 13 hours under UV 254 nm

The converted compound was subjected to thin-layer chromatography-mass spectrometry (TLC-MS), was exhibited a peak at *m/z* 351.1 $[M-H]^-$ ion (molecular weight of viridin: 352.3; Figure 4.5). Therefore, we hypothesized that the converted compound was a stereoisomer of viridin. To confirm this hypothesis, we clarified the absolute configuration of the converted compound using X-ray diffraction. Viridin (150 mg) was dissolved in chloroform, and the solution was evenly spread on a TLC silica gel plate and left for 3 h. Through preparative TLC plate separation and recrystallization using acetone, 21 mg crystal of the converted compound was obtained. Using X-ray crystallography (Figure 4.6, Table 4.4), the absolute configuration of the converted compound was confirmed by refinement of the Flack parameter (−0.06(7)) using anomalous dispersion effects[25], which indicated that it was a stereoisomer of the methoxy group in viridin. Furthermore, vibrational circular dichroism (VCD) technique[26,27], which can analyze the reliable absolute configuration on the comparison of experimental spectrum and theoretical one, provided more detailed

results. (Figure 4.7). Molecular mechanics conformational search was performed using CONFLEX 9 software. Obtained geometries within 3.0 kcal/mol from the most stable (1 conformer for viridin and 2 conformers for β-viridin) were optimized at DFT/B3LYP/6-311+G(d,p) using PCM for chloroform on Gaussian 16 program. The VCD and IR spectra of the resultant conformers were calculated at the same level of theory. The calculated frequencies, dipole strengths and rotational strengths were converted to VCD and IR spectra on GaussView 6 software using a peak half-width at half height of 8 cm^{-1}. The calculated frequencies were scaled with a factor of 0.985. For β-viridin, the VCD and IR spectra of each conformer were averaged based on its Boltzmann populations simulated at 298 K.

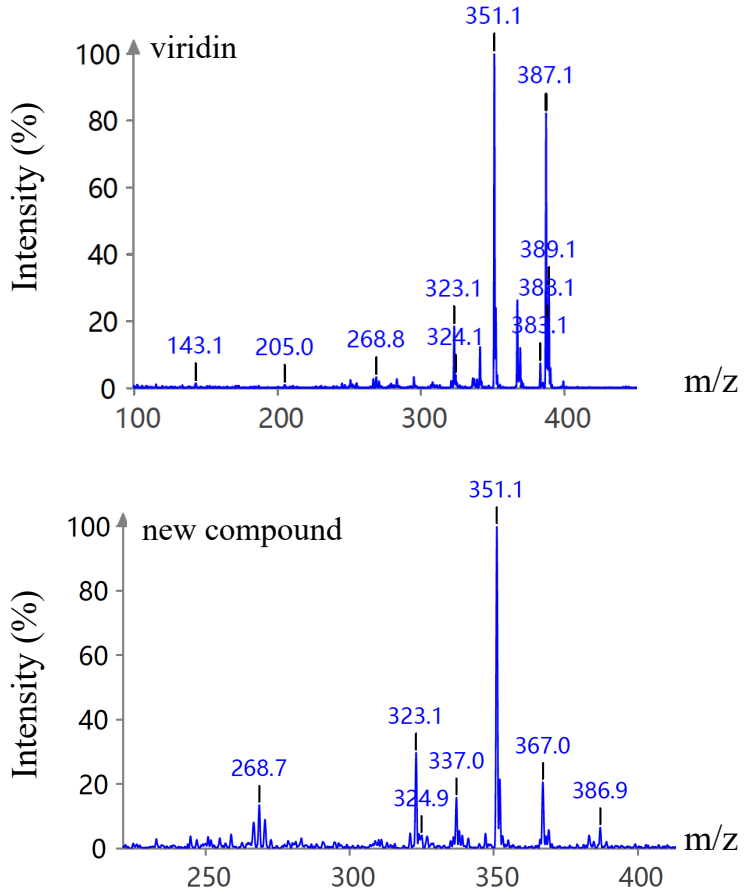

Figure 4.5 TLC-MS spectrum of viridin and the converted compound

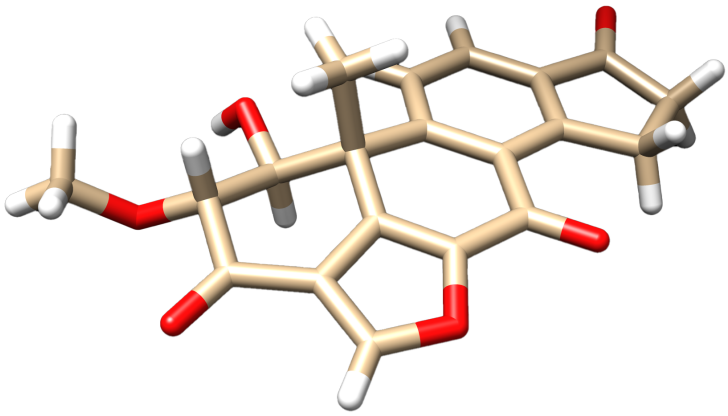

Figure 4.6 X-Ray structure of the compound, β-viridin

Table 4.4 Crystal data and structure refinement for β-viridin: The correct absolute configuration of β-viridin was defined by the Flack parameter, −0.06(7)[87].

Crystal	β-viridin
Empirical formula	$C_{20}H_{16}O_6$
Formula weight	352.33
Temperature/K	103(2)
Crystal system	orthorhombic
Space group	$P2_12_12_1$
a, b, c (Å)	8.25630(10), 10.9299(2), 17.6929(3)
α, β, γ (°)	90, 90, 90
Volume/Å^3	1595.17(4)
Z	4
ρ_{calc}g/cm^3	1.467
μ/mm^{-1}	0.911
F(000)	736.0
Crystal size/mm^3	0.073 × 0.059 × 0.043
Radiation	CuKα (λ = 1.54184)
2Θ range for data collection/°	9.518 to 149.224
Index ranges	$-10 \leq h \leq 10$, $-13 \leq k \leq 13$, $-21 \leq l \leq 21$
Reflections collected	21552
Independent reflections	3162 [R_{int} = 0.0317, R_{sigma} = 0.0210]

Data/restraints/parameters	3162/0/238
Goodness-of-fit on F^2	1.064
Final R indexes [I>=2σ (I)]	R_1 = 0.0310, wR_2 = 0.0797
Final R indexes [all data]	R_1 = 0.0339, wR_2 = 0.0809
Largest diff. peak/hole / e $Å^{-3}$	0.22/-0.21
Flack parameter	0.06(7)

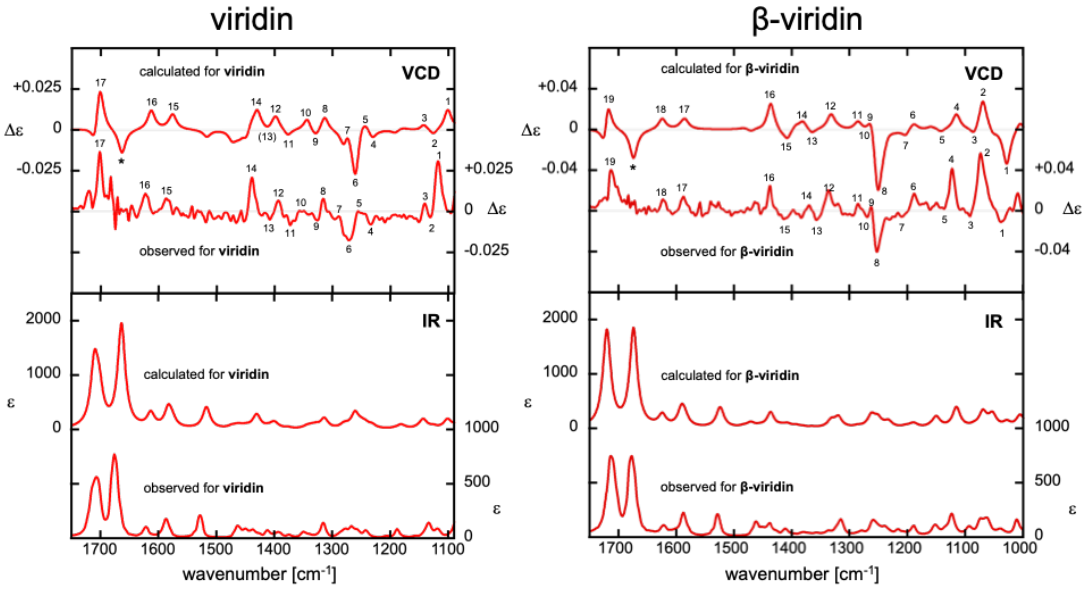

Figure 4.7 VCD analysis of viridin and β-viridin.

This result was verified via ^{1}H-NMR and ^{13}C -NMR (Figures 4.8 and 4.9; Tables 4.5 and 4.6), which revealed that the stereoisomerism of the methoxy group and hydrogen caused a chemical shift at 8.31 ppm, but this was observed at 8.28 ppm for the converted compound. Therefore, the converted compound of viridin on silica gel was confirmed to be β-viridin, and this study provides the first report of the absolute configuration of β-viridin.

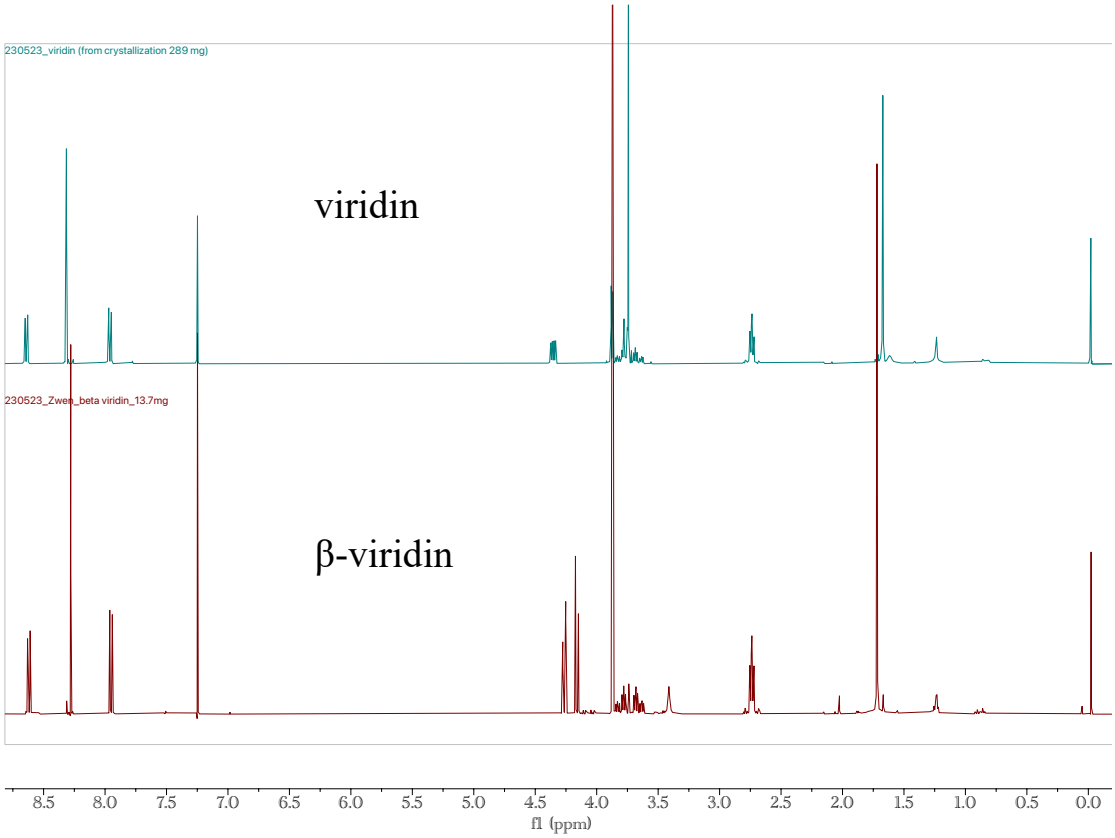

Figure 4.8 ^{1}H NMR spectrum of viridin and β-viridin

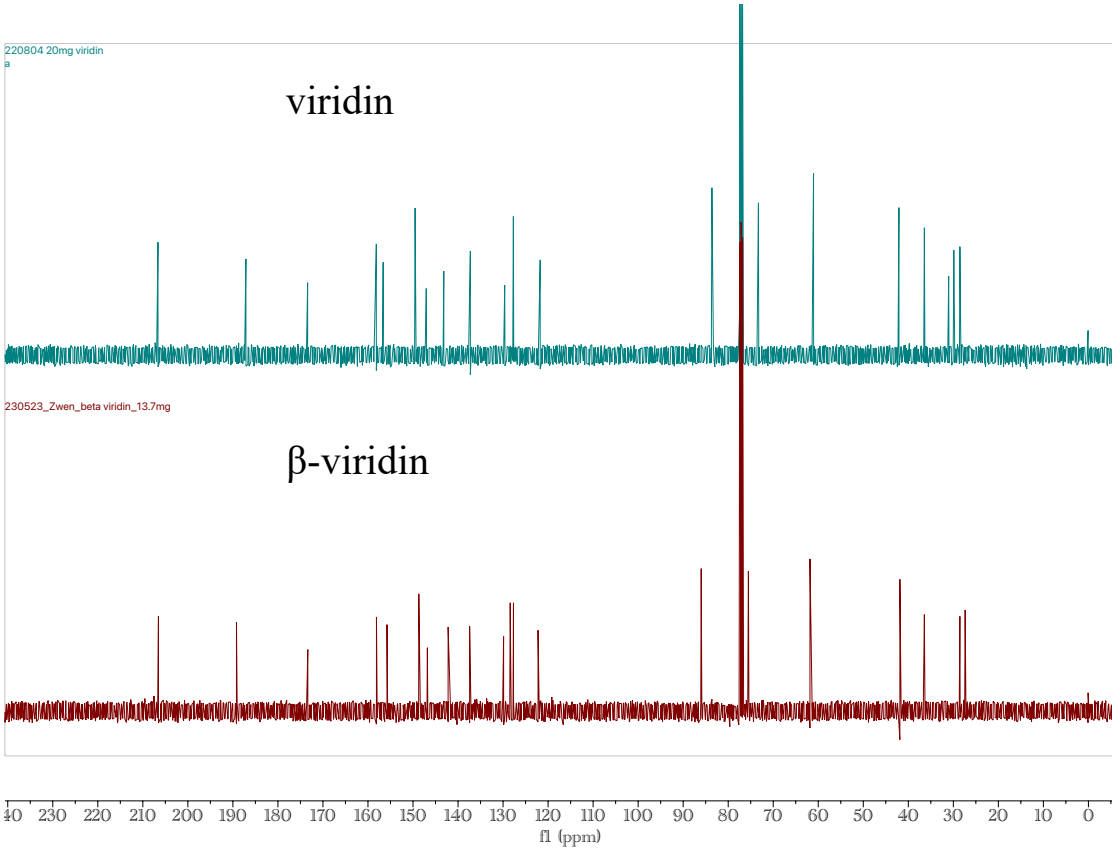

Figure 4.9 ^{13}C NMR spectrum of viridin and β-viridin

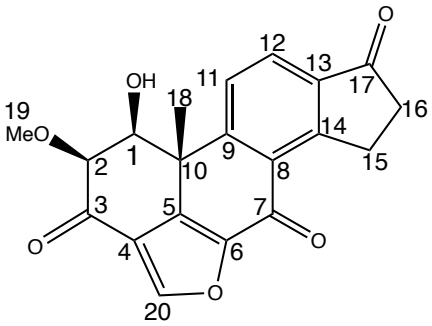

viridin

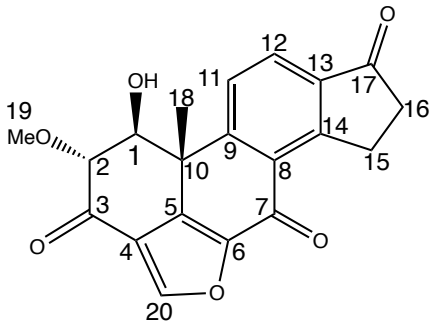

β-viridin

Table 4.5 Comparison of ^{1}H NMR spectroscopic data of Guerrero's synthetic viridin[73] with our biosynthetic viridin and synthetic β-viridin

position	Synthetic viridin reported by Guerrero δ ^{13}C [ppm], 500 MHz	Our biosynthetic viridin δ ^{13}C [ppm], 400 MHz	Our synthetic β-viridin δ ^{13}C [ppm], 400 MHz
1	3.89 (d, 5.0)	3.88 (1H, d, 5.1)	4.26 (1H, d, 9.6)
2	4.37 (bs)	4.35 (1H, dd, 10.8, 5.0)	4.16 (1H, d, 9.6)
11	8.66 (dd, 8.2, 0.8)	8.64 (1H, d, 8.2)	8.62 (1H, d, 8.3)
12	7.98(d, 8.2)	7.96 (1H, d, 8.3)	7.95 (1H, d, 8.3)
15-a	3.87-3.78 (m)	3.81-3.76 (1H, m)	3.85-3.75 (1H, m)
15-b	3.72-3.64 (m)	3.72-3.60 (1H, m)	3.72-3.60 (1H, m)
16	2.79-2.73 (m)	2.88-2.62 (2H, m)	2.77-2.71 (2H, m)
18	1.69 (s)	1.67 (3H, s)	1.72 (3H, s)
19	3.76 (s)	3.74 (3H, s)	3.87 (3H, s)
20	8.33 (s)	8.31 (1H, s)	8.28 (1H, s)
OH	-	-	-

Table 4.6 Comparison of ^{13}C NMR spectroscopic data of Guerrero's synthetic viridin with our biosynthetic viridin and synthetic β-viridin

position	Synthetic viridin reported by Guerrero δ ^{13}C [ppm], 125 MHz	Our biosynthetic viridin δ ^{13}C [ppm], 100 MHz	Our synthetic β-viridin δ ^{13}C [ppm], 100 MHz
1	73.31	73.29	75.51
2	83.58	83.62	86.00
3	187.09	187.10	189.20
4	121.77	121.76	122.23
5	143.13	143.16	142.20
6	147.09	147.06	146.81
7	173.43	173.40	173.36
8	129.65	129.64	129.88
9	156.61	156.63	155.78
10	42.10	42.08	41.87
11	127.95	127.93	128.41
12	127.77	127.71	127.69
13	137.3	137.27	137.42
14	158.18	158.15	158.12
15	28.59	28.54	28.55
16	36.49	36.44	36.44
17	206.66	206.64	206.54
18	29.95	29.89	27.38
19	61.10	61.05	61.84
20	149.53	149.54	148.71

Specific rotations of viridin and β-viridin were determined via optical rotation testing, viridin: $[\alpha]_D^{20}$ = -177° ($CHCl_3$), β-viridin: $[\alpha]_D^{20}$ = -39° ($CHCl_3$), which are also consistent with previous reports [72].

4.2.5. Irreversible conversion from viridin to β-viridin

Viridin readily isomerizes into β-viridin in neutral, alkaline, and weakly acidic media due to keto–enol tautomerism[78]. However, the specific conditions and conversion yields remain unclear. Therefore, in this study, we investigated the isomerization of viridin to triethylamine (TEA), formic acid (FA), and trimethylsilanol (Me_3SiOH) at room temperature. ^{1}H-NMR (Figure 4.10) revealed that Me_3SiOH did not convert viridin into β-viridin. However, small amounts of β-viridin were formed by TEA and FA after 13 h treatment, with more impurities observed with FA than with TEA (Figure 4.11). Notably, viridin completely dissolved in FA, but not in TEA. Addition of $CDCl_3$ to the reaction system turned it into a liquid system. β-viridin was the main conversion product after 10-h reaction in the TEA system, but β-viridin was not detected in the FA system (Figure 4.11(B)).

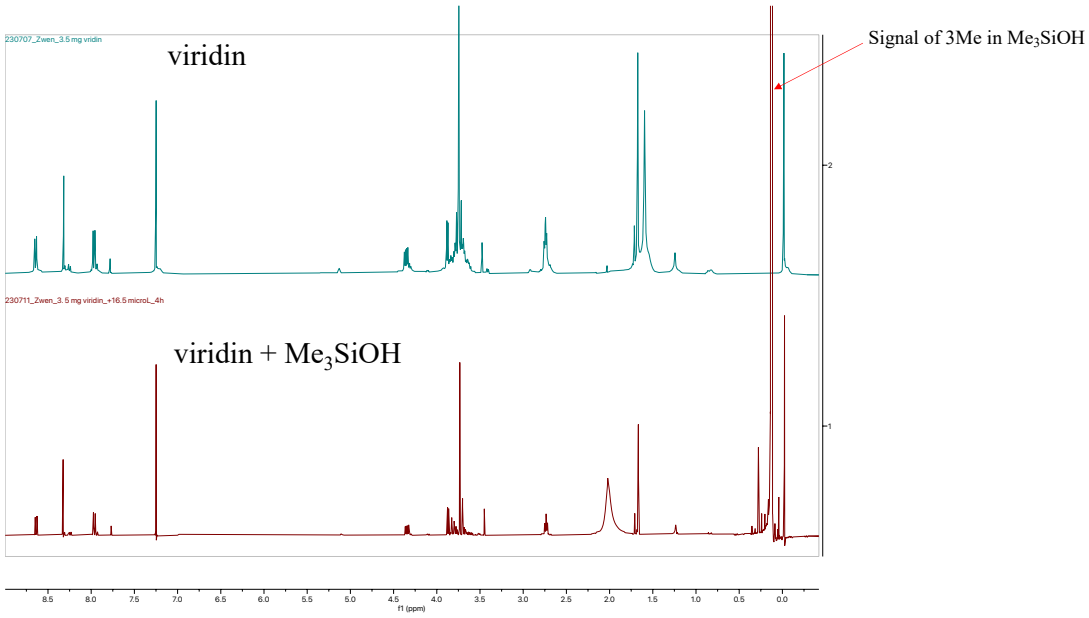

Figure 4.10 ^{1}H NMR spectrum of viridin reacting with trimethylsilanol (Me_3SiOH)

(A)

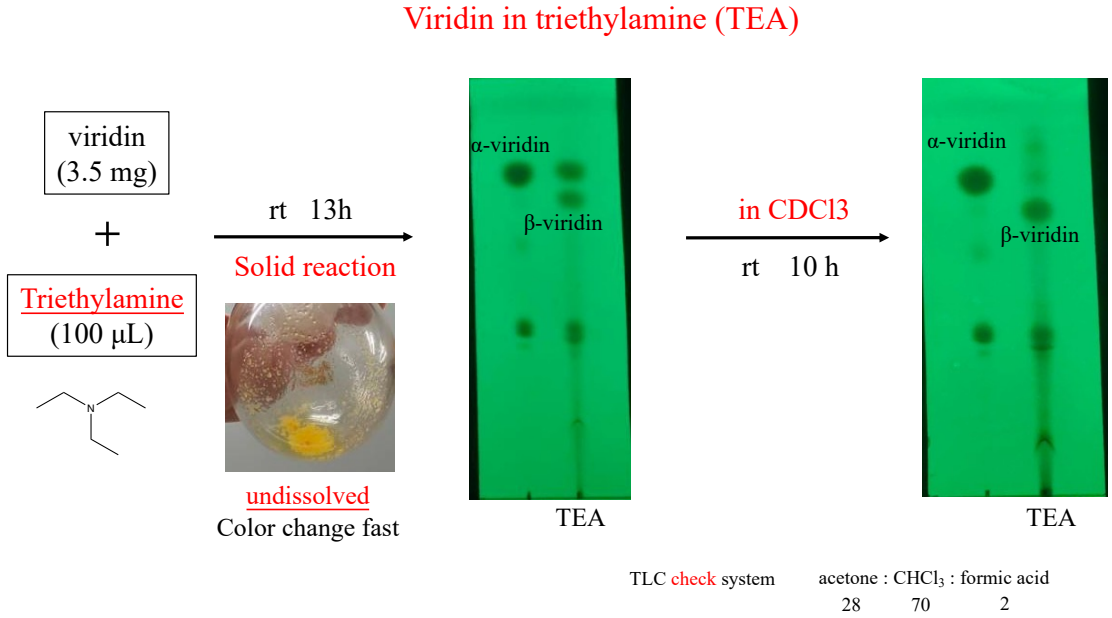

(B)

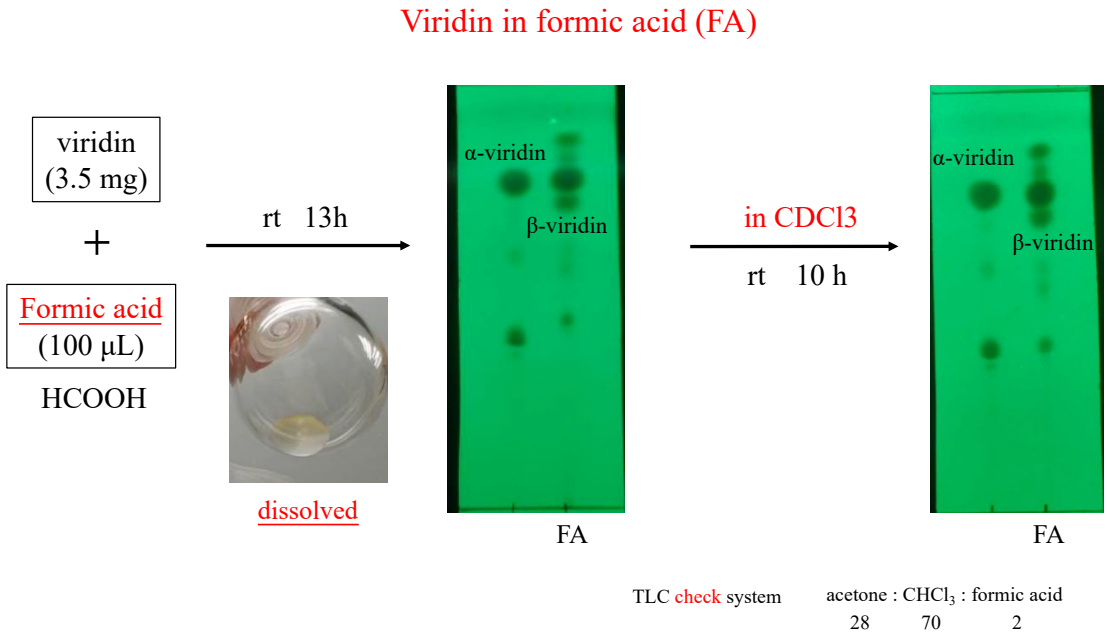

Figure 4.11 TLC results of viridin reacting with TEA (A) and FA (B).

Next, based on the stable conversion into β-viridin using the TEA/$CHCl_3$ system, we determined the optimal conditions and values of conversion. Different amounts of TEA were added to a 10 mM viridin solution in $CDCl_3$ and allowed to react for 1 h. The conversion ratios were calculated by the specific integration value of each compound in ^{1}H-NMR. As shown in Table 4.7, β-viridin ratio increased with increasing TEA

concentration, and 100 eq TEA significantly increased the conversion ratio. It's predicted that the isomerization from viridin to β-viridin is through keto-enol tautomerism due to alkali existing (Figure 4.12). To investigate the conversion in alkaline conditions with high efficiency and fewer by-products, various representative organic and inorganic alkalis were reacted with the viridin solution. Among the different alkaline compounds, TEA exhibited the best potential to convert viridin into β-viridin (Table 4.8). However, purified β-viridin did not yield any α-viridin on TLC. These results indicated that the configuration of β-viridin was more stable than that of α-viridin, which was confirmed via crystallographic analysis. We further assessed our conversion method on a large scale using 31.5 mg of viridin and obtained 24 mg of pure β-viridin with a conversion rate of 76% after separation using the silica gel column. For the first time, we demonstrated the irreversible conversion of viridin to β-viridin at a high yield using TEA.

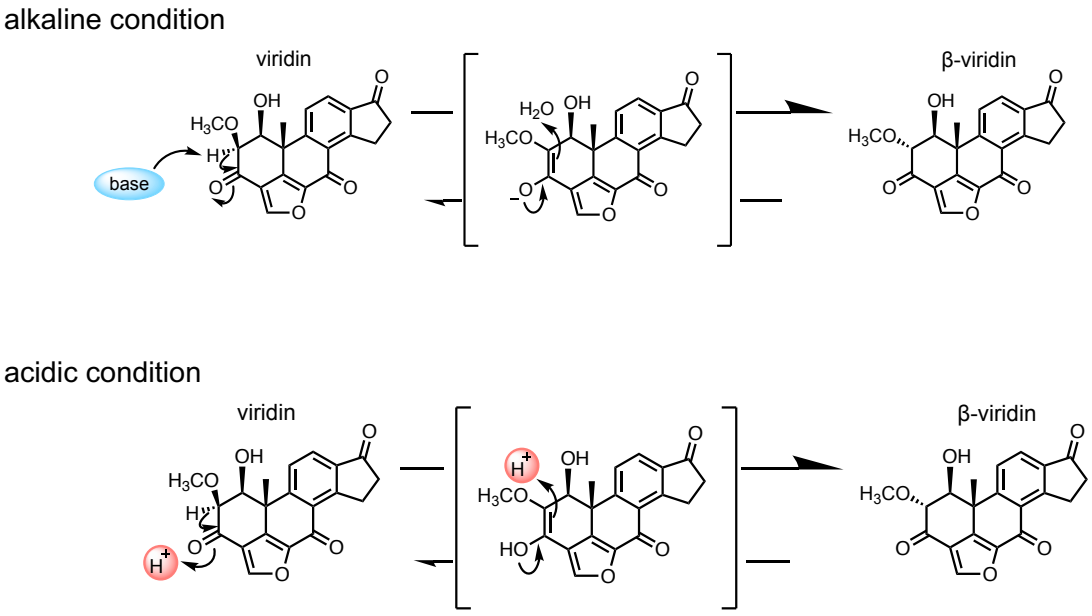

Figure 4.12 Predicted isomerization scheme of viridin to β-viridin.

Table 4.7 Viridin and β-viridin ratios after reacting with different amounts of triethylamine (TEA) for 1 h.

TEA (eq)	1	5	10	50	100	200
α:β	1:0.05	1:0.16	1:0.53	1:1.33	1:6.82	1:7.82

Table 4.8 Viridin and β-viridin ratios after reacting with different alkalis for 1 h.

Base	Conversion rate
triethylamine	1:6.82
diisopropylethylamine	Viridin broken
DBU	Viridin broken
NaOH	No conversion
K_2CO_3	α:β = 1:0.25
$NaHCO_3$	α:β = 1:0.08
Cs_2CO_3	α:β = 1:0.33
CsF	α:β = 1:0.25
t-BuONa	Viridin broken

Note: alkali (100 equiv.) was added into 1 mL of 10 mM viridin solvent in $CHCl_3$ and reacted for 1 h at room temperature.

4.2.6. Biosynthesis of ^{13}C labeled viridin and viridiol using [U-$^{13}C_6$]-glucose in the culture medium

Viridin, derived from mevalonic acid, partly shares the mevalonate pathway with squalene[85]; however, the gene cluster involved in the biosynthesis of viridin and its conversion into viridiol remains unclear. Recently, we bionsynthesized ^{13}C-enriched squalene using [U-$^{13}C_6$]-glucose as a carbon source instead of normal glucose[86]. Here, we attempted to biosynthesize ^{13}C-labeled viridin and viridiol. NBRC 9169 was cultured with 1 g of [U-$^{13}C_6$]-glucose and 0.2 g PI powder in 50 mL of water at pH 3. After separating the culture from the cells, 5.8 mg ^{13}C-labeled viridin was obtained using our established purification method. Consistent with previous reports, ^{13}C-labeled viridiol was obtained at pH 3. ^{13}C incorporation into viridin and viridiol was evaluated via NMR and MS analyses. As shown in Figure 4.13 and Table 4.9 and 4.10, ^{13}C–^{13}C coupling was observed in all carbons of ^{13}C-viridin and ^{13}C-viridiol. In FD-MS analysis of ^{13}C-enriched viridin and viridiol, 20 ^{13}C atoms were incorporated (m/z 372 and 374, respectively) into the structures (Figure 4.14) compared to nor mal viridin and viridiol (m/z 352 and 354, respectively) (Figure 4.15). Compared to our previous study with 78% ^{13}C incorporation into squalene[86], ^{13}C incorporation into viridin and viridiol reached 82 and 76%, respectively, in this study. Additionally, ESI time-of-flight-MS analysis revealed the $[M+H]^+$ ion peaks of ^{13}C-enriched viridin (*m*/*z* = 366–373), with

the major ion peak observed at *m*/*z* = 370, whereas the $[M+H]^+$ ion peak of viridin (*m*/*z* = 353) was rarely detected. For ^{13}C-enriched viridiol, $[M+H]^+$ ion peaks of ^{13}C-enriched viridiol were observed at *m*/*z* 366–375, with the major ion peak observed at *m*/*z* = 372 (Figure 4.16). In negative mode, both ^{13}C-viridin and ^{13}C-viridiol shows peaks after Cl^- addition into the structure (approximately *m/z* 407 and 409, respectively; Figure 4.17). Therefore, 13–20 ^{13}C atoms were incorporated into viridin and 11–20 ^{13}C atoms were incorporated into viridiol, confirming that all carbon atoms of viridin and viridiol were successfully replaced by ^{13}C isotopes. To the best of our knowledge, this is the first report on the biosynthesis of ^{13}C-viridin and ^{13}C-viridiol which can aid in the biosynthetic pathway analysis of other furanosteroids in the future.

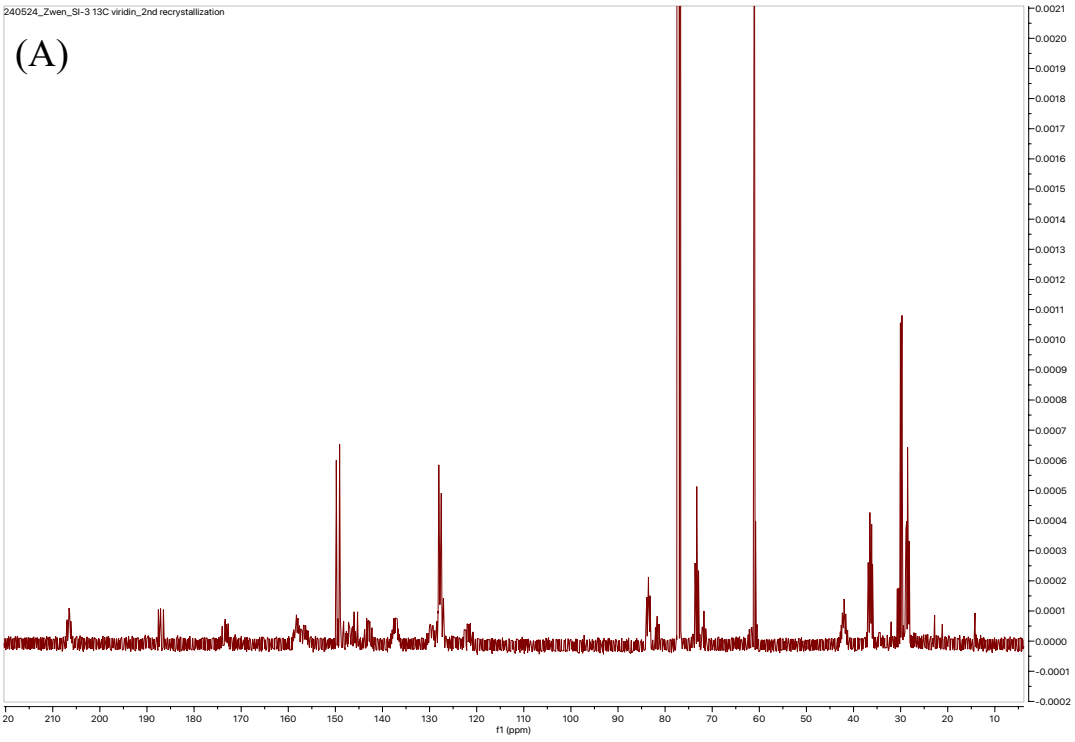

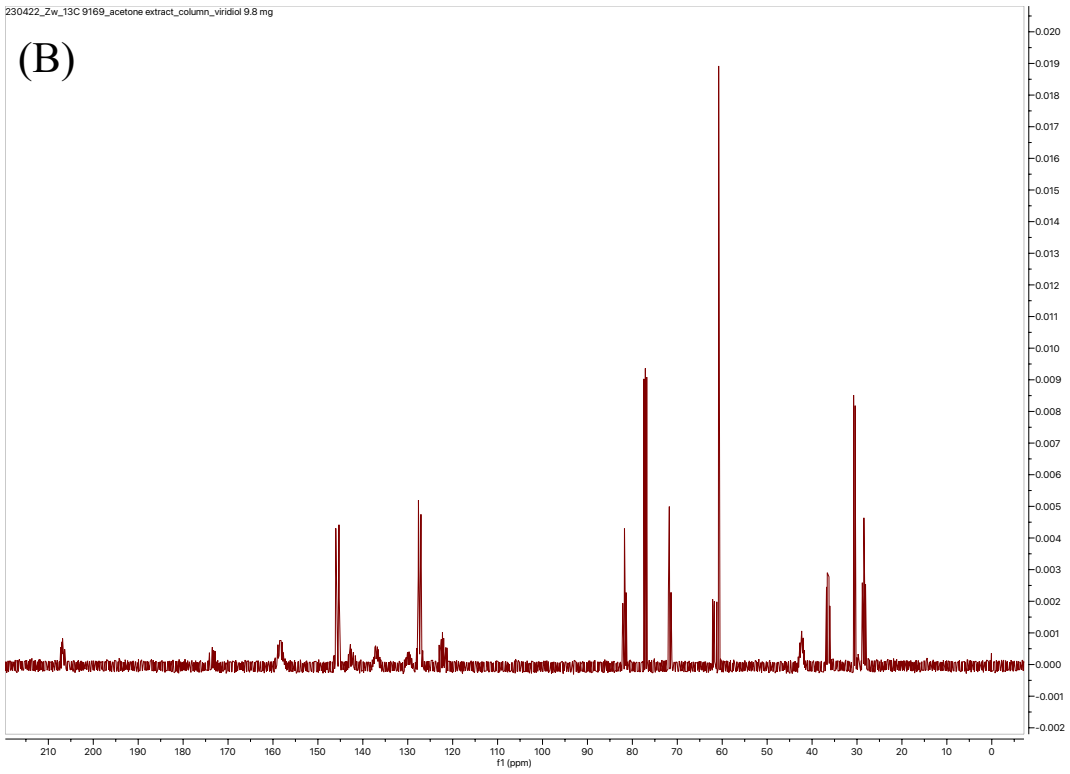

Figure 4.13 ^{13}C NMR spectrum of biosynthesized ^{13}C enriched viridin (A) and viridiol (B) in $CDCl_3$

Table 4.9 ^{13}C-^{13}C coupling constants of ^{13}C-viridin

δ (ppm)	J (Hz)	Carbon-position
28.61	m	15-CH2
29.89	d, 32.27	18-Me
36.43	m	16-CH2
41.82	m	10-C
61.05	m	19-OMe
73.28	m	1-CH
83.55	m	2-CH
121.67	m	4-C
127.29	m	12-CH
128.05	m	11-CH
129.81	m	8-C
137.25	m	13-C
143.02	m	5-C

146.69	m	6-C
149.45	d, 70.80	20-CH
156.38	m	9-C
158.26	m	14-C
173.32	m	7-C
187.04	m	3-C
206.59	m	17-C

Table 4.10 ^{13}C-^{13}C coupling constants of ^{13}C-viridiol

δ (ppm)	J (Hz)	Carbon-position
28.46	m	15-CH2
30.59	d, 32.75	18-Me
36.51	m	16-CH2
42.32	m	10-C
60.8	q, 1.57, 1.57, 1.93	19-OMe
61.7	m	3-C
71.76	m	1-CH
81.76	m	2-CH
122.06	m	4-C
127.14	m	12-CH
127.54	m	11-CH
129.50	m	8-C
137.14	m	13-C
142.59	m	5-C
145.31	d, 73.21	17-C
146.04	m	6-C
157.93	m	14-C
158.71	m	9-C
173.52	m	7-C
206.80	m	20-CH

(A)

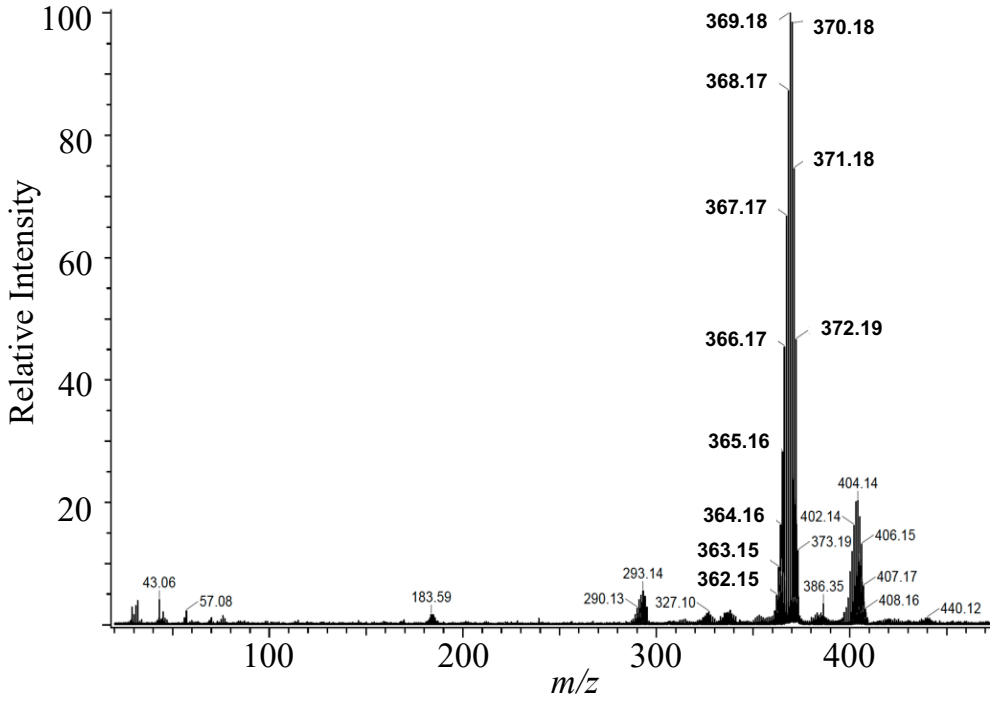
Relative Intensity
m/z
100
80
60
40
20
100
200
300
400
369.18
370.18
368.17
371.18
367.17
366.17
372.19
365.16
404.14
364.16
402.14
373.19
406.15
363.15
362.15
407.17
386.35
408.16
440.12
43.06
57.08
183.59
290.13
293.14
327.10

(B)

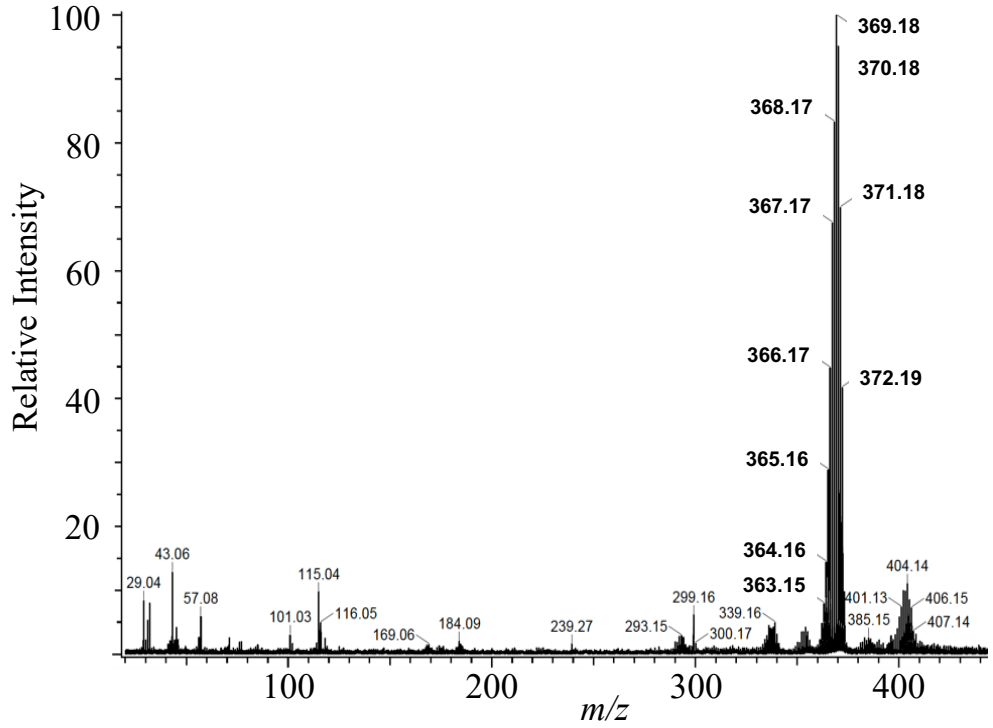
Relative Intensity
m/z
100
80
60
40
20
100
200
300
400
369.18
370.18
368.17
371.18
367.17
366.17
372.19
365.16
364.16
363.15
404.14
406.15
401.13
385.15
407.14
299.16
339.16
300.17
293.15
239.27
184.09
169.06
116.05
115.04
101.03
57.08
43.06
29.04

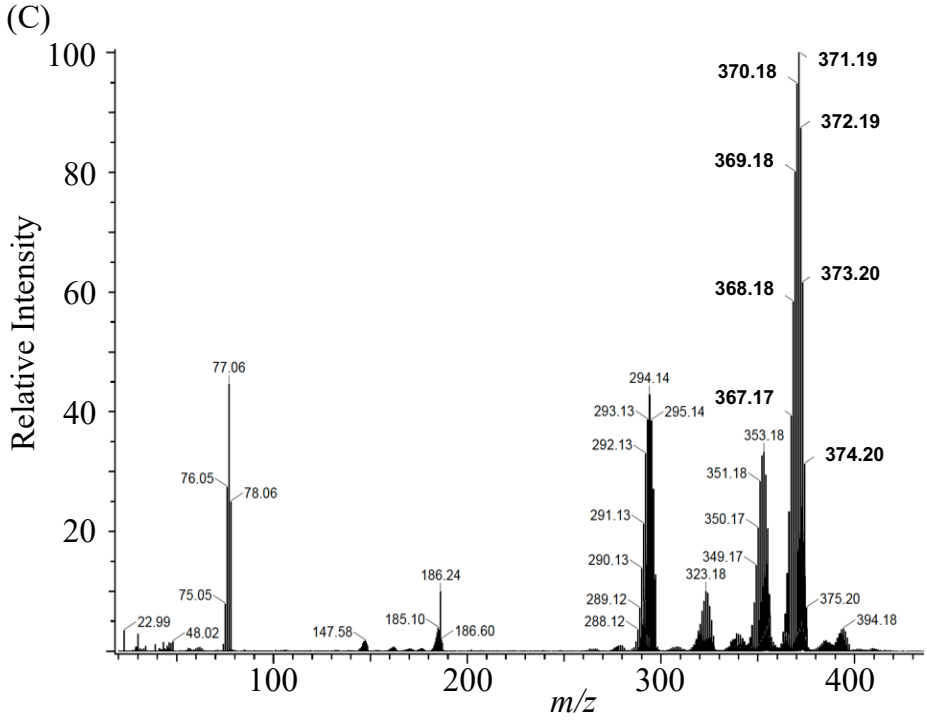

Figure 4.14 Field desorption-mass spectrometry (FD-MS) spectra of (A) ^{13}C-labeled viridin, (B) ^{13}C-labeled β-viridin, and (C) ^{13}C-labeled viridiol.

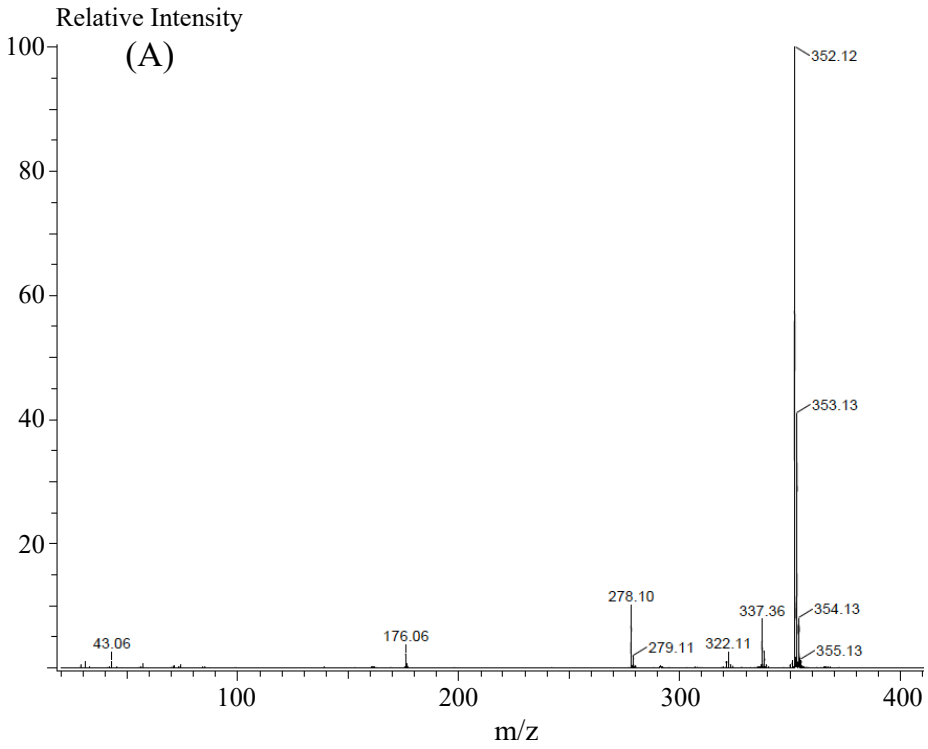

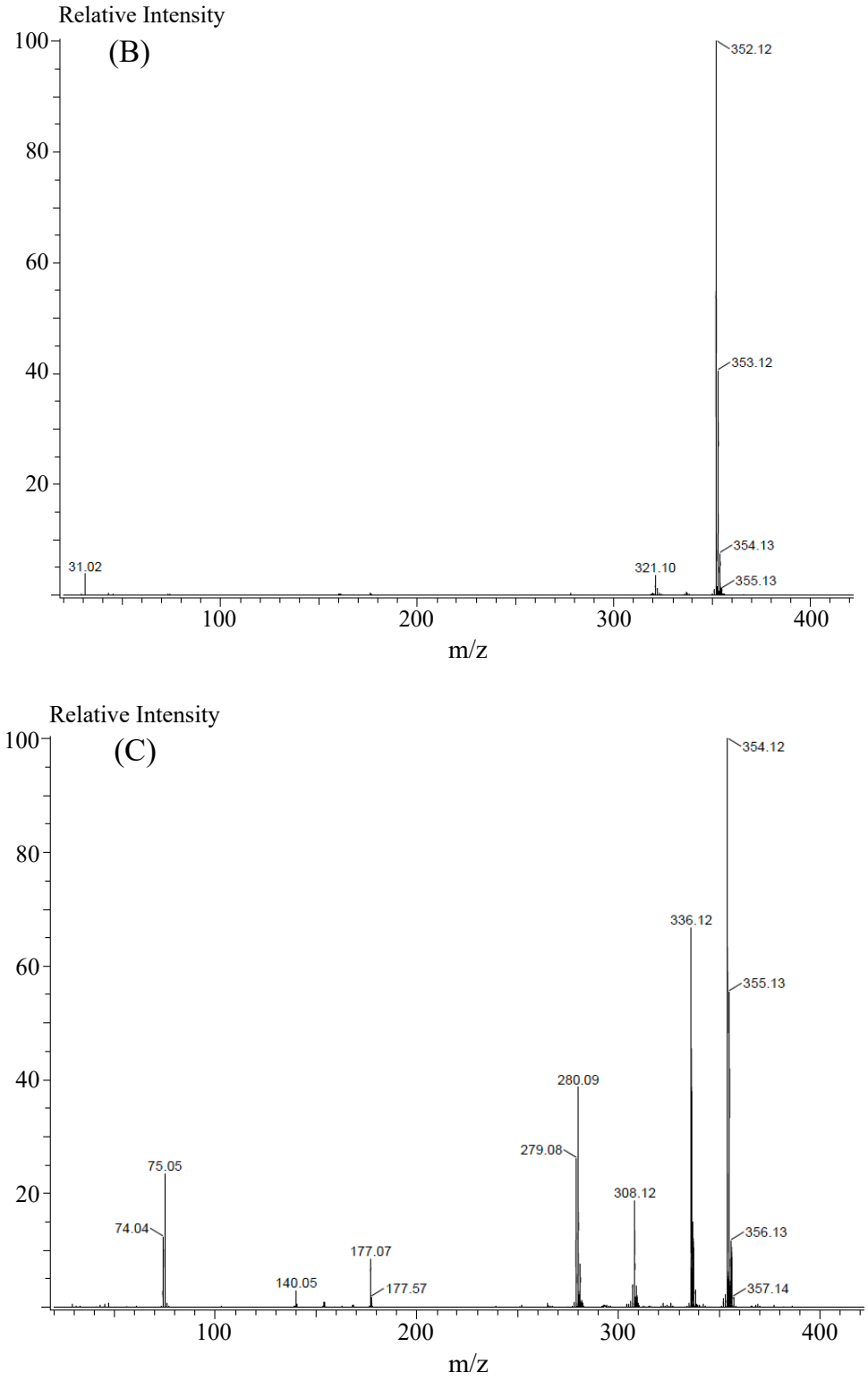

Figure 4.15 FD-MS spectrum (A: viridin; B: β-viridin; C: viridiol)

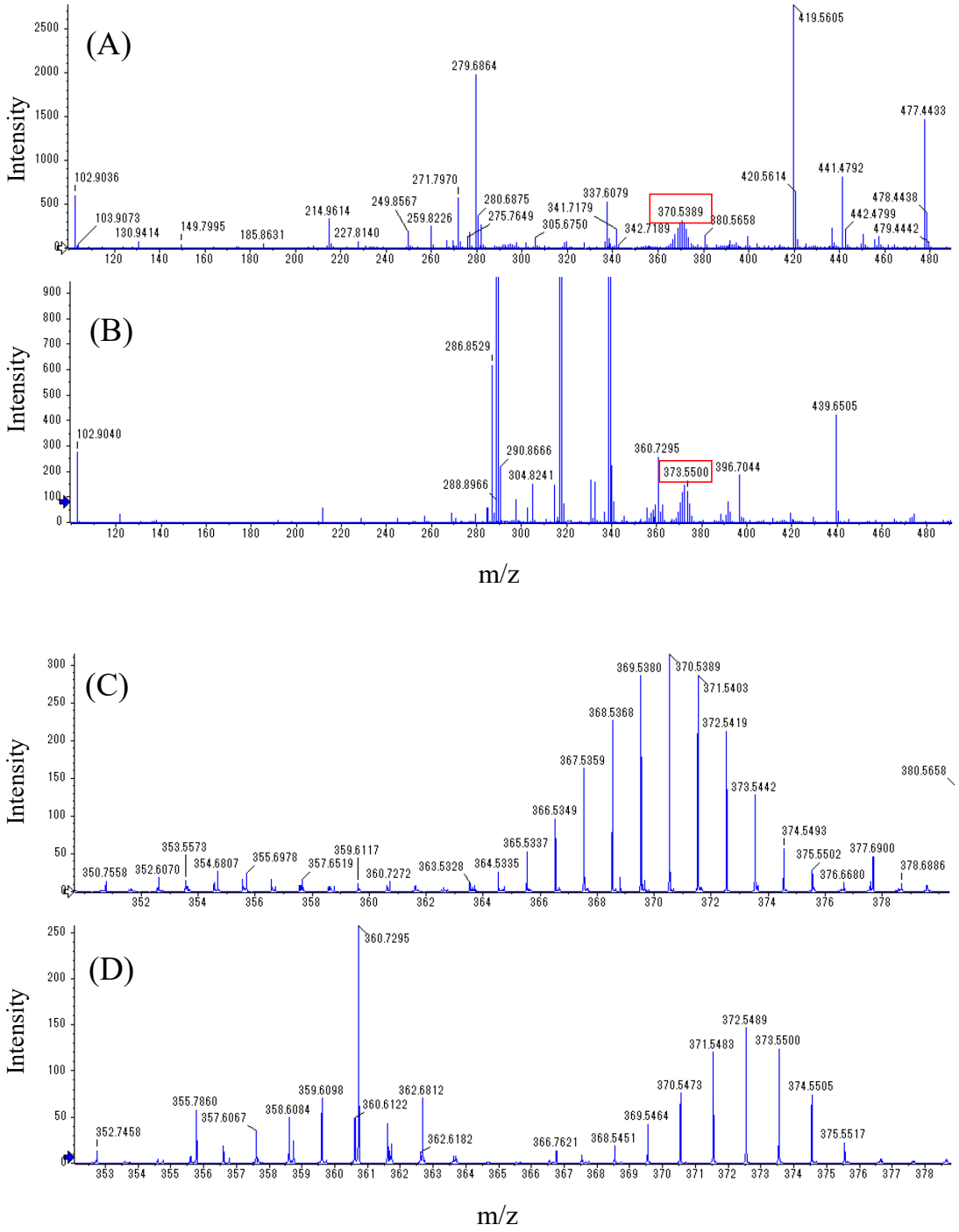

Figure 4.16 Positive mode of TOF-MS spectrum (A: ^{13}C labeled viridin; B: ^{13}C labeled viridiol; C: m/z 352 ~ 378 of ^{13}C labeled viridin; D: m/z 352 ~ 378 of ^{13}C labeled viridiol)

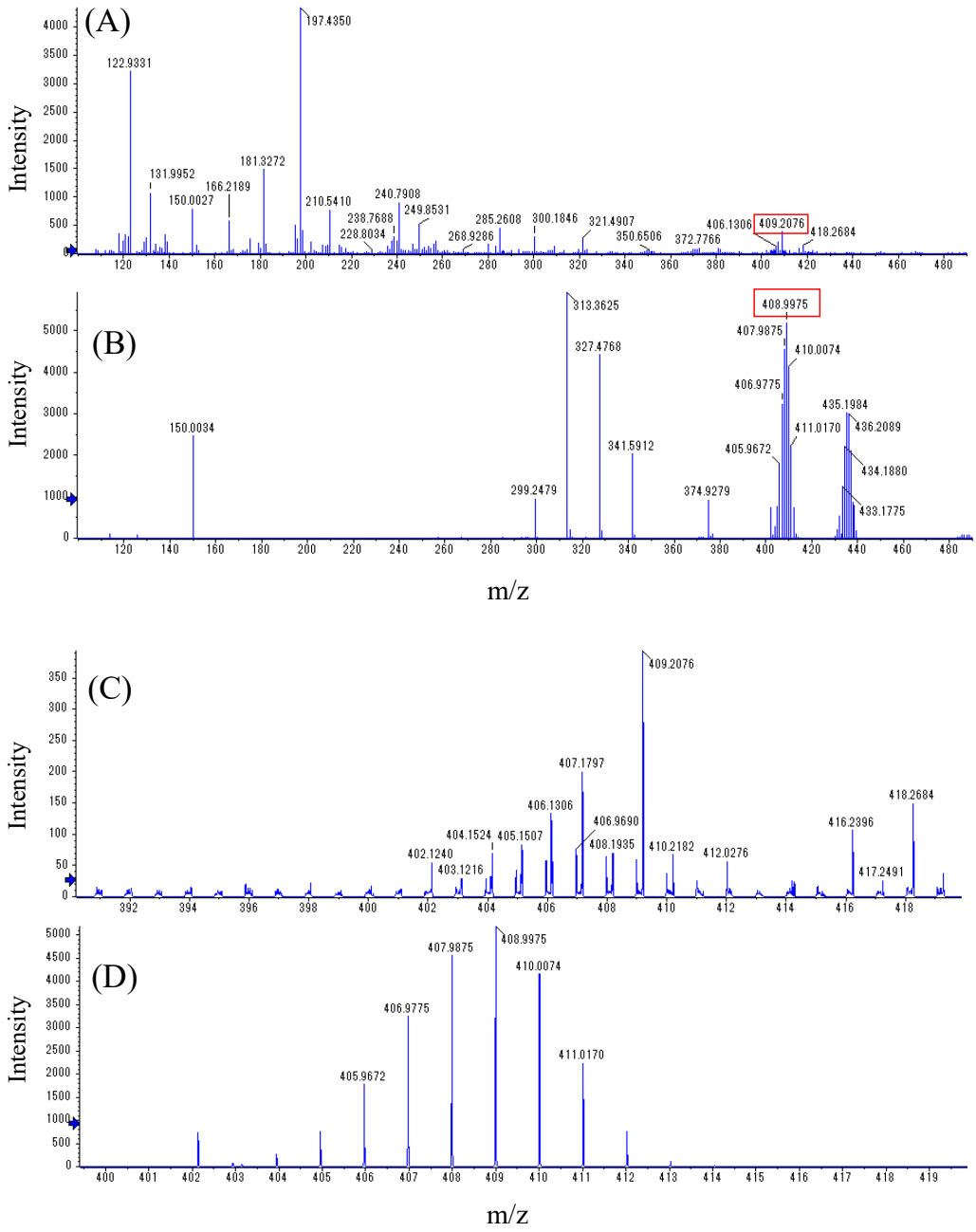

Figure 4.17 Negative mode of TOF-MS spectrum (A: ^{13}C labeled viridin; B: ^{13}C labeled viridiol; C: m/z 352 ~ 480 of ^{13}C labeled viridin; D: m/z 352 ~ 480 of ^{13}C labeled viridiol)

4.2.7. Bioactivities of viridin, β-viridin and viridiol

Viridin and β-viridin, but not viridiol, exhibited high DPPH radical scavenging activity percentages of 84.7 and 64.99%, respectively, at 8 mM. Compared to ascorbic acid (IC_{50}: 0.13 mM), viridin exhibited stronger antioxidant activity (IC_{50}: 2.00 mM), followed by β-viridin (IC_{50}: 4.09 mM).

4.3. Conclusion

Viridin and viridiol are useful compounds with potent bioactivities, including antibacterial and antifungal activities. Additionally, they strongly inhibit phosphoinositide 3-kinases, which are associated with tumor cell survival. However, despite their benefits, methods for the large-scale production of viridin, viridiol, and their derivatives are limited. Therefore, in this study, we developed a simple production and purification method for these compounds. NBRC 9169 showed viridin and viridiol accumulation of 47.80 ± 4.71 and 61.92 ± 4.39 mg/L after seven days of incubation at pH 3 and pH 2, respectively. Additionally, we established an efficient method to irreversibly convert viridin into β-viridin at high yields reaching 76% using the TEA/$CHCl_3$ system, thus facilitating further research on β-viridin. Notably, we determined the absolute configuration of β-viridin, which has been unknown for more than 70 years since its discovery. Our findings revealed the potential of NBRC 9169 for the biosynthesis of ^{13}C-labeled viridin and viridiol using [U-$^{13}C_6$]-glucose. Future studies should elucidate the detailed biosynthetic pathways of ^{13}C-labeled viridin and viridiol. Moreover, it will be expected to reveal a group of unidentified gene clusters responsible for the biosynthesis of viridin and viridiol using our unique culturing techniques to produce highly enriched ^{13}C- furanosteroids.

4.4. Experimental section

4.4.1. General methods or Chemicals

Potato dextrose broth (PDB) was purchased from BD Difco (USA). Potato infusion (PI) was purchased from Millipore (USA). [U-$^{13}C_6$]-glucose was obtained from Cayman (USA). All other chemicals were of commercially available grade.

4.4.2. Microorganisms and culture medium

T. virens PS1-7 was previously isolated in our laboratory[88]. Other *Trichoderma virens* were purchased from the Biological Resource Center of the National Institute of Technology and Evaluation (NBRC, Japan). All strains were maintained in potato dextrose agar at 25 °C. PIG medium contained PI powder (4 g/L) and glucose (20 g/L) in distilled water, and its pH was adjusted using 1 M H_2SO_4.

4.4.3. Growth and cultivation conditions

All fungal cells were incubated with 200 mL of PIG liquid medium (PI + glucose) for seven days in a shaking incubator at 25 ℃ and 100 rpm.

[U-$^{13}C_6$]-glucose (1 g) and PI powder (0.2 g) were dissolved in 50 mL of water, and the pH of the medium was adjusted to 3.0 to produce ^{13}C-labeled viridin and viridiol.

4.4.4. Extraction and purification of metabolites

After incubation, the culture liquid and biomass were separated, and the culture liquid was extracted with ethyl acetate (200 mL × 2) for the quantitative analysis of metabolites. The organic phase was dried (Na_2SO_4) and concentrated under vacuum. For large-scale isolation and purification, the culture liquid was extracted with hexane, ether (viridin), or ethyl acetate (viridiol). Viridins and viridiol were successfully purified by recrystallization or silica gel chromatography before conducting chemical validation.

4.4.5. Quantitation of viridin and viridiol via high-performance liquid chromatography

High-performance liquid chromatography was performed using the Hitachi Model D-2000 Elite system with Inertsil ODS-02 C18 column. Aqueous 0.1% H_3PO_4 (A) and acetonitrile (B) gradient was used as the mobile phase. Metabolites in the residue were dissolved in 1 mL $CHCl_3$/MeOH (7/3), and the solution was eluted at 1 mL/min using a 22-min solvent gradient: 0–15 min 78% A and 22% B to 63% A and 37% B, with a 7 min hold. The analysis was performed at a wavelength of 220 nm. Standard curves were plotted and used to quantify the concentrations of viridin and viridiol in the samples. The standards were isolated and identified in our laboratory.

4.4.6. Mass analysis

The isolated compounds were identified using the high-resolution mass spectrometry field desorption-mass spectrometry (FD-MS) analyzer (JMS-T100GCV; JEOL Ltd., Tokyo, Japan).

4.4.7. NMR analysis

NMR spectra were acquired using the JEOL JNM-ECZ400 spectrometer at 25 °C in $CDCl_3$, at 400 MHz for ^{1}H and 100 MHz for ^{13}C. Chemical shifts (δ) are reported in ppm and coupling constant values (*J*) are in Hertz (Hz0) relative to those of $CDCl_3$ (^{1}H, δ 7.26; ^{13}C, δ 77.00) and tetramethylsilanol. The following abbreviations were used to indicate the signal multiplicity: s = singlet, d = doublet, t = triplet, q = quartet and m = multiplet.

4.4.8. VCD analysis

VCD and IR spectra were recorded for a chloroform-*d* solution at a concentration of 0.125 M placed in a 100-μm BaF_2 cell. These spectra were measured on a JASCO FVS-6000 spectrometer equipped with an optical filter that passes through 2200-850 cm^{-1} light and a MCT-V detector at a resolution of 4 cm^{-1} under ambient temperature. VCD spectra were recorded for 4000 scans, while IR spectra were recorded for 16 scans. Both spectra were corrected by solvent spectra obtained under the identical measurement conditions.

4.4.9. Antioxidant activity: 2, 2-Diphenyl-1-picryl-hydrazyl-hydrate (DPPH) assay

DPPH radical scavenging activity of isolated compounds was determined as previously described [89], with some modifications. Briefly, DPPH dissolved in EtOH as a 0.2 mM solution was mixed with the viridin, β-viridin and viridiol (0.5 – 8 mM) and incubated at 37 ℃ for 30 min in the dark. Then, absorbance of different solutions was measured at 517 nm using a spectrophotometer. The percentage of DPPH scavenging activity was calculated using the following equation (1):

$$\text{DPPH scavenging activity (\%)} = \frac{A_0 - A_1}{A_0} \times 100 \quad (1)$$

where, A_0 and A_1 are the absorbance values of the DPPH solution and sample, respectively. Half-maximal inhibitory concentration (IC_{50}) values were calculated by plotting the percentage inhibition against the concentration.

References

1. Forensics, S.I., An Introduction to the Forensic Applications of Stable Isotope Analysis. *Wiltshire: Wiley*, 2010.
2. O'Brien, D.M., Stable isotope ratios as biomarkers of diet for health research. *Annual review of nutrition*, 2015. **35**(1): 565-594.
3. Fry, B., *Stable Isotope Ecology*. Vol. 521. 2006: Springer.
4. Wolfe, R.R. and D.L. Chinkes, *Isotope Tracers in Metabolic Research: Principles and Practice of Kinetic Analysis*. 2004: John Wiley & Sons.
5. Kao, C.C., et al., Resting energy expenditure and protein turnover are increased in patients with severe chronic obstructive pulmonary disease. *Metabolism*, 2011. **60**(10): 1449-1455.
6. Cuthbertson, D., et al., Anabolic signaling deficits underlie amino acid resistance of wasting, aging muscle. *The FASEB Journal*, 2005. **19**(3): 1-22.
7. Mew, N.A., M. Yudkoff, and M. Tuchman, Stable isotopes in the diagnosis and treatment of inherited hyperammonemia. *Journal of pediatric biochemistry*, 2014. **4**(1): 57-63.
8. Menicucci, A.J., J.A. Matthews, and H.J. Spero, Oxygen isotope analyses of biogenic opal and quartz using a novel microfluorination technique. *Rapid Communications in Mass Spectrometry*, 2013. **27**(16): 1873-1881.
9. Meier-Augenstein, W., et al., An inter-laboratory comparative study into sample preparation for both reproducible and repeatable forensic 2H isotope analysis of human hair by continuous flow isotope ratio mass spectrometry. *Rapid Communications in Mass Spectrometry*, 2011. **25**(21): 3331-3338.
10. Fortunato, G., A. Ritter, and D. Fabian, Old Masters' lead white pigments: investigations of paintings from the 16th to the 17th century using high precision lead isotope abundance ratios. *Analyst*, 2005. **130**(6): 898-906.
11. Arsene, C.G., et al., Protein quantification by isotope dilution mass spectrometry of proteolytic fragments: cleavage rate and accuracy. *Analytical chemistry*, 2008. **80**(11): 4154-4160.
12. Faucher, N., et al., Highly chemoselective hydrogenolysis of iodoarenes. *The Journal of Organic Chemistry*, 2002. **67**(3): 932-934.

13. Ambroise, Y., et al., Consequences of affinity in heterogeneous catalytic reactions: highly chemoselective hydrogenolysis of iodoarenes. *The Journal of Organic Chemistry*, 2000. **65**(21): 7183-7186.
14. Dorman, G., et al., Synthesis of highly tritiated 4-benzoyl-L-phenylalanine, a photoactivatable amino acid. *The Journal of Organic Chemistry*, 1995. **60**(7): 2292-2297.
15. Atzrodt, J., et al., The renaissance of H/D exchange. *Angewandte Chemie International Edition*, 2007. **46**(41): 7744-7765.
16. Ito, N., et al., Synergistic Effect of a Palladium-on-Carbon/Platinum-on-Carbon Mixed Catalyst in Hydrogen/Deuterium Exchange Reactions of Alkyl-Substituted Aromatic Compounds. *Advanced Synthesis & Catalysis*, 2006. **348**(9): 1025-1028.
17. Saito, I., et al., Regio-controlled hydrogen-deuterium exchange of biologically important indoles under uv irradiation. *Tetrahedron Letters*, 1985. **26**(48): 5891-5894.
18. Tachrim, Z.P., et al., Hydrogen-deuterium exchange of histidine and histamine with deuterated trifluoromethanesulfonic acid. *Heterocycles*, 2020. **101**(1): 357-362.
19. Tachrim, Z.P., et al., Synthesis of deuterated cyclodopa with hydrogen/deuterium exchange. *Heterocycles*, 2019. **99**(1): 404-414.
20. Wang, L., et al., Hydrogen/deuterium exchange of cross-linkable α-amino acid derivatives in deuterated triflic acid. *Bioscience, Biotechnology, and Biochemistry*, 2014. **78**(7): 1129-1134.
21. Murai, Y., et al., Rapid and controllable hydrogen/deuterium exchange on aromatic rings of α-amino acids and peptides. *European Journal of Organic Chemistry*, 2013. **2013**(23): 5111-5116.
22. Tachrim, Z.P., et al., Mild and selective hydrogen–deuterium exchange for aromatic hydrogen of amines. *Journal of Labelled Compounds and Radiopharmaceuticals*, 2023. **66**(10): 321-331.
23. Brown, B., S. Neill, and R. Horgan, Partial isotope fractionation during high-performance liquid chromatography of deuterium-labelled internal standards in plant hormone analysis: A cautionary note. *Planta*, 1986. **167**: 421-423.

24. Magnus, V., R.S. Bandurski, and A. Schulze, Synthesis of 4, 5, 6, 7 and 2, 4, 5, 6, 7 deuterium-labeled indole-3-acetic acid for use in mass spectrometric assays. *Plant Physiology*, 1980. **66**(4): 775-781.
25. Yamada, T., et al., Deuteration of Indole Compounds: Synthesis of Deuterated Auxins, Indole-3-acetic Acid-d5 and Indole-3-butyric Acid-d5. *ACS omega*, 2021. **6**(30): 19956-19963.
26. 辻本満丸, 黒子鮫油に就て. *工業化学雑誌*, 1906. **9**(10): 953-958.
27. Heilbron, I.M. and A. Thompson, CXV.—The unsaponifiable matter from the oils of elasmobranch fish. Part VI. The constitution of squalene as deduced from a study of the decahydrosqualenes. *Journal of the Chemical Society (Resumed)*, 1929: 883-892.
28. Spanova, M. and G. Daum, Squalene–biochemistry, molecular biology, process biotechnology, and applications. *European Journal of Lipid Science and Technology*, 2011. **113**(11): 1299-1320.
29. Huang, Z.-R., Y.-K. Lin, and J.-Y. Fang, Biological and pharmacological activities of squalene and related compounds: potential uses in cosmetic dermatology. *Molecules*, 2009. **14**(1): 540-554.
30. Senbagalakshmi, P., et al., Squalene, biosynthesis and its role in production of bioactive compounds, a proper scientific challenge—a review. *J. Emerg. Technol. Innov. Res*, 2019. **6**: 505-526.
31. Garcia-Bermudez, J., et al., Squalene accumulation in cholesterol auxotrophic lymphomas prevents oxidative cell death. *Nature*, 2019. **567**(7746): 118-122.
32. Brown, A.J., N.K. Chua, and N. Yan, The shape of human squalene epoxidase expands the arsenal against cancer. *Nature communications*, 2019. **10**(1): 888.
33. Gohil, N., et al., Engineering strategies in microorganisms for the enhanced production of squalene: advances, challenges and opportunities. *Frontiers in Bioengineering and Biotechnology*, 2019. **7**: 50.
34. Patel, A., et al., Microbial genetic engineering approach to replace shark livering for squalene. *Trends in Biotechnology*, 2022. **40**(10): 1261-1273.
35. Hadinoto, S., et al. *Characteristics squalene of smallfin gulper shark (Centrophorus moluccensis) livers from Aru Islands, Mollucas, Indonesia*. in *Journal of Physics: Conference Series*. 2020. IOP Publishing.

36. Wejnerowska, G., P. Heinrich, and J. Gaca, Separation of squalene and oil from Amaranthus seeds by supercritical carbon dioxide. *Separation and Purification Technology*, 2013. **110**: 39-43.
37. Lozano-Grande, M.A., et al., Plant sources, extraction methods, and uses of squalene. *International Journal of Agronomy*, 2018. **2018**(1): 1829160.
38. Mantzouridou, F. and M.Z. Tsimidou, Observations on squalene accumulation in Saccharomyces cerevisiae due to the manipulation of HMG2 and ERG6. *FEMS yeast research*, 2010. **10**(6): 699-707.
39. Goldberg, I. and I. Shechter, Occurrence of squalene in methanol-grown bacteria. *Journal of bacteriology*, 1978. **135**(2): 717-720.
40. Blagović, B., et al., Lipid composition of brewer's yeast. *Food Technology and Biotechnology*, 2001. **39**(3): 175-181.
41. Kaya, K., et al., Thraustochytrid Aurantiochytrium sp. 18W-13a accummulates high amounts of squalene. *Bioscience, Biotechnology, and Biochemistry*, 2011. **75**(11): 2246-2248.
42. Patel, A., et al., Co-production of DHA and squalene by thraustochytrid from forest biomass. *Scientific Reports*, 2020. **10**(1): 1992.
43. Nakazawa, A., et al., Optimization of culture conditions of the thraustochytrid Aurantiochytrium sp. strain 18W-13a for squalene production. *Bioresour Technol*, 2012. **109**: 287-91.
44. Lu, S.R., et al., Enhancing fluxes through the mevalonate pathway in by engineering the HMGR and β-alanine metabolism. *Microbial Biotechnology*, 2022. **15**(8): 2292-2306.
45. Goldstein, J.L. and M.S. Brown, Regulation of the mevalonate pathway. *Nature*, 1990. **343**(6257): 425-30.
46. Eisenreich, W., et al., Biosynthesis of isoprenoids via the non-mevalonate pathway. *Cell Mol Life Sci*, 2004. **61**(12): 1401-26.
47. Lichtenthaler, H.K., The 1-Deoxy-D-Xylulose-5-Phosphate Pathway of Isoprenoid Biosynthesis in Plants. *Annu Rev Plant Physiol Plant Mol Biol*, 1999. **50**: 47-65.
48. McGarvey, D.J. and R. Croteau, Terpenoid metabolism. *Plant Cell*, 1995. **7**(7): 1015-26.

49. Chappell, J., Biochemistry and Molecular-Biology of the Isoprenoid Biosynthetic-Pathway in Plants. *Annual Review of Plant Physiology and Plant Molecular Biology*, 1995. **46**: 521-547.
50. Han, J.Y., et al., High-level recombinant production of squalene using selected Saccharomyces cerevisiae strains. *J Ind Microbiol Biotechnol*, 2018. **45**(4): 239-251.
51. Desmond, E. and S. Gribaldo, Phylogenomics of Sterol Synthesis: Insights into the Origin, Evolution, and Diversity of a Key Eukaryotic Feature. *Genome Biology and Evolution*, 2009. **1**: 364-381.
52. Garaiová, M., et al., Squalene epoxidase as a target for manipulation of squalene levels in the yeast Saccharomyces cerevisiae. *FEMS yeast research*, 2014. **14**(2): 310-323.
53. Laranjeira, S., et al., Arabidopsis Squalene Epoxidase 3 (SQE3) Complements SQE1 and Is Important for Embryo Development and Bulk Squalene Epoxidase Activity. *Mol Plant*, 2015. **8**(7): 1090-102.
54. Fuglseth, E., et al., Chiral derivatives of Butenafine and Terbinafine: synthesis and antifungal activity. *Tetrahedron*, 2009. **65**(47): 9807-9813.
55. Song, X.J., et al., High Production of Squalene Using a Newly Isolated Yeast-like Strain Pseudozyma sp SD301. *Journal of Agricultural and Food Chemistry*, 2015. **63**(38): 8445-8451.
56. Bhavani, G.V.L. and V. Muvva, Optimization of Process Parameters for Improved Production of Bio-Active Metabolites by Endophytic Fungus Cladosporium Cladosporioides Isolated from Mangrove Plant Lumnitzera Racemosa Linn. *International Journal of Pharmaceutical Sciences and Research*, 2020. **11**(7): 3260-3267.
57. Yogabaanu, U., et al., Antimicrobial properties and the influence of temperature on secondary metabolite production in cold environment soil fungi. *Polar Science*, 2017. **14**: 60-67.
58. Shakeri, S., F. Khoshbasirat, and M. Maleki, Rhodosporidium sp. DR37: a novel strain for production of squalene in optimized cultivation conditions. *Biotechnology for Biofuels*, 2021. **14**(1).
59. Matsuda, T., et al., Antimicrobial Activities of Organic-Acids Determined by Minimum Inhibitory Concentrations at Different Ph Ranged from 4.0 to 7.0.

Journal of the Japanese Society for Food Science and Technology-Nippon Shokuhin Kagaku Kogaku Kaishi, 1994. **41**(10): 687-702.

60. Lu, S.R., et al., Enhancing fluxes through the mevalonate pathway in Saccharomyces cerevisiae by engineering the HMGR and beta-alanine metabolism. *Microbial Biotechnology*, 2022. **15**(8): 2292-2306.
61. Moran, N.E., et al., Biosynthesis of highly enriched 13C-lycopene for human metabolic studies using repeated batch tomato cell culturing with 13C-glucose. *Food Chem*, 2013. **139**(1-4): 631-9.
62. Peacock, G.A. and M.W. Goosey, Separation of Fungal Sterols by Normal-Phase High-Performance Liquid-Chromatography - Application to the Evaluation of Ergosterol Biosynthesis Inhibitors. *Journal of Chromatography*, 1989. **469**: 293-304.
63. Gadher, P., et al., A Comparison of the Potency of Some Fungicides as Inhibitors of Sterol 14-Demethylation. *Pesticide Biochemistry and Physiology*, 1983. **19**(1): 1-10.
64. Sandmann, G., W. Hilgenberg, and P. Boger, Enzymatic Preparation of C-14-Labeled Phytoene, Squalene, and Geranylgeranyl Pyrophosphate from [2-C-14-Labeled Mevalonic Acid. *Zeitschrift Fur Naturforschung C-a Journal of Biosciences*, 1980. **35**(11-1): 927-930.
65. Kato, T. and Y. Kawase, Selective inhibition of the demethylation at C-14 in ergosterol biosynthesis by the fungicide, Denmert (S-1358). *Agricultural and Biological Chemistry*, 1976. **40**(12): 2379-2388.
66. Hoshino, T., et al., Synthesis of 10,15-[(C-13)2]-Squalene and 10,15-[(C-13)2]-Dl-Squalene Oxide. *Journal of Labelled Compounds & Radiopharmaceuticals*, 1990. **28**(11): 1285-1292.
67. Kawano, Y., et al., Degradation by oxidation of squalene. *Journal of Japan Oil Chemists' Society*, 1997. **46**(11): 1361-1367.
68. Howell, C. and R. Stipanovic, Phytotoxicity to crop plants and herbicidal effects on weeds of viridiol produced by Gliocladium virens. *Phytopathology*, 1984. **74**(11): 1346-1349.
69. Fujiwara, H., et al., Halenaquinone, a novel phosphatidylinositol 3-kinase inhibitor from a marine sponge, induces apoptosis in PC12 cells. *European journal of pharmacology*, 2001. **413**(1): 37-45.

70. Wipf, P., et al., Synthesis and biological evaluation of synthetic viridins derived from C (20)-heteroalkylation of the steroidal PI-3-kinase inhibitor wortmannin. *Organic & Biomolecular Chemistry*, 2004. **2**(13): 1911-1920.
71. Ihle, N.T., et al., Molecular pharmacology and antitumor activity of PX-866, a novel inhibitor of phosphoinositide-3-kinase signaling. *Molecular Cancer Therapeutics*, 2004. **3**(7): 763-772.
72. Ji, Y., et al., Total synthesis of viridin and viridiol. *Journal of the American Chemical Society*, 2019. **141**(41): 16208-16212.
73. Del Bel, M., et al., Enantioselective chemical syntheses of the furanosteroids (-)-viridin and (-)-viridiol. *Journal of the American Chemical Society*, 2017. **139**(20): 6819-6822.
74. Anderson, E.A., E.J. Alexanian, and E.J. Sorensen, Synthesis of the furanosteroidal antibiotic viridin. *Angewandte Chemie-International Edition*, 2004. **43**(15): 1998-2001.
75. Grove, J., P. McCloskey, and J. Moffatt, The structure of viridin. *Chemical Communications (London)*, 1965(15): 343-344.
76. Avent, A.G., J.R. Hanson, and A. Truneh, Metabolites of Gliocladium flavofuscum. *Phytochemistry*, 1992. **32**(1): 197-198.
77. Grove, J.F., J. Moffatt, and E. Vischer, 696. Viridin. Part I. Isolation and characterisation. *Journal of the Chemical Society (Resumed)*, 1965: 3803-3811.
78. Hanson, J.R., The viridin family of steroidal antibiotics. *NATURAL PRODUCT REPORTS*, 1995. **12**(4): 381-384.
79. Vischer, E., S. Howland, and H. Raudnitz, Viridin. *Nature*, 1950. **165**(4196): 528-528.
80. Golder, W.S. and T.R. Watson, Lanosterol derivatives as precursors in the biosynthesis of viridin. Part 1. *Journal of the Chemical Society, Perkin Transactions 1*, 1980: 422-425.
81. Simpson, T.J., M.W. Lunnon, and J. MacMillan, Fungal products. Part 21. Biosynthesis of the fungal metabolite, wortmannin, from [1, 2-$^{13}C_2$]-acetate. *Journal of the Chemical Society, Perkin Transactions 1*, 1979: 931-934.
82. Hanson, J.R. and H.J. Wadsworth, Biosynthesis of demethoxyviridin. *Journal of the Chemical Society, Chemical Communications*, 1979(8): 360-361.

83. Grove, J.F., Viridin. Part VI. Evidence for a steroidal pathway in the biogenesis of viridin from mevalonic acid. *Journal of the Chemical Society C: Organic*, 1969(4): 549-551.
84. Jones, R.W. and J.G. Hancock, Conversion of viridin to viridiol by viridin-producing fungi. *Canadian Journal of Microbiology*, 1987. **33**(11): 963-966.
85. Wang, G.Q., et al., Biosynthetic pathway for furanosteroid demethoxyviridin and identification of an unusual pregnane side-chain cleavage. *Nature communications*, 2018. **9**.
86. Zhang, W., et al., Accumulation of squalene in filamentous fungi PS1-7 in the presence of butenafine hydrochloride, squalene epoxidase inhibitor: biosynthesis of ^{13}C-enriched squalene. *Bioscience Biotechnology and Biochemistry*, 2023. **87**(10): 1129-1138.
87. Parsons, S., H.D. Flack, and T. Wagner, Use of intensity quotients and differences in absolute structure refinement. *Acta Crystallographica Section B: Structural Science, Crystal Engineering and Materials*, 2013. **69**(3): 249-259.
88. Wang, M., M. Hashimoto, and Y. Hashidoko, Carot-4-en-9,10-diol, a conidiation-inducing sesquiterpene diol produced by Trichoderma virens PS1-7 upon exposure to chemical stress from highly active iron chelators. *Applied and Environmental Microbiology*, 2013. **79**(6): 1906-14.
89. Rashid, H.M., et al., Antioxidant and Antiproliferation Activities of Lemon Verbena (Aloysia citrodora): An In Vitro and In Vivo Study. *Plants (Basel)*, 2022. **11**(6).